AEDC-TR-66-177

HIGH TEMPERATURE, LOW DENSITY BOUNDARY-LAYER CONTROL BY CRYOGENIC PUMPING

W. N. MacDermott, R. E. Dix, and J. E. Shepard

ARO, Inc.

December 1966

PROPULSION WIND TUNNEL FACILITY
ARNOLD ENGINEERING DEVELOPMENT CENTER
AIR FORCE SYSTEMS COMMAND
ARNOLD AIR FORCE STATION, TENNESSEE

NOTICES

When U. S. Government drawings specifications, or other data are used for any purpose other than a definitely related Government procurement operation, the Government thereby incurs no responsibility nor any obligation whatsoever, and the fact that the Government may have formulated, furnished, or in any way supplied the said drawings, specifications, or other data, is not to be regarded by implication or otherwise, or in any manner licensing the holder or any other person or corporation, or conveying any rights or permission to manufacture, use, or sell any patented invention that may in any way be related thereto.

Qualified users may obtain copies of this report from the Defense Documentation Center.

References to named commercial products in this report are not to be considered in any sense as an endorsement of the product by the United States Air Force or the Government.

HIGH TEMPERATURE, LOW DENSITY BOUNDARY-LAYER CONTROL BY CRYOGENIC PUMPING

W. N. MacDermott, R. E. Dix, and J. E. Shepard
ARO, Inc.

AF - AEDC
Arnold AFS Tenn

FOREWORD

The work reported herein was sponsored by the Arnold Engineering Development Center (AEDC), Air Force Systems Command (AFSC), under Program Element 62410034.

The results of the research presented were obtained by ARO, Inc. (a subsidiary of Sverdrup & Parcel and Associates, Inc.), contract operator of the AEDC, AFSC, Arnold Air Force Station, Tennessee, under Air Force Contract AF 40(600)-1200. The research was conducted from July 1964 to September 1965 under ARO Project No. PL2291, and the manuscript was submitted for publication on August 11, 1966.

This technical report has been reviewed and is approved.

Carl E. Simmons
1 Lt, USAF
Research Division
Directorate of Plans and Technology

Donald R. Eastman, Jr.
Acting Director
Directorate of Plans and Technology

ABSTRACT

Results are presented of a study of the flow in a hypersonic nozzle operated at low densities and high stagnation enthalpy levels with both natural and controlled boundary layers. The boundary-layer control was established by cryogenic pumping on the nozzle walls, using liquid hydrogen as the cryogen. A flow calibration procedure was evolved for this nozzle which included a fully frozen (in vibration) nitrogen flow model, large low density corrections to pitot and static pressure measurements, and a non-Sutherland viscosity variation. The regimes of isentropic flow in the nozzle were identified by this calibration, and flow conditions within these regimes are given. The boundary-layer control technique permitted the attainment of indicated Knudsen numbers one order of magnitude greater than those produced with no boundary-layer control. At the lowest levels of static density produced in the nozzle with boundary-layer control, evidence of an entropy-increasing process was found which was tentatively identified as a departure from rotational equilibrium in the flow.

CONTENTS

ILLUSTRATIONS

NOMENCLATURE

A	Area
C	Cryogenic capture coefficient
D	Diameter
Kn	Knudsen number

Kn_{cm}	Knudsen number for L_c = 1 cm
K_w	Wall heat-transfer parameter, Eq. (III-3)
k	Boltzmann constant
L	Length of nozzle along wall
L_c	Characteristic length
L_{mean}	Mean free path = $\frac{32\mu}{5\pi\ \rho\ \overline{v}}$
ℓ	Characteristic length defined by Eq. (II-1)
M	Mach number
$\dot{m}$	Mass flux
Pr	Prandtl number
p	Pressure
Q	Volumetric pumping speed
$\dot{q}$	Heat flow rate
R	Gas constant for undissociated nitrogen
Re	Reynolds number
T	Temperature
V	Velocity
$\overline{v}$	Mean molecular velocity = $\sqrt{\frac{8RT}{\pi}}$
x	Length of developed boundary layer
γ	Specific heat ratio
ΔM	Mach number difference defined by Eq. (4)
δ	Boundary-layer thickness
δ^*	Momentum thickness
ϵ	Potential energy at minimum of intermolecular potential energy curve
θ	Nozzle expansion half-angle
μ	Absolute viscosity or microns of Hg
ρ	Mass density
σ	Molecular separation at zero potential energy of interaction
ψ	Nonequilibrium value normalized by equilibrium value, Fig. (II-1)

SUBSCRIPTS

1	Static condition at nozzle exit
$\mathfrak{L}$	Centerline of nozzle
core	Useful test core
e	Edge of useful test core
g	Condition in gas
L	Parameter based on nozzle length
L_c	Parameter based on characteristic length
o_1	Upstream reservoir condition
o_2	Impact condition at nozzle exit
orif	Orifice
p	Condition at pumping surface
w	Wall

SUPERSCRIPT

*	Sonic condition

SECTION I
INTRODUCTION

The Reynolds numbers characteristic of low density wind tunnel nozzle flows are so low that boundary layers on the nozzle walls are not thin layers at the flow boundaries, but are major portions of the flow. In fact, the boundary layer can develop until a fully viscous flow profile exists at the nozzle exit. This "merged" condition represents a natural limit to the usefulness of the nozzle for low density aerodynamic testing.

A minimum attainable Reynolds number, based on nozzle length, is formed at the "merged" flow limit. This minimum Reynolds number is given in Fig. 1 as a function of Mach number for stagnation temperatures of 1000 and 4000°K in nitrogen, a wall temperature of 300°K, and for both an equilibrium and a vibrationally frozen flow model. These data are based on a simplified analysis using the flat plate boundary-layer thicknesses of Ref. 1 and a typical hypersonic nozzle length-to-diameter ratio of 2.0. Similar data were presented for a stagnation temperature of 300°K in Ref. 2, where it was also shown that the flat plate boundary-layer approximation was accurate to within ±15 percent for a large number of low density nozzles. Within this approximation, then, referring to Fig. 1 for M = 10, minimum nozzle Reynolds numbers will range from 6500 to 3500 at merge, for stagnation temperatures between 1000 and 4000°K and for vibrationally frozen flow. These Reynolds number limits are independent of the nozzle scale. In small nozzles they will be attained with relatively large unit Reynolds numbers and in large nozzles with relatively small unit Reynolds numbers and low densities.

The merged boundary-layer condition also defines a maximum Knudsen number in the nozzle exit flow

$$Kn = \frac{L_{mean}}{L_c} = \frac{32\mu}{5\pi\rho\bar{v}L_c} = 1.512\,\frac{M}{Re_{L_c}} \qquad (1)$$

It is convenient to define the degree of rarefaction produced in a nozzle as the Knudsen number for a 1-cm characteristic length:

$$(Kn_{cm})_{merge} = 1.512\,\frac{ML}{(Re_L)_{merge}} \qquad (2)$$

where L is the nozzle length in centimeters. Curves of this rarefaction parameter are given on the bottom half of Fig. 1 for the same conditions as for the minimum Reynolds number data and for a 1-ft-exit-diam nozzle. It is to be noted that this rarefaction parameter is directly proportional to the nozzle scale. It can be seen that for natural boundary-layer growth in a 1-ft-diam hypersonic nozzle at M = 10, the maximum

attainable Kn_{cm} is 0.15 to 0.275 for stagnation temperature between 1000 and 4000°K, again with vibrationally frozen flow.

There have been numerous investigations of the possibility of circumventing these limits by some form of boundary-layer control (Refs. 2 through 6). At AEDC, the form of boundary-layer control (BLC) investigated has been wall suction produced by cryogenic pumping action. In Ref. 5, preliminary results were reported of tests using a small, unheated, low Mach number nozzle with liquid nitrogen as the refrigerant and carbon dioxide as the test gas. In Ref. 2, results were given for a combination of liquid hydrogen as the refrigerant and nitrogen as the test gas in a 1-ft-diam hypersonic nozzle. Extensive Mach number calibrations and flow profiles were given for a stagnation temperature of 300°K, and it was shown that the attainable degree of rarefaction in the nozzle, Kn_{cm}, was increased by at least an order of magnitude by the use of the cryogenic BLC. A limited amount of data on useful test core size at a single mass flow was also presented for operation of the BLC nozzle with arc-heated nitrogen at stagnation temperatures up to 4000°K. No information on the degree of rarefaction at high stagnation temperature was provided, since this high temperature data had not been subjected to an accurate Mach number calibration. It was verified, however, that the cryopumping process did function at high stagnation temperature. A time-dependency related to the thickness of the condensate layer was noted. There was also reported an isolated case which appeared to demonstrate large gains in performance of the BLC system by means of precooling the boundary layer to liquid-nitrogen temperature at the wall upstream of the cryopumping section of the nozzle.

This report represents an extension of the high temperature results to both a broader range of nozzle operating conditions and a detailed calibration of the nozzle flows. In Fig. 2, it can be seen that stagnation pressures were varied from 200 to 1000 torr and stagnation temperatures from 800 to 4000°K. Largely by trial and error, that combination of special assumptions and modifications to conventional nozzle flow calibration procedure was found which was necessitated by these operating conditions. These modifications included a vibrationally frozen flow model, indirect determination of stagnation temperature, large low density corrections to pitot and static pressures, and a non-Sutherland viscosity for nitrogen at temperatures below 80°K. A reasonably reliable calibration of the nozzle flows was finally obtained, and the low density performance of the BLC nozzle at high stagnation temperatures was evaluated. The preliminary conclusions of Ref. 2 which related to high temperature operation have been confirmed and extended, except for the beneficial effects of precooling of the boundary layer.

SECTION II
EXPERIMENTAL APPARATUS

The apparatus assembled for the experimental investigation of nozzle boundary-layer reduction by cryopumping included a vacuum chamber and vacuum pumps, a cryopump, an aerodynamic expansion nozzle, an arc heater, stilling chamber, a test section with impact pressure probes, and necessary instrumentation. Accessory and support equipment required for the adequate and safe storage and handling of liquid hydrogen was also installed.

2.1 VACUUM CHAMBER AND VACUUM PUMPS

The nozzle, test section, and cryopump were contained in a vacuum chamber whose inside diameter and length were approximately 3 and 9 ft, respectively. The chamber was fabricated of 3/8-in.-thick mild steel, and consisted of three separate sections whose O-ring-sealed flanges were joined with lever-action clamps. Each section had four legs with casters which rolled on floor-mounted rails for ease of movement and alignment. Several instrument feedthrough ports and Plexiglas®-covered viewing ports provided convenient physical and visual access to the lighted chamber interior. A side view incorporating a half cross section of the facility is shown in Fig. 3.

The chamber was connected by mild steel piping to a roughing pump-diffusion pump system. For initial chamber evacuation to 10^{-3} torr, a 1400-liter/min, two-stage rotary volumetric displacement pump was used, and to attain and hold the desired pretest vacuum of approximately 10^{-4} torr, a 1500-liter/sec oil diffusion pump (exhausted by the above mechanical pump) was employed. Vacuum valves in the pump lines allowed isolation of the chamber and pumps from each other as required for both proper operational procedures and necessary maintenance.

2.2 CRYOPUMP

During design of the low density nozzle, the predicted operating conditions included nitrogen test gas mass flows of up to 1.2 gm/sec, and nozzle exit static pressures of at most 5×10^{-3} torr. These figures, together with the desire to operate the nozzle in an underexpanded mode, indicated that the vacuum roughing and holding pumps described in Section 2.1 would have insufficient pumping capacity. To provide adequate pumping speed, the technique of cryopumping was selected, implemented by a liquid-hydrogen system operated in an open-cycle manner.

The cryopump was an annular right cylinder with open ends, whose axis was coincident with the axis of symmetry of both the nozzle and vacuum chamber (Figs. 3 and 4). It was fabricated of 304 stainless steel, and had outside and inside diameters of 16 and 15 in., respectively. Its 30-in. length defined a surface area of approximately 2970 $in.^2$ and an annular volume of 8 liters. To minimize the conductive parasitic heat load on the cryopump, it was mounted on three knife-edged supports 1 in. long.

When the cryopump was filled with liquid hydrogen and allowed to "soak" for a length of time sufficient to ensure thermal equilibrium, a cryopump surface temperature of approximately 20°K was established, well below the 63°K triple point of the nitrogen test gas. The pumping speed actually provided by the cold surface is determined from the following equation, whose key factor is the pressure in the vicinity of the cryopump for a given mass flow:

$$Q_p = \frac{\dot{m}}{\rho_p} = \frac{RT_p}{p_p} \dot{m} \tag{3}$$

For a specific case, in which $\dot{m}$ = 1.2 gm/sec, p_{o1} = 880 torr, and T_{o1} = 2000°K, p_p was held at 5 x 10^{-3} torr. Assuming a sufficient number of collisions of the gas molecules with the vacuum chamber wall to establish $T_p \approx 300°K$, the effective Q_p was 160,000 liters/sec, several orders of magnitude greater than the diffusion pump capacity.

2.3 CRYONOZZLE

The cryonozzle was of axisymmetric conical design, with an included expansion angle of 30 deg, a minimum section diameter of 0.150 in., and an exit plane diameter of 12 in. (Figs. 3 and 5). The nozzle was fabricated of 304 stainless steel.

The nozzle may be considered as two major subassemblies: the throat insert, and the cryojacketed segment (Fig. 6). The nozzle throat insert was comprised of the converging region, the minimum area station, or throat, and the initial 4 in. of the conical expansion. The cryojacketed segment included the remaining 19 in. of the nozzle expansion, which was of double-wall construction. The chamber, or jacket, formed by the double wall could be filled with a cryofluid, thereby converting the nozzle to a cryopump, or cryonozzle. The cryojacket was assembled as four separate but contiguous compartments, serviced by both a cryofluid input manifold and an evolved gas vent manifold. To achieve a desired pattern of nozzle cryopumping, the manifold connections to selected compartments could be broken and sealed.

During operation, the nozzle throat insert would receive a much greater heat flux than the cryojacketed segment, hence a cooling system independent of the cryojackets was used for it. There were three nozzle throat inserts available, each of which incorporated a different coolant passage design (Fig. 6). The first insert utilized copper tubing silver-soldered to its backside contour. Both water and liquid nitrogen could be used as the coolant for this insert. It had the least efficient nozzle cooling performance of the three, however, since the nonuniform tube-to-nozzle bond established poor thermal conductivity. The second insert had an integral coolant chamber, with machined blocks defining the coolant passages. While more efficient water cooling of the nozzle was realized, it was not possible to use liquid nitrogen with this insert, since its O-rings could not maintain the required vacuum seal when chilled to 77°K. A third insert was available, incorporating two separate chambers for bifluid cooling: water for the converging nozzle entrance and minimum area regions, and liquid nitrogen for the initial expansion region. If desired, water could be used in both chambers.

The nozzle throat inserts and their coolant chambers were thermally isolated from the cryojacketed segment of the nozzle by a properly contoured insulator of 0.5-in. axial thickness. The insulator was fabricated of a low thermal conductivity, heat resistant, nonmetallic material. The final inch of the nozzle contour was made of Plexiglas and contained a 0.2485-in.-diam static pressure orifice. A low thermal conductivity material was selected for this component to ensure that no cryopumping would occur into or around the orifice.

2.4 ARC HEATER – STILLING CHAMBER

Large values of nozzle reservoir stagnation enthalpy were obtained by passing the nitrogen test gas through a Gerdien-type dc arc heater (Fig. 7). The heater had a tungsten-tipped cathode and a copper anode, both water cooled. The gas was introduced upstream of the cathode-anode gap through an orifice which intersected the arc chamber tangentially. The ensuing swirling of the gas served to rotate the arc attachment point, reducing wear of the electrodes.

The arc heater power supply consisted of four 400-amp dc welding machines, connected in series so that a maximum power of approximately 60 kw was available - a continuous duty output of some 300 amp at about 50 v from each of the four machines.

The arc-heated gas issued from the anode exit into a stilling chamber which served as the nozzle reservoir. There were three stilling

chamber configurations, identified as A, B, and C, whose dimensions were:

Stilling Chamber Configuration	Length, in.	Diameter, in.
A	13	3.9
B	5	1.4
C	5	6.1

The various stilling chamber configurations permitted adjustment of reservoir stagnation temperatures within a wider range than by merely varying the current input to the arc heater. Stilling chamber A was constructed with a water-cooled copper pipe liner in which a cooling water flow rate could be adjusted to allow a range of stagnation temperatures from 800 to 1600°K. Chamber B was shorter and incorporated a length of radiation-cooled stainless steel or tungsten pipe as a liner which confined the arc, hence established much greater temperatures, viz from 2000 to 4000°K (Fig. 7). The C configuration was the same as B, except that there was no liner; hence, the stagnation temperatures spanned a middle range of from 1000 to 1900°K.

2.5 IMPACT PRESSURE PROBES

Stagnation pressures on the horizontal centerline of the nozzle exit plane were sampled by an impact probe rake which consisted of five separate probes, whose tip axes were mounted in the same plane, mutually parallel, and 0.75 in. apart (Fig. 8a). Each probe tip was machined on one end of a length of stainless steel tubing, as shown in Fig. 8b. The tubing terminated in a fitting to which an Alphatron® pressure measuring head was attached.

Rather than seal the pressure tubes individually as they penetrated the vacuum chamber wall, they were formed into a bundle and passed through a length of 1.25-in.-diam stainless steel tubing and silver-soldered to its inside wall. The chamber vacuum was then preserved by one O-ring shaft seal around the outside diameter of the large tubing. The rake could be positioned on the nozzle exit plane centerline by translation through the shaft seal fitting. A photograph of the installed rake is shown in Fig. 5.

2.6 FLOW ANGULARITY PROBE

Flow angles at the nozzle exit were measured with a null-type probe which consisted of a flat plate with a stagnation pressure probe

mounted on each side (Fig. 8c). The probe tips were finished like those illustrated in Fig. 8b.

For aligning the plate with the local flow velocity, a rotational degree of freedom was provided by mounting the plate on a pivot. Adjustment of the plate angle about its pivot was accomplished by gears, driven from outside the vacuum chamber by a flexible cable. A translational degree of freedom was available too, since the probe was mounted on a sliding tube similar to the rake system depicted in Fig. 8a. The correct alignment of the plate relative to the flow vector was assumed accomplished when the difference in stagnation pressures sensed on each side of the plate was nullified. The plate angle was read on a calibrated dial whose pointer was attached to the end of the flexible drive cable outside the vacuum chamber.

The probe described here was preferred over the more common fixed angularity probes because of the very large boundary-layer effects at the low Reynolds numbers expected in the cryonozzle test series. The null-type probe is not error free, however, especially in regions of stagnation pressure gradients; e. g., an exit plane gradient in p_{o2} creates a Δp_{o2} in the probe readings, even with zero flow angle. The probe used here had a spacing of only 0.2 in. between the axes of the stagnation probes on either side of the plate, which reduced the error attributable to pressure gradients to a small fraction of a degree for reasonably uniform core flows. In the region of strong p_{o2} gradients, e.g., in the boundary layer outside an isentropic core, errors of more than a degree were probable; therefore, flow-angle measurements with the null-type probe were restricted to the region of useful test cores.

2.7 INSTRUMENTATION

Briefly, the experiments discussed herein involved supplying nitrogen gas to an arc heater, whose efflux was then used as the reservoir supply for a hypersonic expansion nozzle. Measurements of the experimental parameters were made with appropriate instrumentation as discussed below.

The mass flow rate of the nitrogen test gas, up to 1.5 gm/sec, was measured with a tapered-tube rotameter. The pressure of the gas at the input of the rotameter was measured with a bellows-type absolute pressure gage.

The power input to the arc heater was determined by measuring the applied voltage and current with dc galvanometers of ±0.5-percent full-scale accuracy.

All pressure measurements required for aerodynamic description and calibration of the flow produced by the expansion nozzle, i. e., nozzle reservoir pressure, nozzle exit impact and static pressures, and vacuum chamber static pressures, were made with Model 520 Alphatron vacuum gages, manufactured by the NRC Equipment Corporation. For increased resolution in determining the values of pressures indicated by the Alphatrons, their output voltages were applied to the input of a millivolt indicator.

The NRC Equipment Corporation stated that the accuracy of the Alphatron was ±2 percent of full-scale for all decades from 1×10^{-3} to 1×10^{3} torr. At least once every six months, the sensing heads were disassembled, repaired if necessary, cleaned, reassembled, baked out under vacuum, and sealed at their joints with a low vapor pressure wax compound. Their indicated readings were then compared with a McLeod gage standard. Given this maintenance procedure, it is felt that the ±2-percent of full-scale error quoted by the manufacturer, together with a ±3-percent error of the reading being made, represents a conservative estimate of the data accuracy.

Quite often the Alphatrons were used to measure pressures of from 1×10^{-4} to 1×10^{-3} torr; e. g., the nozzle exit static pressures. Even though the manufacturer did not quote a specific accuracy for this model of the instrument for pressures in this range, it is felt that ±5 percent of full-scale of this span; i. e., $\pm 5 \times 10^{-5}$ torr, plus the ±3-percent reading error as above, is a conservative estimate of the data accuracy.

2.8 CRYOFLUID STORAGE

Consideration of test objectives, cryofluid requirements, and test area safety regulations determined that only a relatively small quantity of liquid hydrogen would be used during one test run. To serve within these restrictions, a portable dewar of 150-liter capacity was purchased and used for local storage immediately outside the test building.

SECTION III
TEST RESULTS

The primary goal of the study reported herein was the evaluation of the rarefaction performance of the BLC nozzle at high stagnation temperatures. This evaluation, of course, required the determination of flow properties at the nozzle exit for a large range of operating conditions.

The combination of high stagnation temperature, low stagnation pressure, and very low free-stream density was found to require several important modifications to the conventional nozzle calibration procedure. These modifications were verified by a comparison of two independent calibration calculations, one based on pitot pressure and one based on static pressure. Since entropy conservation was a common factor in each of these calculations, equality of results not only verified the modifications which had been made to each, but also identified the regimes of nozzle flow for which the entropy was constant between the reservoir and the nozzle exit. Only after this dual purpose had been served were extensive flow calibrations performed with the resulting validated calibration procedure.

3.1 VALIDATION OF FLOW CALIBRATION AND IDENTIFICATION OF ISENTROPIC FLOW REGIMES

In determining the ranges of operation of the nozzle for which there is isentropic flow, that flow regime characterized by merged boundary layers was first excluded by a simple inspection of the pitot pressure profiles. It proved to be a simple matter to locate the apparent edge of the boundary layer from such profiles, even when the cores were not uniform. Having thus restricted attention to flows with some area of lateral isentropy, the reservoir conditions which also produced longitudinal or streamwise isentropy were next sought. They were determined by comparing Mach number based on pitot pressure at the edge of the core, $M(p_{o2}/p_{o1})_e$, and Mach number based on wall static pressure, $M(p_{1_w}/p_{o1})$. Equality of these two Mach numbers is generally accepted as evidence of isentropic flow from the reservoir to the point of pitot pressure measurement. Conversely, divergence of these two Mach numbers, beyond the experimental scatter, is regarded as evidence of the occurrence of some nonisentropic process in the flow. (The use of Mach number for this comparison is purely a matter of convenience. Any one of a number of thermodynamic variables would serve the same purpose.)

In Ref. 2 this procedure was followed for room stagnation temperature nitrogen, and it was found that only two modifications to conventional wind tunnel practice were required to establish a valid flow calibration, namely, an adjustment of measured pitot pressure for a low Reynolds number effect and the use of a non-Sutherland viscosity at very low temperatures. In addition, however, the high stagnation temperatures used in the present investigation necessitated three more modifications, so that the complete list of required modifications to the flow calibration became:

a. Indirect Stagnation Temperature Determination

A sonic flow method was used to determine T_{o1}, as described in Appendix I. This calculation included a correction for the throat boundary layer and an assumed freezing of vibrational energy mode.

b. Flow Model

It is shown in Appendix II that the reservoir pressures used in the BLC nozzle were low enough to justify the assumption of complete freezing of the vibrational mode of excitation of the molecular nitrogen. Also, reservoir temperatures were low enough to allow neglecting dissociation. Rotational excitation was assumed to remain in equilibrium with the translational motion of the molecules, thereby allowing use of the familiar $\gamma = 1.4$ isentropic flow tables in the flow calibration.

c. Low Reynolds Number Correction to Pitot Pressure

The measured pitot pressure was corrected for a low Reynolds number effect by using data of Ref. 7 as described in Appendix III.

d. Low Density Correction to Static Pressure

The pressure sensed in the wall static pressure orifice was corrected for the effect of heat transfer to the wall at low densities by use of the data given in Ref. 8, described in Appendix III. In many cases, this correction amounted to over 100 percent of the measured pressure level.

e. Low Temperature Viscosity

For static temperatures below 80°K, the viscosities used in calculating the pressure corrections were obtained by an extension of the calculated viscosities of Ref. 9, using collision integrals for the Lennard-Jones (6-12) intermolecular potential and appropriate constants for nitrogen, as discussed in Appendix IV. The difference between this viscosity and a Sutherland-formula extrapolation to low temperatures is quite large.

3.1.1 Natural Boundary Layer on Nozzle Wall

The nozzle reservoir conditions which resulted in merged boundary layers with no suction, as determined by inspection of pitot pressure profiles, are indicated by the "merge" line in Fig. 2. Thus, the search for isentropic flow conditions was immediately restricted to reservoir

conditions falling below this limit curve. As was also found in Ref. 2, the core nonuniformities were such that the Mach number based on pitot pressure was selected at the edge of the boundary layer, $M(p_{o_2}/p_{o_1})_e$, for comparison with $M(p_{1_w}/p_{o_1})$. Of course, there is a further assumption implied here that there is negligible variation of static pressure within the boundary layer in a direction perpendicular to the flow. A typical comparison of these two Mach numbers is given in Fig. 9 for data obtained with a minimum arc-heater power and stilling chamber configuration B. These data do not form smooth curves because fluctuations in arc-heater performance did not permit operation on repeatable smooth trajectories in the p_{o_1}, T_{o_1} plane. However, there can clearly be seen an agreement of these Mach numbers (within experimental scatter) for $p_{o_1} > 520$ torr and a rapid divergence below this pressure. The location of this divergence was found to correlate closely with the boundary-layer merge point at $p_{o_1} = 520$ torr and $T_{o_1} = 2900°K$, Fig. 2. Thus, for $p_{o_1} < 520$ torr, the flow is nonisentropic and for $p_{o_1} > 520$ torr, the flow is isentropic from the nozzle reservoir to all points of the core at the exit of the nozzle. The solid points at $p_{o_1} = 612$ torr give an indication of the magnitude of the low density corrections to the flow calibration.

Since it was not possible to operate on smooth trajectories in the p_{o_1}, T_{o_1} plane, the final evaluation of the Mach number difference was made without regard to the reservoir condition. In Fig. 10, the frequency distribution of

$$\Delta M = M\left(\frac{p_{1_w}}{p_{o_1}}\right) - M\left(\frac{p_{o_2}}{p_{o_1}}\right)_e \tag{4}$$

is given for 36 runs without suction and without regard to reservoir conditions, except that all points are below the merge line of Fig. 2. It is seen that an approximation to a normal frequency distribution was obtained with a mean value of $\overline{\Delta M} = 0.2$, roughly 2 percent of the Mach number level. The mean width of this distribution about $\Delta M = 0.2$, a measure of the experimental scatter, is 0.3 of a Mach number. Within the small systematic difference of 0.2 of a Mach number, Fig. 10 is regarded both as evidence of isentropic nozzle flow below the merge line and as a validation of the flow calibration procedure represented by the five special assumptions listed in Section 3.1 above.

It is noted that these assumptions are interrelated to an appreciable degree. If any one of them were omitted or took a different form (as was the case during formulation of the proper combination), the Mach number agreement would suffer. For example, the ΔM frequency distribution obtained when the low density corrections to p_{o_2} and p_{1_w}

are not made is given as the dashed curve of Fig. 10. The spread of the distribution is increased by a factor of two and the mean value is $\overline{\Delta M} = 0.87$. By an approximate analysis it was found that use of an equilibrium, rather than frozen, flow model would give $\overline{\Delta M} \cong -0.6$, and the use of a Sutherland viscosity law would give $\overline{\Delta M} \cong +0.65$. In view of the different signs on these $\overline{\Delta M}$ values, it is clear that there could exist more than one combination of assumptions concerning the nozzle flow which would yield an apparent equality of $M(p_{o2}/p_{o1})_e$ and $M(p_{1_w}/p_{o1})$. It is important to the validation process, then, that the particular combination of assumptions represented by (a) through (e) in Section 3.1, above, not only gave $\Delta M \approx 0$, but also formed the most likely combination based on subsequent evaluation of the flow process in the nozzle.

3.1.2 Cryogenic Suction on the Nozzle Wall

Although the flow calibration procedure was considered well verified for nozzle flows with no suction, additional verification was considered necessary when cryogenic suction was applied to the nozzle walls, because of the unknown effect of the drastic change in the wall boundary condition. Furthermore, there were a number of reasons for expecting greater difficulty in obtaining this verification:

a. The absolute magnitude of the static pressure at the nozzle exit was reduced to 1×10^{-3} torr and below. Further, because of the low density orifice effect, the pressures actually sensed by the Alphatron pressure gage were even less (5×10^{-4} torr and lower). In this range the decreasing accuracy of the Alphatron gage begins to dominate any flow calibration.

b. Sporadic fluctuations in the nozzle cryopumping speed would require that test data be sorted for runs in which a maximum pumping speed was continuously effective. Otherwise, the differing time responses of the pitot and static pressure measuring systems would automatically introduce Mach number divergences.

c. There was an uncertainty about the boundary condition at the wall in the vicinity of the static pressure orifice which affected the low density correction to static pressure. The heat-transfer calculation was based on a zero-slip boundary-layer approximation, even though the indicated mean free path at the wall temperature of 300°K at this location was of the order of 6 cm or more. This was justified by the fact that the mean free path at the end of the cryopumping section, only 1/2-in. upstream of the orifice centerline, was much lower - on the order of 0.4 cm and less.

d. It was necessary to define a useful "core" of the flow, arbitrarily taken to be that portion of the nozzle flow around the centerline within which there was a variation of pitot pressure of no more than ±5 percent. This was necessitated by the fact that the pitot pressure profiles with suction (Fig. 18) did not exhibit a well-defined boundary between the relatively flat distribution around the centerline and the regions of large gradients of pitot pressure near the wall. The average Mach number variation in the "core" was 0.35. Thus the Mach number based on pitot pressure at the edge of the core was taken to be

$$M\left(p_{o_2}/p_{o_1}\right)_e = M\left(p_{o_2}/p_{o_1}\right)_{\mathbb{Q}} + 0.35 \qquad (5)$$

Except for the above qualifications, the Mach number comparison with suction was made in the same general way as described in Section 3.1.1 for flows with no suction. Plots similar to Fig. 9, but with BLC active, exhibited an almost identical behavior, with an unexpected Mach number divergence in the low density direction. The relative flatness of all the pitot pressure profiles with suction appeared to eliminate the possibility of transverse entropy gradients of the type generated by regions of strong shear in the flow. It was decided, then, that this divergence was the result of some nonisentropic process occurring somewhere upstream in the nozzle.

Attempts to link the onset of this Mach number divergence to various physical flow parameters revealed that the static density in the flow provided the best correlation. Figure 11 presents the parameter ΔM, defined by Eqs. (4) and (5), plotted versus the static density computed from the $M(p_{o2}/p_{o1})$ calibration. The Mach number divergence appears to begin at approximately $\rho_1 = 1.7 \times 10^{-8}$ gm/cm^3 for a large range of reservoir pressure and temperature. Above this limiting density there seems to be a reasonable approximation to isentropic flow, as shown by the ΔM frequency plot, Fig. 12. Again, a curve similar to a normal frequency distribution is observed, with a mean value of $\overline{\Delta M} = 0.06$. The fact that the mean value of this distribution is closer to zero than for the no suction case is fortuitous, since there are many additional sources of uncertainty when operating with suction. The ΔM distribution when the low density corrections are not applied to the pitot and static pressures is indicated by the dashed curve of Fig. 12. These corrections are seen to be relatively more important than for the flow with no suction.

The data of Figs. 11 and 12 were interpreted as a validation of the flow calibration when operating with cryogenic suction and with a static

density at the nozzle exit no lower than 1.7×10^{-8} gm/cm^3. For expansions to lower densities, the test data gave indication of an apparent entropy generating process somewhere in the nozzle upstream of the exit. Possible sources of this entropy generation are discussed in Section IV.

3.2 CALIBRATED FLOW PROPERTIES AT THE NOZZLE EXIT

Following the validated flow calibration procedure and using $M(p_{o2}/p_{o1})_{\mathbb{C}}$ as an independent variable, the usual flow variables of interest at the nozzle exit were computed as a function of nozzle reservoir pressure and temperature. For convenience in performing a systematic set of calculations, faired curves of constant $M(p_{o2}/p_{o1})_{\mathbb{C}}$ on the p_{o1}, T_{o1} plane were used rather than discrete calibrated values of Mach number at specific p_{o1} and T_{o1}. Differences between the individual experimental values and the faired curves were small as can be seen in Fig. 13. This curve expresses the distribution of experimental Mach number data about the faired curves and should not be confused with the ΔM frequency distributions of Figs. 10 and 12 which were used in validating the calibration. Both with and without suction, the mean of absolute values of deviations from the faired curves is approximately 0.15 of a Mach number.

3.2.1 No Suction

Figure 14a gives the faired Mach number curves versus p_{o1} and T_{o1} with no suction. Also given on the same plot are the static pressure and static temperature at the nozzle exit, as computed from the faired Mach numbers. The Mach number curves are repeated in Fig. 14b, together with curves of unit Reynolds number at the nozzle exit. Figure 14c gives the nozzle exit Knudsen number for a 1-cm length. It should be noted that these data are presented only within the merge limit and above the heater minimum power curve. Experimental deviations from each of these sets of curves would correspond to the Mach number deviations of Fig. 13.

3.2.2 With Suction

Figures 15a, b, and c present the same flow calibration data of Mach number, pressure, temperature, unit Reynolds number, and Knudsen number for flows with suction on the nozzle walls as were given in Figs. 14a, b, and c for the no-suction case. There are two qualifications to be noted with respect to these curves. First, there has been

observed a variation of the flow calibration with time when using cryogenic BLC. For the reason discussed in Section 4.2.2, there is a steady decrease of the Mach number with time, as shown in Fig. 16. Since interest centers on the most highly rarefied conditions, the data of Figs. 15a, b, and c are for the first 5 min of operation of runs with suction.

The second qualification concerns the validity of the calibration for flows expanded below a free-stream density of 1.7×10^{-8} gm/cm^3. The values of p_{o1} and T_{o1} which give this value of density at the nozzle exit are indicated by dashed lines of Figs. 15a, b, and c. For reservoir conditions below these lines, the flow calibrations are on a reasonably secure foundation as described in Section 3.1.2. Above this line, there is a progressive uncertainty in the calibrations because of increasing suspicion of nonisentropic flow.

3.3 SPATIAL VARIATION OF FLOW AT EXIT OF NOZZLE

3.3.1 Pitot Pressure Profiles

Pitot pressure profiles at the nozzle exit with natural boundary layer and T_{o1} = 300°K were given in Fig. 4 of Ref. 2, and are reproduced here as Fig. 17a. Except for the distribution at p_{o1} = 730 torr, these profiles exhibit a large but nonuniform core at high p_{o1}, smaller and more uniform cores at lower p_{o1}, and finally, a fully merged profile at p_{o1} = 45 torr. The pitot pressure profiles for elevated stagnation temperature and no suction show a similar progression of characteristic shapes when arranged in groups having reservoir conditions lying on a relatively smooth curve of approximately constant power in the p_{o1}, T_{o1} plane, Figs. 17b, c, and d. It was concluded in Ref. 2 that the nonuniform cores at high p_{o1} are the result of nonlinear contouring of the nozzle by the boundary-layer displacement thickness. The magnitude of nonuniformity in some cases is as large as 25 percent of the pitot pressure level in the core, e.g., the profile for p_{o1} = 643 torr, T_{o1} = 990°K in Fig. 17b.

When cryogenic suction is applied to the nozzle walls the mean level of the pitot pressure ratio is reduced, and the profiles become relatively flat around the centerline of the nozzle. There is also remarkably little variation in shape of the profiles for a large range of reservoir conditions. A selection of pitot pressure profiles with suction is given in Figs. 18a through f, each compared with a corresponding profile with no suction. Figure 18a presents a comparison of a merged profile with no suction and a relatively flat profile obtained with suction at a fairly low stagnation temperature. In Fig. 18b, a nearly merged

profile obtained with no suction is compared with two suction profiles obtained at virtually the same reservoir conditions but with different modes of operation. The flatter profile was obtained with the nozzle wall upstream of the cryopumping section cooled with liquid nitrogen. This mode of operation, which produces a precooled boundary layer, is discussed in Section 3.4.1. The less flat profile was produced by the normal mode of operation with suction, i.e., with water-cooled nozzle walls upstream of the cryopumping section. This profile is typical of a large number of suction profiles. In comparison with the suction profile of Fig. 18a, it exhibits a more definite contrast between the uniform central core and the region of large pitot pressure gradient in the shear flow surrounding the central core. These suction profiles also exhibited a gradual variation with time, as previously noted in Section 3.2.2. This is shown in Fig. 18c, where six profiles with suction obtained during a long run are compared with a no-suction profile having a 2-in.-diam core with a 9-percent nonuniformity. These are the profiles on which the Mach number variation of Fig. 16 is based. A comparison of a merged no-suction profile and the corresponding suction profile obtained at $T_{o1} \cong 1800°K$ with stilling chamber configuration C is given in Fig. 18d. The comparison is made in Fig. 18e at $T_{o1} \cong 1550°K$ for a no-suction profile with a 2.1-in. core diameter. A higher temperature comparison obtained with stilling chamber configuration B is presented in Fig. 18f. Here, a merged, no-suction profile is compared with a suction profile at $T_{o1} \cong 2500$ to $2800°K$.

It is noted that all of the pitot pressure profiles presented in Figs. 17 and 18 are given in terms of uncorrected pressures. True pitot pressure profiles would require the application to p_{o2} of the low density correction described in Appendix III. The major effect of making this correction would be a downward displacement of the profiles, although small changes in shape would also result, since the correction would vary with radial position in the nozzle.

3.3.2 Useful Core Sizes

The isentropic core diameters obtained with no suction were determined by simple inspection of the pitot pressure profiles and are presented as functions of p_{o1} and T_{o1} in Fig. 19. These curves represent fairings of experimental data similar to the constant Mach number fairings of Fig. 14, as discussed in Section 3.2. A majority of the experimental data agrees with these curves to within 0.1 and 0.2 in., but a few points diverge by as much as 0.5 in. The merge line ($D_{core} = 0$) was established not only by reference to the pitot pressure profiles, but also by reference to ΔM plots similar to Fig. 9.

With suction on the nozzle walls, determining a core diameter was not as straightforward as with no suction because of the lack of a sharply defined boundary between the regions of relatively uniform flow near the nozzle centerline and the region of strong shear flow near the wall. As discussed in Section 3.1.2, a "useful" core diameter has been defined as that within which there is no more than a ±5-percent variation of pitot pressure. Curves of core diameters thus defined for the suction case are given in Fig. 20. Possibly because of the arbitrary definition of core size and possibly because of the time-dependency experienced with suction, experimental deviations from these curves were greater than from the corresponding curves with no suction. Most of the deviations were less than 0.5 in., but a few isolated cases were found which deviate from these curves by as much as 0.9 in., e.g., the profile of Fig. 18a. Thus, although appreciable experimental scatter about the core diameter curves of Fig. 20 exists, these curves do represent a consistent map from which logical conclusions concerning the rarefaction performance of the BLC nozzle can be made.

3.3.3 Flow Angularity

Flow angles for T_{o1} = 300°K were measured at the nozzle exit with the null-type flow angle probe described in Section 2.6. With no suction these angles are all less than source flow angles because of the effective contouring of the nozzle wall by the boundary layer, Fig. 21. The boundaries of the useful test cores are indicated by terminal bars on the curves. Since the displacement of the boundary layer is decreased at high reservoir pressure, the maximum flow angles vary directly with p_{o1}.

The effect of nozzle wall suction is a general increase in flow angles, Fig. 22. For the lower range of reservoir pressure, below p_{o1} = 76 torr, flow angles with suction vary inversely with p_{o1}. This is consistent with other evidences of an inverse dependence of capture coefficient on density discussed in Section 4.2.2. For higher p_{o1} with suction, however, the flow angles appear to increase with p_{o1}. It is perhaps significant that this occurs in the approximate range of p_{o1} in which wall suction decreases rather than increases the useful core size.

No flow angles were measured at elevated stagnation temperatures, but it is considered likely that such data would be similar to those of Figs. 21 and 22.

3.4 SUPPLEMENTARY EXPERIMENTAL DATA

3.4.1 Performance of Nozzle with Precooling of Boundary Layer

A single observation of core size obtained by cooling the nozzle throat insert with liquid nitrogen was given in Fig. 8 of Ref. 2. Such a mode of operation appeared to offer a significant increase in core size over the normal mode of operation with suction, which incorporated a water-cooled throat insert. A typical pitot pressure profile obtained with liquid nitrogen as the throat coolant is given in Fig. 18b. It is clear that precooling of boundary layer to near-liquid-nitrogen temperature produced a large increase in pumping speed of the nozzle walls and a flatter test core. However, this flow characteristic proved very difficult to maintain because of repeated and frequent formation of gaseous nitrogen in the cooling coils of throat insert No. 1. As noted, the precooled profile of Fig. 18b was obtained prior to 50 sec after start of flow. At this instant, a vapor lock in the cooling coils immediately restored the pitot pressure profile to a normal-mode profile.

This problem of gasification of liquid nitrogen in the cooling coils was obviously the result of imposing too high a heat load on the coolant. Throat insert No. 3 was designed specifically to alleviate this gasification problem by subjecting the liquid nitrogen to only the relatively low heat-transfer rates downstream of the throat, while retaining water cooling for the high heat-transfer areas at the throat and upstream of the throat. Subsequent operation of the BLC nozzle with throat insert No. 3 demonstrated that this separation of regions of high and low heat-transfer rates did, in fact, allow operation with liquid nitrogen precooling and no gasification problem. However, the reduction in heat load to the liquid-nitrogen coolant defeated its own purpose, since then there appeared to be insufficient precooling of the boundary layer. In fact, pitot pressure profiles obtained with throat insert No. 3 and its reduced precooling were hardly distinguishable from those which resulted from use of the regular throat insert No. 2 with water cooling alone.

It was concluded that the very real benefits of precooling could only be obtained by cooling the entire throat insert with liquid nitrogen. This could be accomplished with a high pressure liquid-nitrogen coolant system, which would allow increased flow rates of the coolant without gasification.

3.4.2 Nozzle Back Pressure

For most runs, static pressures were measured outside of the free jet at the nozzle exit and also in the vacuum chamber around the cryopump. Under all conditions of operation of the BLC nozzle, the static pressure outside the nozzle exit was found to be less than the nozzle exit static pressure measured at the wall orifice. Thus, both with and without suction, the nozzle flow was slightly underexpanded, requiring an expansion on the free jet flowing out of the nozzle.

In contrast, the static pressure at the cryopump was observed to vary over wide limits relative to the nozzle exit static pressure. For operating conditions involving very low mass flows, the pumping capacity of the cryopump was so large relative to the throughput of the nozzle that pressures at the cryopump as low as 1 percent (1×10^{-5} torr) of the nozzle static pressure were observed. In such cases, the flow underwent continuous expansion from the nozzle exit to the cryopumping surfaces. As the nozzle mass flow was increased, higher pressures at the cryopump were observed, because of accommodation to the increased throughput. In the most extreme case, the static pressure at the cryopump was observed to exceed the nozzle static pressure by a factor of two, indicating a definite recovery in the free jet between the nozzle and cryopump.

SECTION IV
DISCUSSION

4.1 RAREFACTION PERFORMANCE OF CRYONOZZLE

4.1.1 Knudsen Number and Core Size Comparison

The purpose of the BLC nozzle is to produce a low density flow with boundary-layer effects reduced, hence providing as large a uniform test core as possible. The use of wall suction did increase the core size for most of the operating range shown in Figs. 19 and 20. There are some reservoir conditions, however, for which the suction produces a smaller useful core diameter. These are the p_{o1} and T_{o1} points lying to the right of the equal core size curve in Fig. 20. This cannot be considered an adverse effect, however, because the flow conditions are also more rarefied, as can be seen by reference to Figs. 14 and 15.

A legitimate comparison of the nozzle performance with and without suction should include both the core diameter and the corresponding

degree of rarefaction attained. Such a comparison is made in Fig. 23, where the degree of rarefaction, expressed as the Knudsen number at the nozzle exit for a 1-cm characteristic length, is plotted versus the useful core diameter for constant stagnation temperatures. Note that, by definition, the ordinate is numerically equal to the mean free path in centimeters. The curves for T_{o1} = 300°K are identical to those given in Ref. 2. The data of Fig. 23 are the main results of the study of the cryogenically pumped BLC nozzle, and except for small sections of the curves, a universal improvement is shown in the rarefaction performance when suction is employed. The no-suction curves exhibit the usual boundary-layer effect at low density, a decreasing core size as rarefaction is increased. With cryogenic suction the trend is in the opposite direction, an increasing core size as rarefaction is increased. This implies that the capture coefficient of molecules striking the cryopumping surfaces of the nozzle increases with decreasing density. The reversal of the Mach number gradient in the p_{o1}, T_{o1} plane shown in Figs. 14 and 15 is further evidence of the same phenomenon.

The improvement in rarefaction performance resulting from the use of the suction technique is simply the increase in Kn_{cm} for a given stagnation temperature and core diameter. For T_{o1} = 300°K, D_{core} = 4.3 in., the increase in Kn_{cm} from 0.024 with no suction to 1.75 with suction represents an improvement of nearly two orders of magnitude. Although this was the maximum performance increment experimentally observed, it by no means represents an inherent limit. On the contrary, since the suction curves were terminated at their upper ends only by arbitrary considerations of experimental convenience, it is probable that further improvement in rarefaction could easily be obtained simply by operating the nozzle at lower densities. This is also the case for the higher stagnation temperatures, where the maximum rarefaction increase observed experimentally was approximately a single order of magnitude at all values of T_{o1}. Since the suction and no-suction curves for T_{o1} > 300°K appear to diverge as rapidly as do those at T_{o1} = 300°K, it is considered probable that this order-of-magnitude increase could easily be extended to the two orders of magnitude actually observed with room temperature nitrogen.

4.1.2 Effect of Irreversibility at Low Densities

The indicated irreversibility for reservoir conditions giving $\rho_1 < 1.7 \times 10^{-8}$ gm/cm^3 extends an uncertainty in flow calibration to roughly the upper half of each of the suction curves of Fig. 23. Unfortunately, these are the more important halves of these curves. This uncertainty is quite large for some of the flow variables, but for the static density it is less than 10 percent, as discussed in Section 4.3.

Since the Knudsen number is primarily determined by the density, and D_{core} values are directly measured, then it is true that the curves of Kn_{cm} versus D_{core} with suction are not greatly affected by the onset of the nonisentropic process.

4.1.3 Comparison with a Porous-Wall Nozzle

The results of an investigation of BLC in a supersonic nozzle incorporating suction through a porous wall section were reported in Ref. 6. This nozzle had a 1-ft exit diameter, an expansion half-angle of 13 deg, and a geometric Mach number of 12.9. It was thus quite similar to the AEDC cryonozzle in general aerodynamic configuration. The porous section of the nozzle began at a geometric Mach number of 5.9 with a linear variation of porosity ranging from 0 percent at that station to 40 percent at the nozzle exit.

The measured increases in core size and Mach number produced by the suction through the porous wall compared very favorably with an integral-type boundary-layer calculation incorporating a suction velocity at the wall. However, the rarefaction performance of the nozzle was poor when evaluated in terms of the Kn_{cm} parameter for a given core diameter, as was done in Fig. 23 for the AEDC cryonozzle. The maximum Kn_{cm} obtained was only 0.24 and the maximum increase of Kn_{cm} produced by the suction through the porous wall was only a factor of 1.5, compared to factors of from 10 to 100 shown in Fig. 23 for the cryonozzle.

The explanation for this marked difference in performance of these two nozzles lies in two inherent characteristics of the porous-wall nozzle. First, for structural reasons the average porosity is low (about 20 percent), which limits the percent of ideal free-molecule suction flow that can be attained. Second, the pressure drop in the suction passages further reduces the suction flow by a factor of from 2 to 3, so that the effective suction area is only from 7 to 10 percent of the nozzle surface area. In the cryonozzle, the effective suction area is given by the capture coefficient which, as discussed in Section 4.2.2, apparently ranges from 45 to 90 percent for the conditions tested.

4.2 COMPARISON OF NOZZLE PERFORMANCE WITH THEORY

4.2.1 Natural Boundary Layer

The feasibility of predicting boundary-layer thicknesses within a 15-percent accuracy in low density hypersonic nozzles by use of simple

flat plate theory was discussed in Ref. 2. The feasibility of this method, of course, results from the fact that the velocity gradient over the greatest part of the diverging section of a hypersonic nozzle is negligible. In Fig. 24, experimental values of boundary-layer thickness for the no-suction case, taken from Fig. 19, are compared with calculated values based on the Van Driest flat plate solutions of Ref. 1. The agreement between the two values is exceptional for the adiabatic wall case (T_{o1} = 300°K). For nonadiabatic cases (T_{o1} > 300°K, T_w = 300°K), the agreement is not as good, although in all cases it is within the ±15-percent limits referred to in Ref. 2.

Note that the theoretical and experimental comparison of Fig. 24 is more comprehensive than the simple comparison of the $\delta/L\sqrt{Re_L}$ parameter at known Mach number, as was given in Ref. 2. In the present case, the Mach number itself is part of the theoretical solution by virtue of the displacement thickness correction to the geometric nozzle area ratio. Values of the ratio δ^*/δ were obtained by integrating the Van Driest velocity and temperature profiles. An approximate axisymmetric correction to δ^*/δ was also included. The nozzle exit Mach numbers predicted by the δ^* calculation are compared with calibrated values of Mach number in Fig. 25. Again, the agreement is exceptional for the adiabatic wall case, but only mediocre for cases with heat transfer. In the worst case, the displacement thickness effect on the nozzle Mach number is overestimated by 1.3 Mach numbers.

A comparison of theoretical and experimental boundary-layer thicknesses in a form which does not include the displacement thickness effect is made in Fig. 26. (A similar comparison is made in Ref. 2.) Here, the dimensionless parameter $\delta/L\sqrt{Re_L}$ is normalized by the theoretical Van Driest value and plotted versus Re_L, using calibrated Mach numbers to determine the Reynolds numbers. High stagnation temperature data for the BLC nozzle with no suction are presented, as well as data for T_{o1} = 300°K. (Four points are also given for the porous wall nozzle of Ref. 6 for cases where the suction flow is zero.) There appears to be a small downward shift of these data compared to the correlation given in Ref. 2 for ten different low density nozzles. The correlation of experimental with theoretical values of $\delta/L\sqrt{Re_L}$ is 0.94 ±11.5 percent for all the BLC nozzle data, regardless of whether the boundary layer is adiabatic or not. This implies that the observed effect of heat transfer on the correlations of Figs. 24 and 25 results from some inadequacy of the calculation of the displacement effect, since this calculation has no bearing on the correlation of Fig. 26.

4.2.2 With Suction

A theoretical boundary-layer analysis was developed in Ref. 10 for nozzle flows with cryogenic suction applied to the walls. This was an asymptotic solution which used both an assumed independence of the streamwise coordinate and a y-momentum equation to allow for large suction rates. The suction rate used in this theory was obtained from the free-molecule pumping speed equation

$$\frac{Q}{A} = C\sqrt{\frac{RT_g}{2\pi}} \tag{6}$$

The initial application of this analysis to the flow in the BLC nozzle revealed, by comparison with test data, that the average capture coefficients in the nozzle flow were appreciably less than those observed for nitrogen in static test chambers, Ref. 11. Whereas capture coefficients in static test chambers were independent of density, and had values of $C \approx 0.9$, the average capture coefficients inferred from the theoretical calculations and the test data reported herein varied from $C = 0.36$ at the highest density to $C = 0.90$ at the lowest density in the nozzle expansions.

In Fig. 27 a calculated Mach number distribution is given for the BLC nozzle at $p_{o1} = 422$ torr and $T_{o1} = 1160°K$, Ref. 10. The average capture coefficient has been arbitrarily adjusted to $C = 0.45$ to give a good agreement with the calibrated exit Mach number. The value of the theoretical solution lies in the information it provides concerning the distribution of Mach number in the nozzle, even though the magnitude of the Mach number depends upon an empirical selection of the capture coefficient. The result of an approximate calculation based on the flat plate boundary layer with no suction is also given in Fig. 27. This approximation merely requires that mass be conserved under the combined effect of the boundary-layer displacement and the mass flux to the wall given by Eq. (6). Although this is a very crude approximation, it is noted that the Mach number distribution supports that of Ref. 10.

The distribution of mass flux to the wall obtained in Ref. 10 is given in Fig. 28. An order-of-magnitude difference exists between the beginning and end of the cryopumping section. For a typical run of 30 min, the curve of Fig. 28 would indicate a condensate-layer thickness of 0.21 in. at the beginning of the cryojacket and 0.012 in. at the exit of the cryojacket. Actual measurements of cryodeposit thickness were not made, but these values are entirely consistent with visual observations of the frost layers. It is of interest that an integration of

the curve of Fig. 28 yields a cryopumped fraction of 22 percent of the total mass flow through the nozzle throat.

The density dependence of the average capture coefficient is simply another expression of both the increase in core size with increasing Kn_{cm}, Fig. 23, and the reversal of Mach number gradient in the p_{o1}, T_{o1} plane when operating with suction, Fig. 15. It would be extremely difficult to infer detailed information on local values of the capture coefficient from nozzle test data because the pumping speed of Eq. (6) is strictly valid only in the free-molecule regime. Even in the most highly rarefied case, the flow at the nozzle exit is in the transitional regime with respect to the nozzle dimension, whereas at the upstream end of the cryopumping section, continuum conditions prevail. The simple dependence of pumping speed on $\sqrt{T_g}$ is maintained throughout the transition from the free-molecule to the continuum regime, but the limiting value (for C = 1.0) increases by a factor of approximately three. Thus, the actual pumping speed along the nozzle should be represented by Eq. (6) modified by another factor, varying from 1.0 to 3.0, to express the dependence on the local Knudsen number.

It is possible, however, to use the known behavior of local capture coefficients in static test chambers to explain the variation with time of Mach number at constant reservoir conditions when using suction, Fig. 16. In Ref. 11 it is shown that, with other variables held constant, the local capture coefficient decreases as the temperature of the condensate surface increases. For a constant reservoir condition and an essentially constant heat load transmitted across the frost layer, the surface temperature of the condensate will increase with time as the thickness of the layer increases, according to the quasi-steady heat conduction equation. This increasing surface temperature yields a decreasing capture coefficient all along the nozzle and a consequent slow decrease in Mach number with time, Fig. 16. The simple dependence of Mach number on the condensate-layer thickness has been convincingly demonstrated by interrupting the nozzle flow for varying lengths of time while maintaining the liquid-hydrogen flow. Upon resumption of mass flow through the nozzle, the exit Mach number was observed to return to the value existing at the moment of interruption of the flow.

4.3 SOURCE OF IRREVERSIBILITY AT VERY LOW DENSITY

A number of possible explanations have been considered for the apparent onset of irreversibility in the nozzle expansions with suction for free-stream densities less than 1.7×10^{-8} gm/cm^3. The source of

this irreversibility must have a low density threshold and must increase in severity as this threshold is exceeded. This immediately eliminates as a possible explanation the liquefaction of the flowing nitrogen for the simple reason that it would be characterized by a high density threshold. Also, the saturation temperature for nitrogen in the pressure range of interest here is from 32 to 36°K, so that there is only a very small portion of the operating range of the BLC nozzle for which supersaturated conditions are indicated (Fig. 15a).

Inaccuracies in the low density corrections to the pitot and static pressures could conceivably create an indicated or apparent increase in entropy. However, the corrections were verified in the no-suction calibrations for conditions producing up to a 15-percent correction in p_{o2} and up to a 40-percent correction in p_1. It does not seem likely that above this established level there would be a change in the character of these corrections sufficiently sudden to explain the rapid divergence of $M(p_{o2}/p_{o1})_e$ and $M(p_{1_w}/p_{o1})$ shown in Fig. 11.

Consideration has been given to the possibility of attenuation of the pitot pressure by invasion of the free jet by background molecules from the region around the jet. Such a phenomenon has been observed in molecular beam facilities, Ref. 12. However, data presented in Ref. 12 indicate that the background pressures normally found in the test section (from 0.001 to 0.002 torr) are not high enough to generate any large attentuation of p_{o2}.

Another phenomenon which could explain the low density irreversibility, and which has only recently become of interest in nozzle flows, is that of rotational nonequilibrium. Rotational relaxation times for nitrogen are many orders of magnitude shorter than vibrational relaxation times (1.4×10^{-9} sec compared to 8.0×10^{-3} sec at atmospheric conditions) so that in most cases a very good assumption is that the rotational states remain in equilibrium in all parts of a flowing gas. However, the rotational relaxation times are inversely proportional to the pressure, and in highly rarefied expansions it is recognized that departure from rotational equilibrium is possible, Ref. 13. The rotational relaxation times are not known for the very low static temperatures attained in the BLC nozzle expansions, but a calculation based on room temperature collision numbers for rotational adjustment, Ref. 13, predicts rotational freezing in the BLC nozzle for reservoir conditions which are well within an order of magnitude of those for which the pressure calibration of the nozzle indicates the irreversibility.

It is considered at this time that rotational nonequilibrium is the most likely source of the irreversibility. If this is the case, then it is the same type of phenomenon as chemical or vibrational freezing, for

which it is known that the density and velocity in the flow are little affected (usually less than 10 percent). However, for the other parameters of interest in the flow, i. e., the pressure, temperature, and Mach number, departure from equilibrium can produce changes of from 70 to 80 percent.

SECTION V
CONCLUSIONS

The following conclusions are drawn from the results of a study of the flow in a hypersonic nozzle operated at low densities and high stagnation enthalpy levels with both natural and controlled boundary layers.

1. It was determined that the boundary-layer merge limit for low density operation of a supersonic nozzle can be appreciably lowered by cryogenic control of the boundary layer. Between one and two orders of magnitude increase in the attainable degree of rarefaction was demonstrated in a 1-ft-diam hypersonic nozzle operated with nitrogen at reservoir pressures of from 45 to 1000 torr and reservoir temperatures of from 300 to 4000°K.

2. A valid flow calibration for these reservoir conditions can be obtained only by assuming a vibrationally frozen flow of undissociated nitrogen and applying large low density corrections to the pitot and static pressures. In turn, the low density corrections require the use of non-Sutherland viscosity variation below 80°K.

3. When operating with cryogenic suction on the nozzle walls, an indication of irreversibility in the flow was found for cases in which the static density was less than 1.7×10^{-8} gm/cm^3. The irreversibility has tentatively been identified as the result of departure from rotational equilibrium in the flow, and results in large uncertainties in the pressure, temperature, and Mach number in this regime. The density and velocity, however, are probably affected by less than 10 percent.

4. With natural boundary layer, the flow angles in the useful core of the flow were observed to be less than source-flow angles. With suction on the nozzle walls the flow angles were equal to, or slightly in excess of, the source-flow angles.

5. The thickness of the nozzle boundary layer with no suction was found to agree within 15 percent with a flat plate boundary-layer solution over the entire range of operation.

6. It was not possible to predict the flow in the nozzle with suction by using capture coefficients obtained from static experiments. The capture coefficients inferred from the BLC nozzle performance were found to be density-dependent and, in some cases, less than half of the values found in static experiments. The density-dependence was such that the integrated effective pumping speed on the nozzle walls was an inverse function of density level. As a result, both the effective core size and the Mach number were observed to increase as the degree of rarefaction was increased by operating with suction on the walls.

7. A gradual decrease in Mach number with time was observed when the cryogenic suction was applied. This was considered to be the result of the increasing condensate thickness, and consequently, surface temperature, with time.

REFERENCES

1. Van Driest, E. R. "Investigation of Laminar Boundary Layer in Compressible Fluids Using the Crocco Method." NACA TN 2597, January 1952.

2. MacDermott, W. N., Dix, R. E., and Shirley, B. H. "Low Density Boundary Layer Control by Liquid Hydrogen Cryopumping." AEDC-TR-65-148 (AD467446), August 1965.

3. Stalder, J. R., Goodwin, G., and Creager, M. O. "Heat Transfer to Bodies in a High-Speed Rarefied-Gas Stream." NACA Report 1093, 1952.

4. Enkenhus, K. R. "The Design, Instrumentation and Operation of the UTIA Low Density Wind Tunnel." UTIA 44, University of Toronto, June 1957.

5. MacDermott, W. N. "Preliminary Experimental Results of the Reduction of Viscous Effects in a Low Density Supersonic Nozzle by Wall Cryopumping." AEDC TN 61-71, (AD 264656), October 1961.

6. Bottorf, M. R. and Rogers, K. W. "Theoretical and Experimental Investigation of Boundary Layer Control in a Low-Density Nozzle by Wall Suction and Cooling." USCEC 90-101, University of Southern California Engineering Center, March 1963.

7. Kosterin, S. I., Yuschenkova, N. I., Belova, N. T., and Kamaev, B. D. "An Investigation into the Effect of Rarefaction of a Supersonic Stream on the Readings of a Total Head Probe." International Chemical Engineering, Vol. III. No. 2, April 1963.

8. Potter, J. L., Kinslow, M., and Boylan, D. E. "An Influence of the Orifice on Measured Pressures in Rarefied Flow." AEDC-TDR 64-175 (AD447734), September 1964.

9. Hilsenrath, J., et al. "Tables of Thermal Properties of Gases." National Bureau of Standards Circular 564, November 1, 1955.

10. White, J. J., III. "Calculation of the Boundary Layer for Low-Density, Hypervelocity Flows in Nozzles with Cryogenic Boundary-Layer Removal." A Thesis presented to the Graduate Council of The University of Tennessee, March 1966.

11. Collins, J. A. and Dawson, J. P. "Cryopumping of 77°K Nitrogen and Argon on 10-25°K Surfaces." AEDC-TDR-63-51 (AD404174), May 1963.

12. Fenn, J. B. and Anderson, J. B. "Background and Sampling Effects in Free Jet Studies by Molecular Beam Measurements." Project Squid Technical Report PR-108-P, September 1964.

13. Knuth, E. L. "Rotational and Translational Relaxation Effects in Low Density Hypersonic Free Jets." University of California, Los Angeles, Report No. 64-53, November 1964.

14. Cohen, C. B. and Reshotko, E. "Similar Solutions for the Compressible Laminar Boundary Layer with Heat Transfer and Pressure Gradient." NACA Report 1293, 1956.

15. Erickson, W. D. "Vibrational Non-Equilibrium Flow of Nitrogen in Hypersonic Nozzles." NASA TN D-1810, June 1963.

16. Hirschfelder, J. O., Curtiss, C. F. and Bird, R. B. Molecular Theory of Gases and Liquids, John Wiley and Sons, New York, 1954.

17. Munn, et al. "Transport Collision Integrals for Quantum Gases Obeying a 12-6 Potential." Journal Chem. Phys., Vol. 42, No. 2, p. 537, January 1965.

APPENDIX I
DETERMINATION OF RESERVOIR TEMPERATURE

Since many of the reservoir temperatures used in the BLC nozzle were in the range where conventional measurements were impossible, the sonic flow technique was adopted as the standard technique for determining T_{o1}. The sonic flow relation for $\gamma = 1.4$ was used:

$$\dot{m} = \frac{\rho^*}{\rho_{o_1}} \left(\frac{T^*}{T_{o_1}}\right)^{1/2} \left(\frac{\gamma}{RT_{o_1}}\right)^{1/2} p_{o_1} A^* \qquad \text{(I-1)}$$

$$= 402.3 \frac{p_{o_1} A^*}{\sqrt{T_{o_1}}} \qquad \text{(I-2)}$$

where p_{o1} is in atmospheres, T_{o1} is in degrees Kelvin, and A* is in square centimeters. Clearly, if $\dot{m}$, p_{o1}, and A* are known, the stagnation temperature can be determined. The BLC nozzle operates at such low Reynolds numbers that there is a significant effect of boundary-layer displacement on the sonic area,

$$\frac{A^*_{eff}}{A^*_{geom}} = \left(\frac{D_{geom} - 2\delta^*}{D_{geom}}\right)^2 = \left(1 - 2\frac{\delta^*}{D_{geom}}\right)^2 \qquad \text{(I-3)}$$

The displacement thickness was computed by an approximate procedure involving use of the total boundary-layer thickness parameter $\frac{\delta}{x}\sqrt{Re_x}$ from Ref. 1 and δ^*/δ ratios computed from the solutions of Ref. 14 for an infinitely favorable pressure gradient. This calculation was verified by actual measurement at $T_{o1} = 300°K$ with both an adiabatic nozzle wall and a highly cooled wall ($T_W = 77°K$). Below $T_{o1} = 1400°K$, a displacement correction in the usual sense was found, but above $T_{o1} = 1400°K$ the calculated displacement effect was found to be negative, i. e., giving an effective sonic area greater than geometric throat area. The displacement correction corresponded to 700°K at the lowest p_{o1} and 50°K at the highest p_{o1}.

APPENDIX II
THERMODYNAMIC MODEL OF NOZZLE EXPANSION

Since the flow calibration of the nozzle is to be made on the basis of parameters measured only at the nozzle exit and in the nozzle reservoir, the thermodynamic model of the expansion process between these two points must be known or assumed. The characteristics of the flow model will depend upon whether or not certain elementary molecular processes such as chemical reaction and excitation are present, and if present, whether or not they remain in equilibrium with the translational temperature during the expansion.

The possibility of chemical reaction (dissociation/recombination of N_2) is eliminated by the restriction of T_{o1} to values less than 4000°K. For p_{o1} in the range of from 100 to 1000 torr, this means that equilibrium dissociation of nitrogen in the stagnation reservoir is less than 0.5 percent and therefore negligible.

The range of T_{o1} from 1000 to 4000°K is such that strong excitation of molecular vibration exists, while the reservoir pressures are low enough that departure from vibrational equilibrium should be expected. However, analysis of results of Ref. 15 indicates that a particularly simple limiting form of nonequilibrium is indicated, viz, fully frozen flow. In this reference, nozzle expansions were computed with finite-rate vibrational de-excitation. The main results are summarized in Fig. II-1. The values of various nozzle flow parameters in the nonequilibrium expansions are normalized by equilibrium values and presented as functions (ψ) of the scale parameter, $p_{o1}\,\ell$. The subscripts of the ψ symbols specify the particular flow variable involved. Here, p_{o1} is the nozzle reservoir pressure in atmospheres and ℓ is a characteristic length defined by

$$\ell = \frac{D^*}{2} \cot \theta \qquad \text{(II-1)}$$

with D* in centimeters. For the BLC nozzle, the scale parameter is in the range of from 0.1 to 1.0 atm-cm, for which all of the flow parameters are within 1 percent of the fully frozen values. In other words, the vibrational energy freezes so early in the expansion that there is essentially no de-excitation of vibrational states, and a simple $\gamma = 1.4$ expansion can be assumed. This assumption is postulatory in nature and must be verified by a flow calibration.

The rotational energy states of nitrogen are fully excited for all temperatures above 5°K, and since the rotational relaxation times are

so very short, this degree of freedom is conventionally regarded as an active degree of freedom in all fluid dynamic applications. It was so regarded in the thermodynamic model of the BLC nozzle expansions; however, as discussed in Section 4.3, evidence of rotational nonequilibrium in the lowest density expansions was tentatively identified.

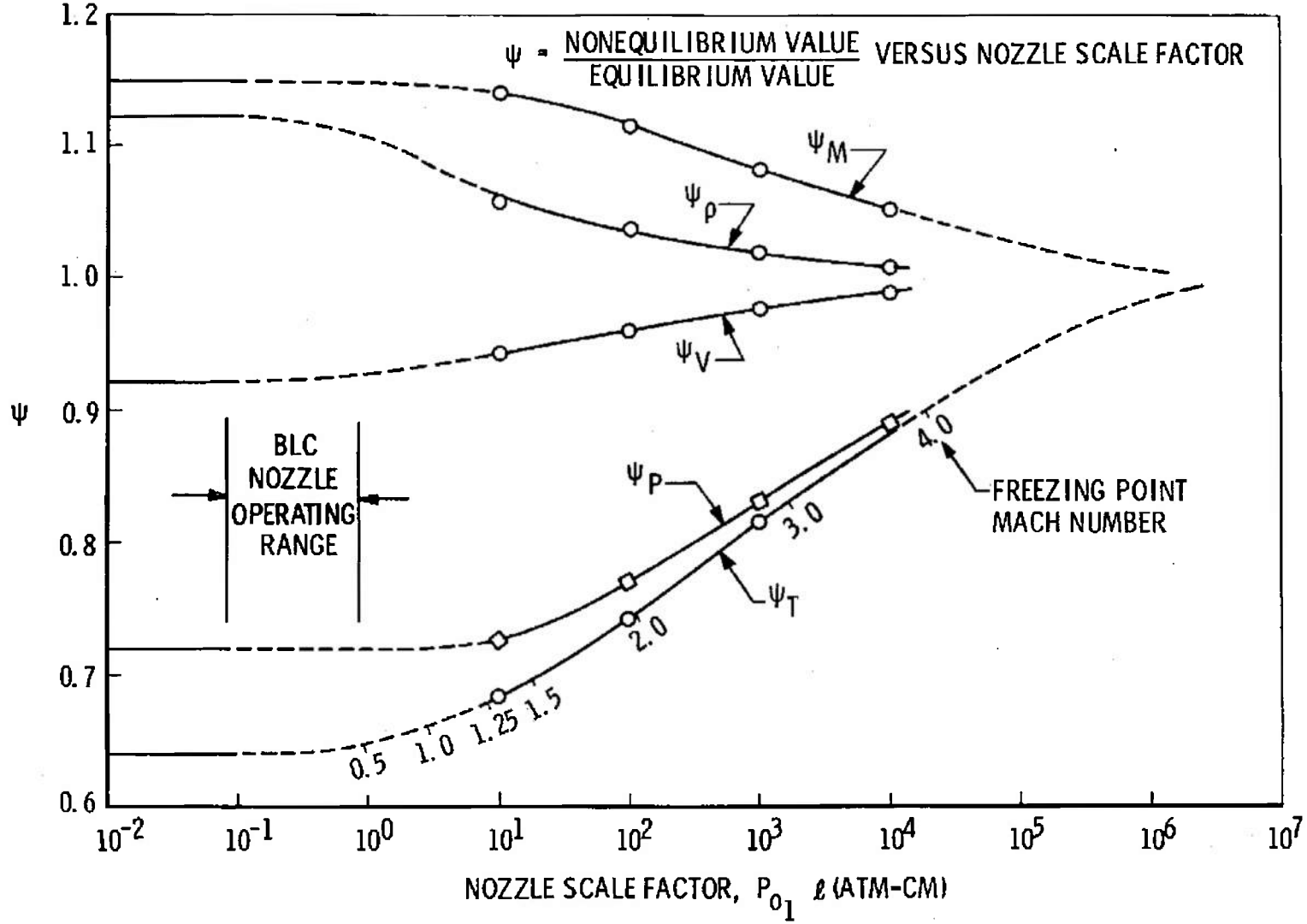

Fig. II-1 Transition from Equilibrium to Frozen Flow in Nitrogen Expansions at T_o = 4000 °K (Ref. 15)

APPENDIX III
LOW DENSITY CORRECTIONS TO PITOT AND STATIC PRESSURE MEASUREMENTS

The BLC nozzle is operated at such rarefied conditions that there are significant low density effects on both the pressure measured by a pitot probe and the static pressure measured in a wall orifice cavity.

The effect on pitot pressure is the familiar low Reynolds number correction to the pressure sensed by a pitot tube. This is basically an influence of the normal viscous stresses at the stagnation point, which, usually insignificant compared to the inertial stresses in the flow field, approach the value of the inertial stresses when the density is sufficiently low. Initially, this effect can be expressed in the form

$$\frac{(P_{o_2})_{measured}}{(P_{o_2})_{ideal}} = f(Re_D) \qquad \text{(III-1)}$$

with a weak dependence on Mach number. As density is steadily reduced, the pitot tube response undergoes a continuous transition to a free-molecule response, requiring Knudsen-number-dependent corrections on the order of 2.0. The pitot probe response curve used in this investigation is that given in Ref. 7 in which the factor $\frac{(p_{o2})_{measured}}{(p_{o2})_{ideal}}$ is correlated as a function of Re_D/M, which is inversely proportional to the Knudsen number.

As was found in the flow calibration, an even more importance influence of low density affects the pressure sensed by the wall orifice. Since the nozzle wall at the orifice location is of Plexiglas, the orifice remains at essentially room temperature, as verified by actual measurement. Hence, there is no thermal transpiration correction in the usual sense. However, in Ref. 8, the dissimilar molecular velocity distribution for molecules entering and leaving the orifice when heat transfer is present was found to produce a large difference between the gas pressure at the wall and the pressure inside the orifice cavity. This effect, referred to as the "influence of the orifice," is given by a function

$$\frac{\text{pressure in cavity}}{\text{pressure on wall}} = \frac{(P_{1_w})_{measured}}{(P_{1_w})_{ideal}} = F\left(K_w, \frac{D_{orif}}{(L_{mean})_{1_w}}\right) \qquad \text{(III-2)}$$

where

$$K_w = \frac{\dot{q}/A\ Pr_w\ (\gamma - 1)}{\gamma (P_{1_w})_{measured} (RT_w)^{1/2}} \qquad \text{(III-3)}$$

To fully cover the range of the BLC nozzle, the curves of F given in Ref. 8 were extrapolated to $K_W = 3.0$, using the theoretical values for the $\frac{D_{orif}}{(L_{mean})_{1_W}} = 0$ curve (free-molecule limit) as a guide.

The heat-transfer rate required for evaluation of K_W was computed using simple flat plate boundary-layer theory with wall reference conditions, Ref. 1. The sense of this correction is such that for heat transfer to the wall, the pressure in the orifice cavity is less than the static pressure on the wall outside the orifice. For conditions of calibration of the BLC nozzle, values of $\frac{(p_{1_W})_{measured}}{(p_{1_W})_{ideal}}$ as low as 0.42 were found.

APPENDIX IV
LOW TEMPERATURE VISCOSITY OF NITROGEN

Because the nozzle expansions in the BLC nozzle produced static temperatures of 30°K and lower, viscosity data for nitrogen at these low temperatures were required for evaluation of the low density corrections of Appendix III. The tabulated data of Ref. 9 stop at 100°K, and it is shown that fourteen different sources of experimental data agree with the tabulation to within ±2 percent between T = 80°K and T = 400°K. The tabulated data are the result of a collision-integral calculation based on the Lennard-Jones (6-12) intermolecular force potential with the force field constants

$$\sigma = 3.68\ \text{Å};\ \epsilon/k = 91.5°\text{K} \qquad \text{(IV-1)}$$

These data were extended to low temperatures by use of the tabulated collision integrals for the Lennard-Jones potential in Ref. 16. The result is given in Fig. IV-1. The lowest temperature collision integral for nitrogen was for T = 27.5°K, necessitating an extrapolation of the data below this limit. Subsequent to this calculation, Ref. 17 was published, in which the collision integrals with quantum mechanical corrections were extended to lower temperatures. It was observed that the extrapolation upon which Fig. IV-1 was based was in error by no more than 10 percent at 10°K.

It is noted that the viscosity variation below 100°K can be represented by a straight line within an accuracy of 4 percent. However, this straight line does not pass through the origin, and the frequently used linear law

$$\mu = (\text{constant})(T) \qquad \text{(IV-2)}$$

introduces large errors below 30°K. A Sutherland curve is also shown in Fig. IV-1. The unnatural requirement of the Sutherland relation that $d\mu/dT = 0$ at T = 0 means that any Sutherland curve will form a very poor approximation in this same temperature range.

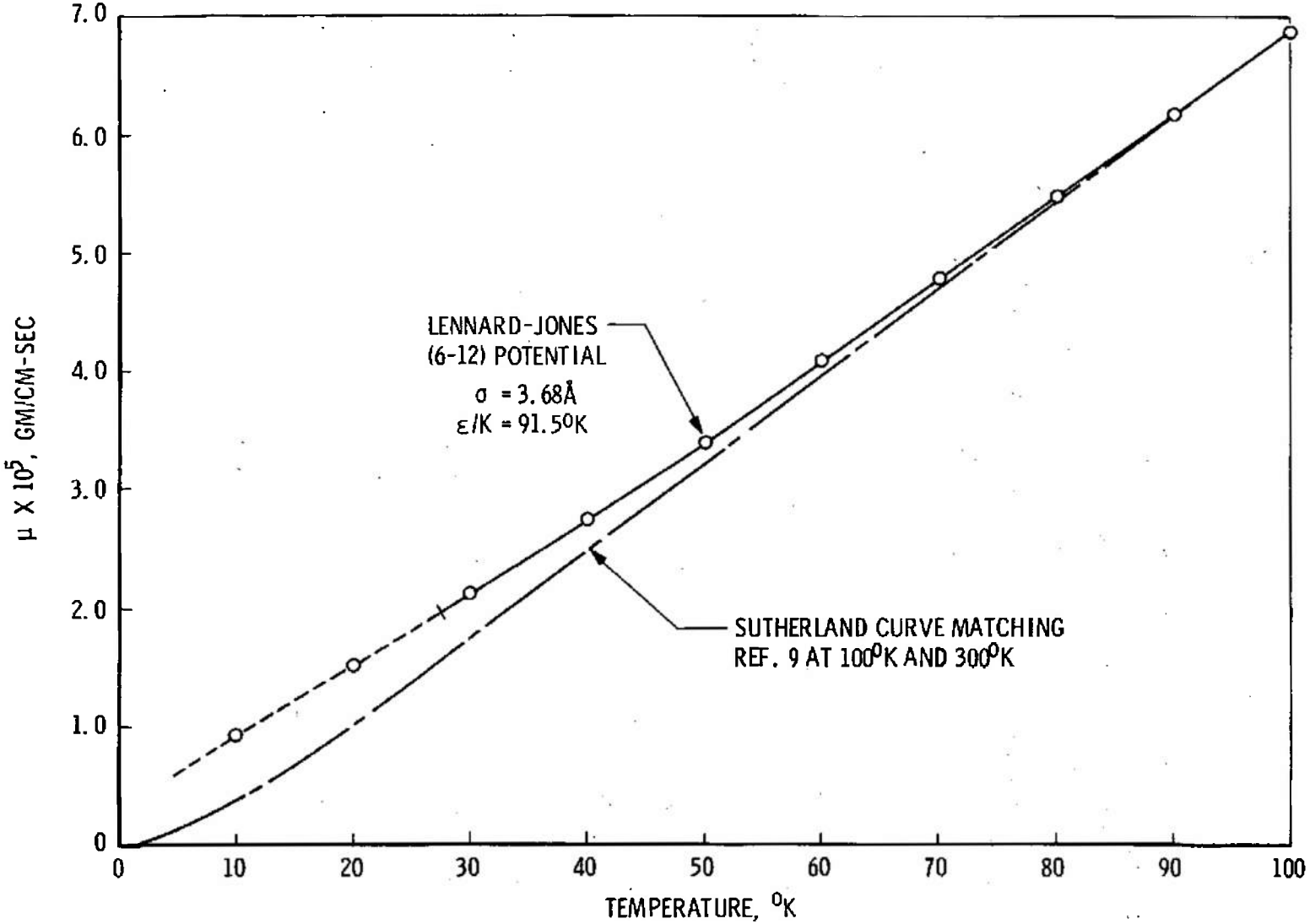

Fig. IV-1 Low Temperature Viscosity of Nitrogen

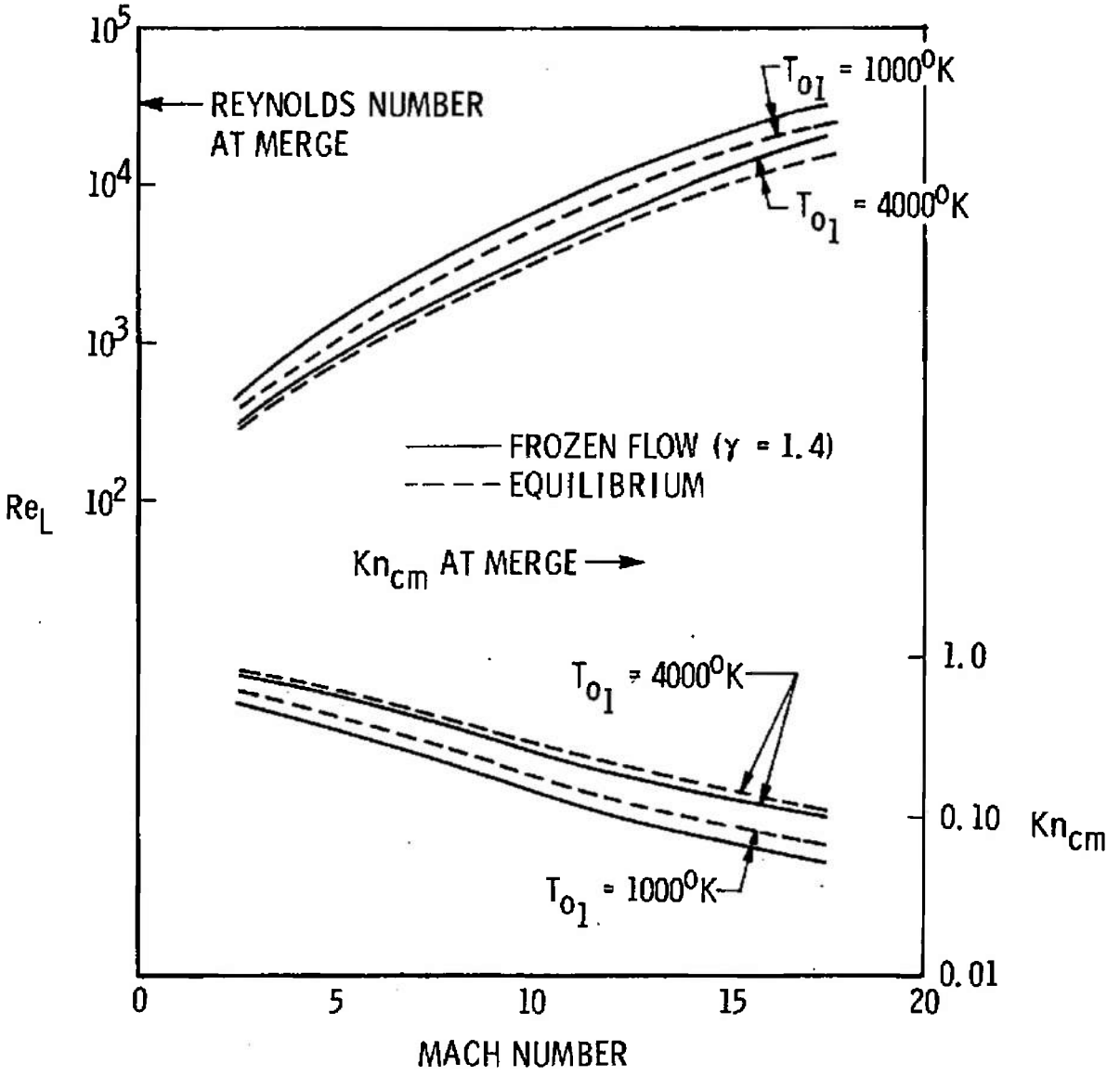

Fig. 1 Maximum Knudsen Number and Minimum Reynolds Number in 1-ft-diam Hypersonic Nozzle with a Merged Natural Boundary Layer, T_w = 300°K

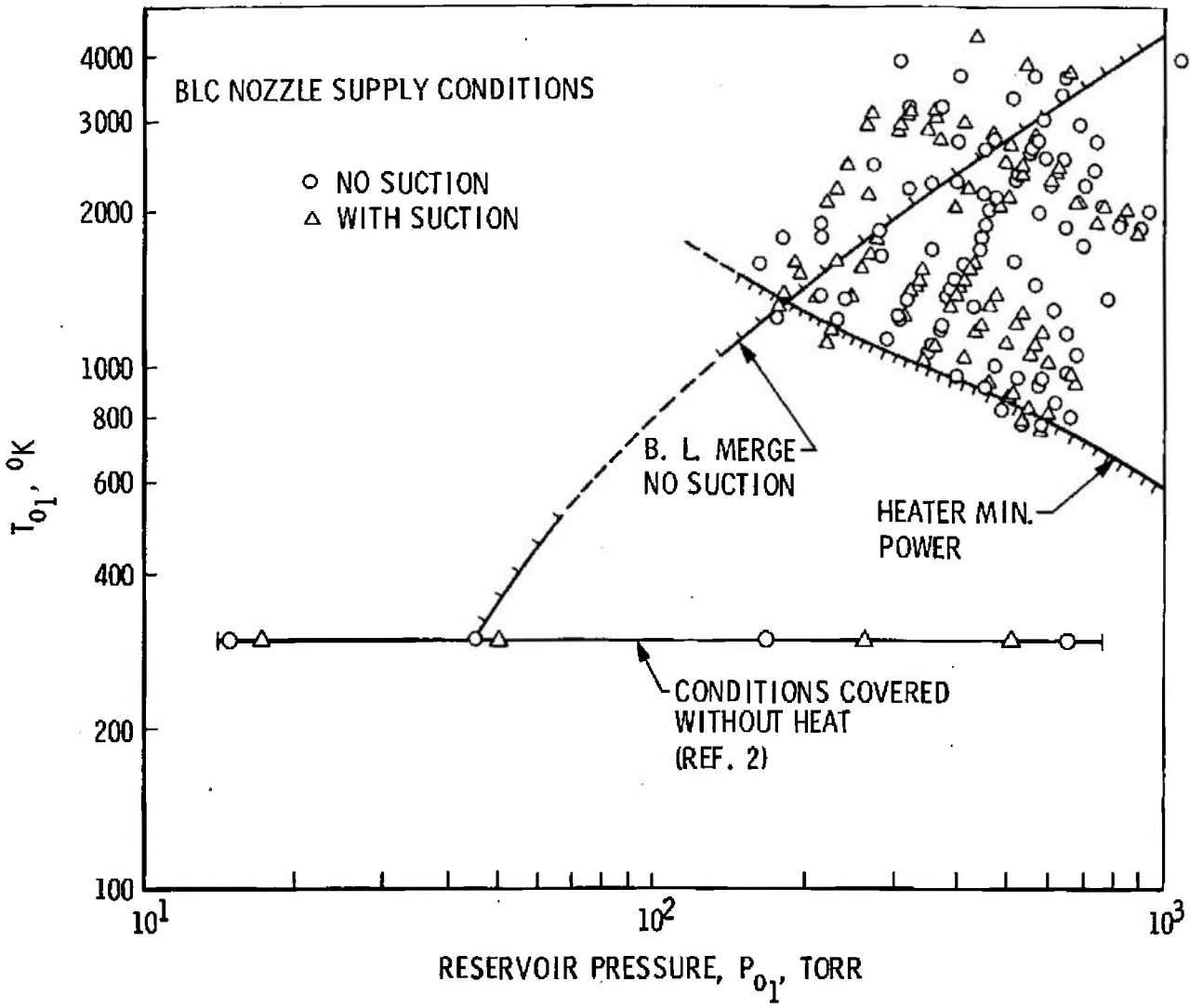

Fig. 2 Reservoir Conditions at which the BLC Nozzle Has Been Operated

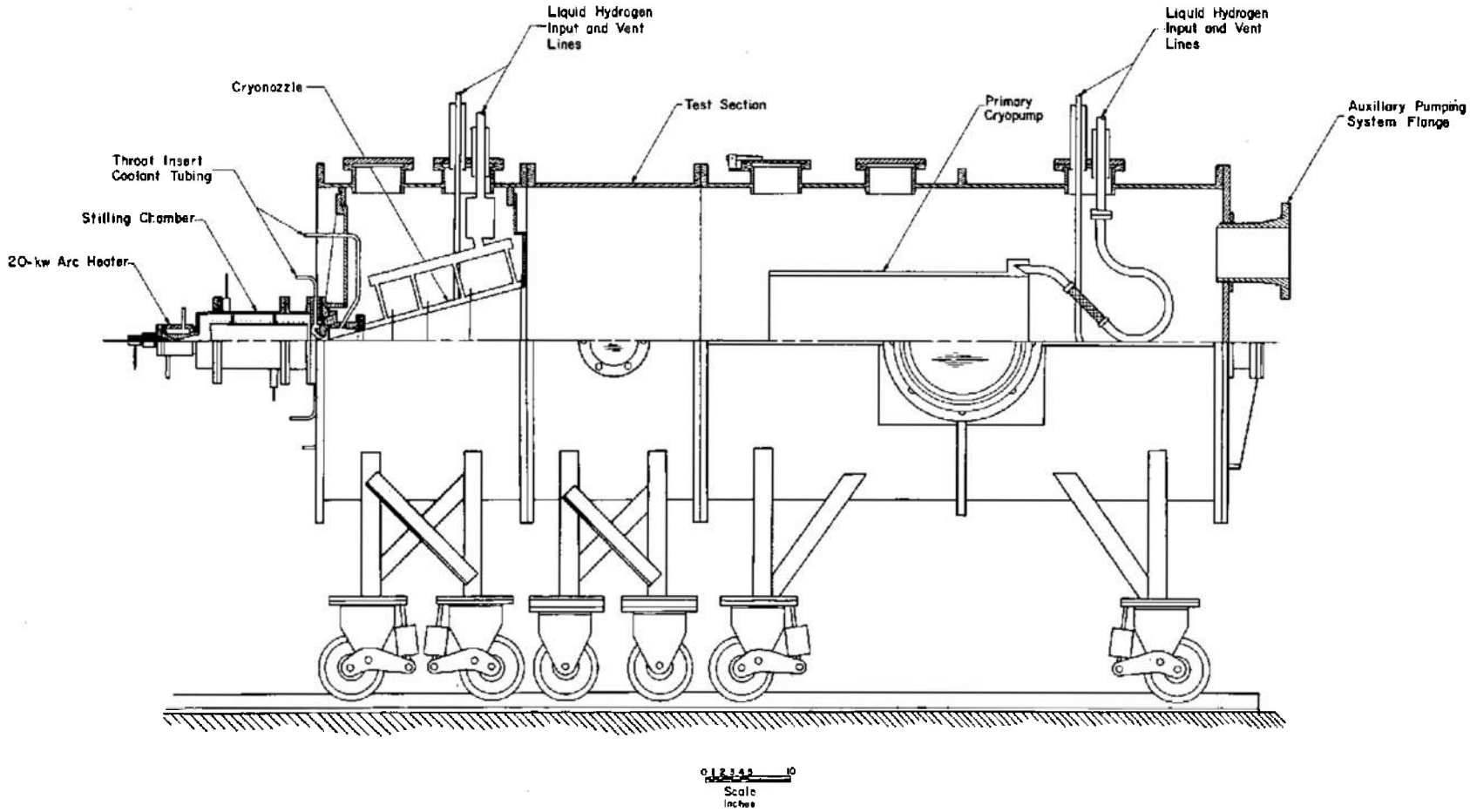

Fig. 3 Cryogenic BLC Nozzle and Test Chamber

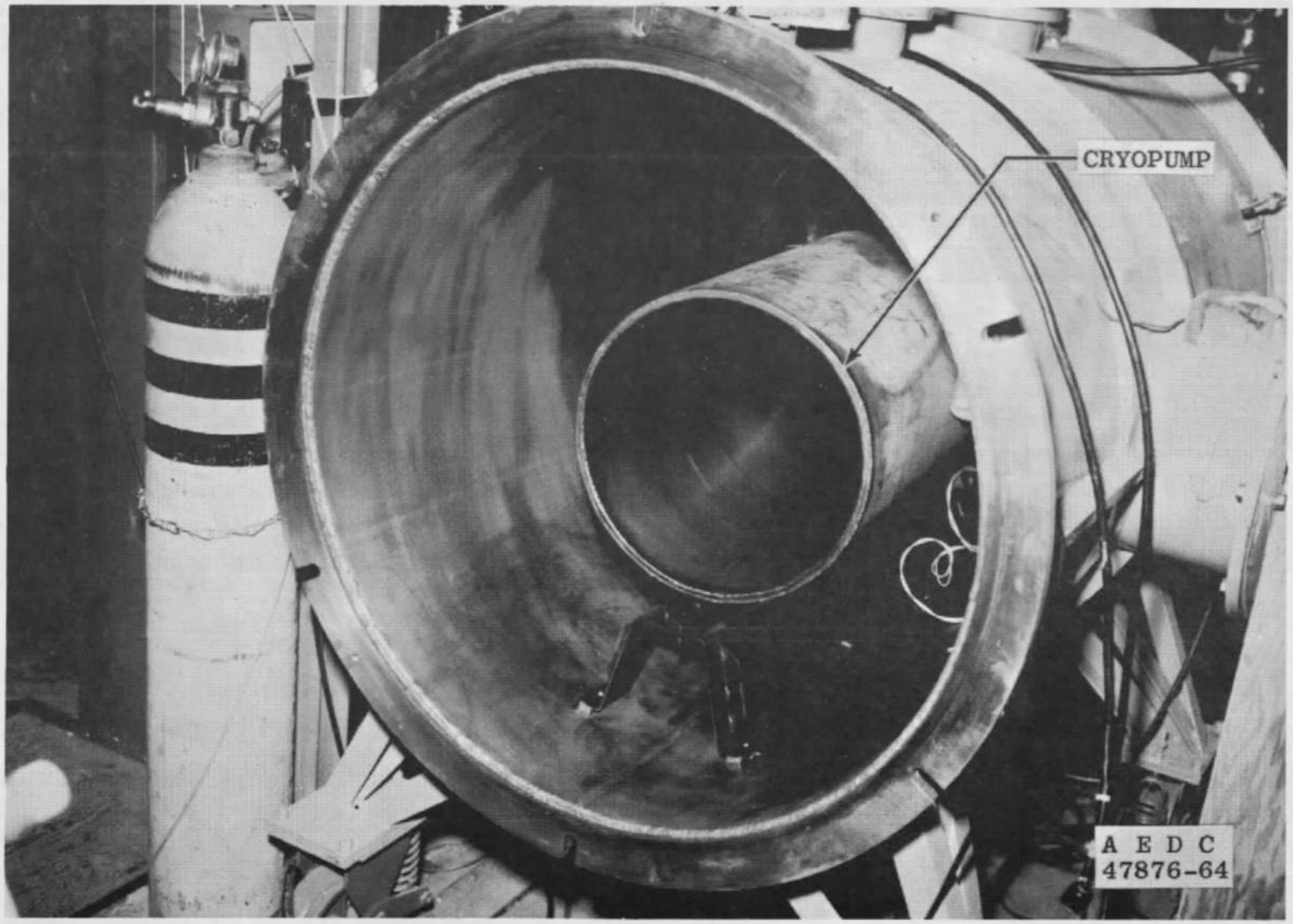

Fig. 4 View of Cryopump inside Vacuum Chamber

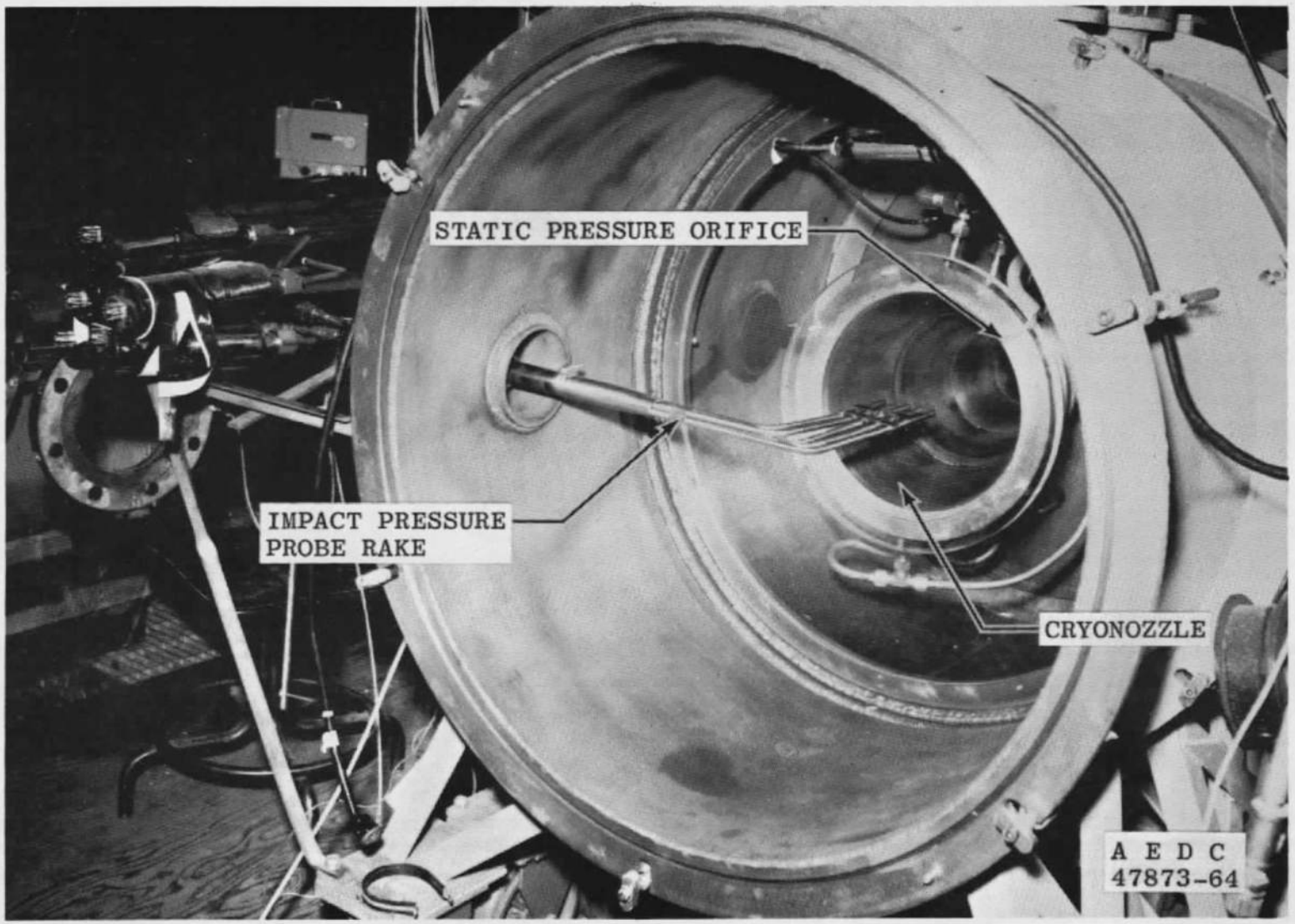

Fig. 5 View of Cryonazzle Exit, Test Sectian, and Impact Pressure Probe Rake

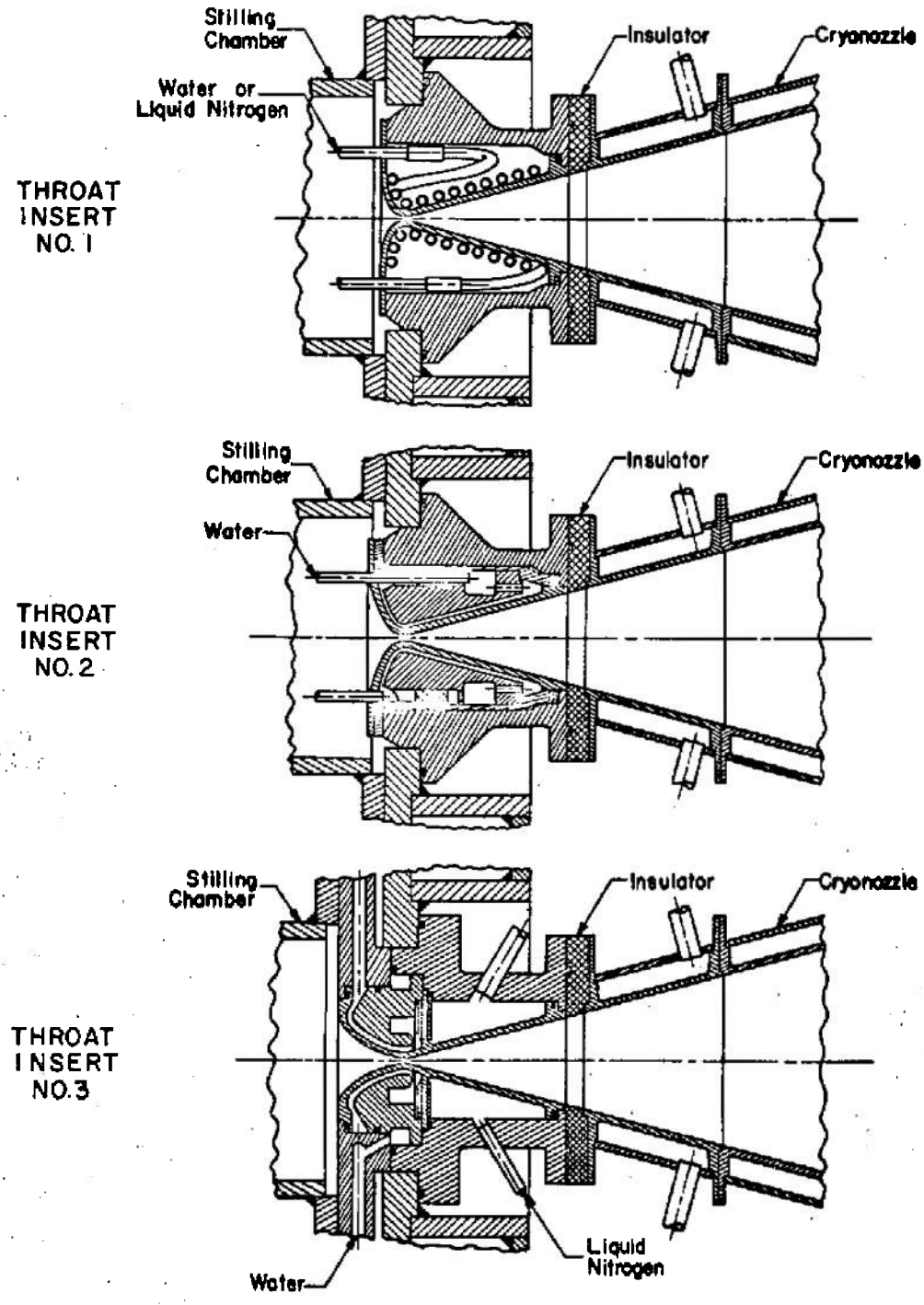

Fig. 6 Throat Inserts

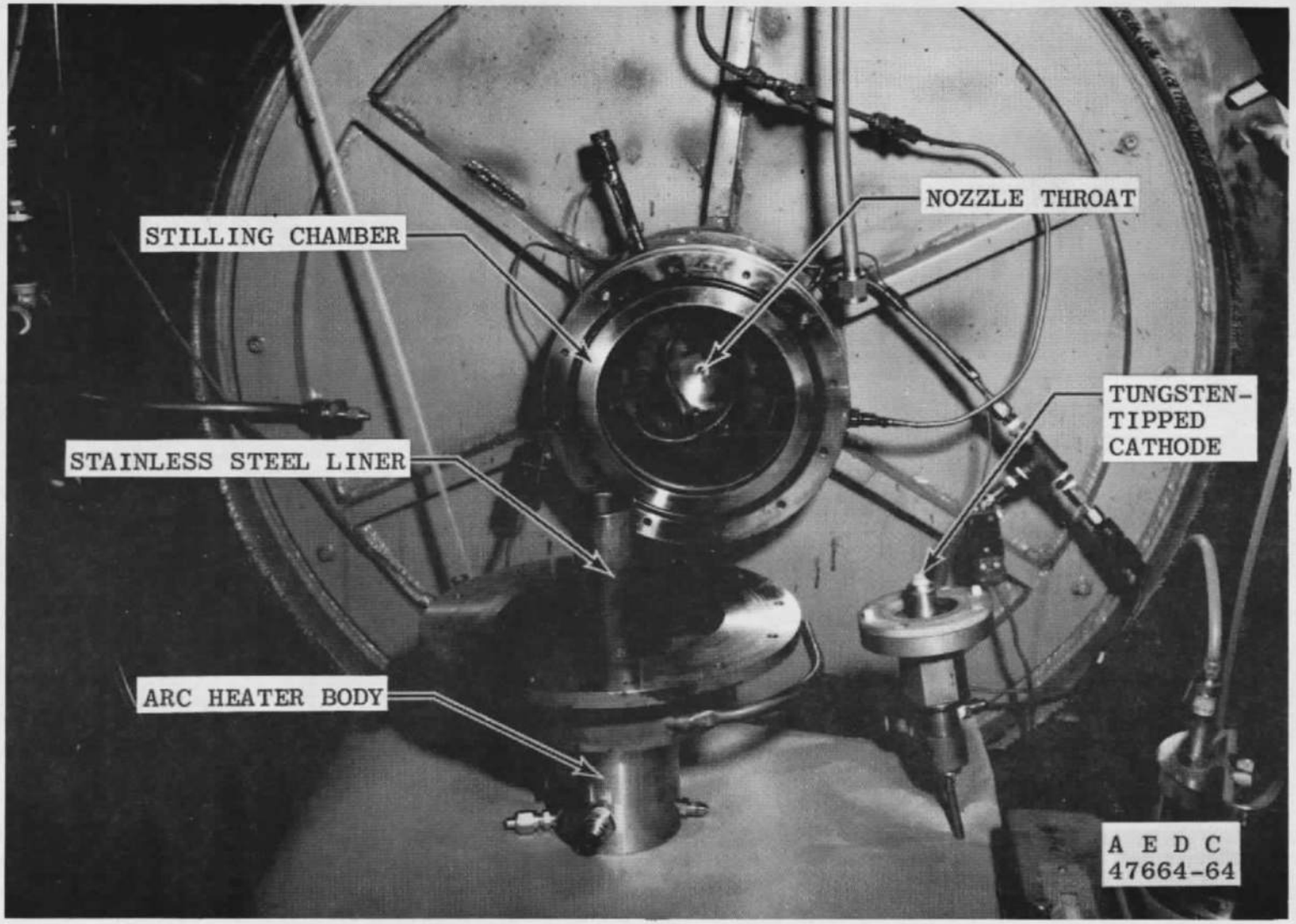

Fig. 7 Arc Heater and Stilling Chamber B

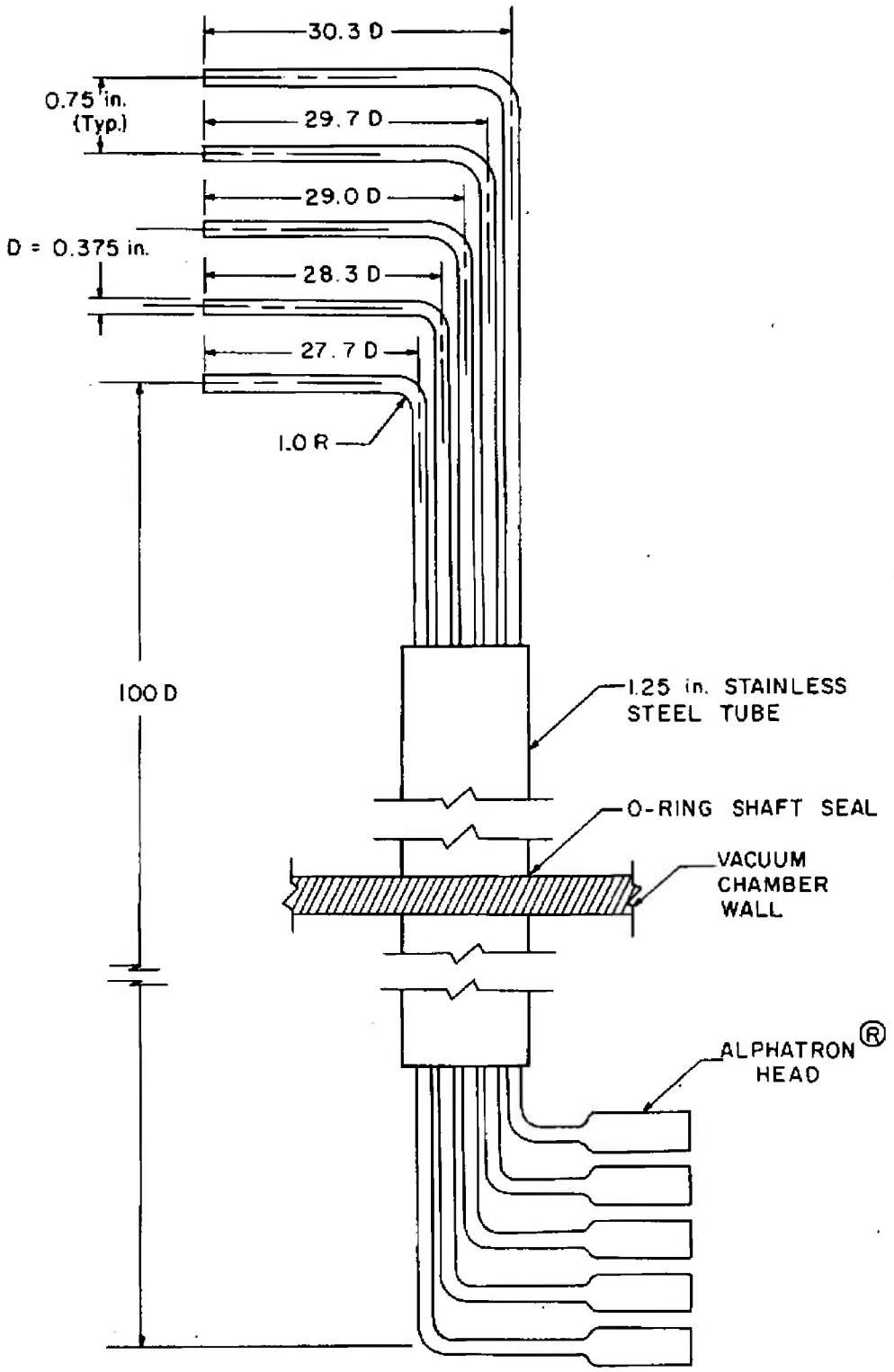

a. Impact Pressure Probe Rake Schematic

Fig. 8 Test Probes

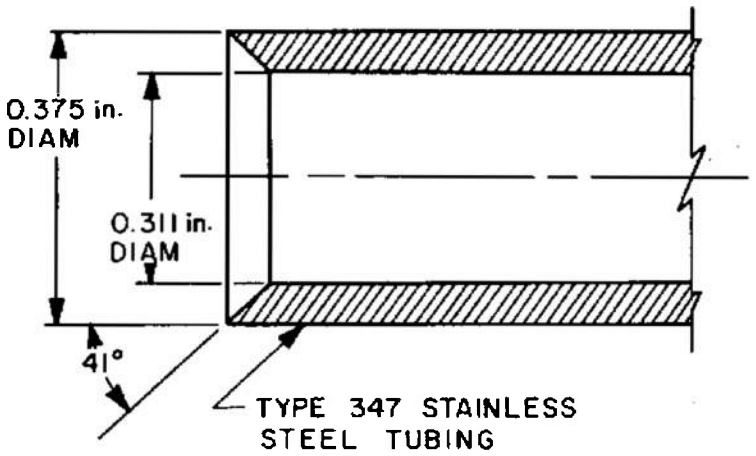

b. Impact Pressure Probe Tip Detail

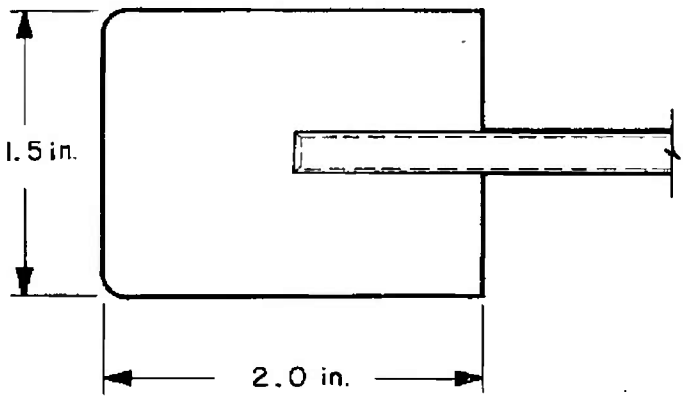

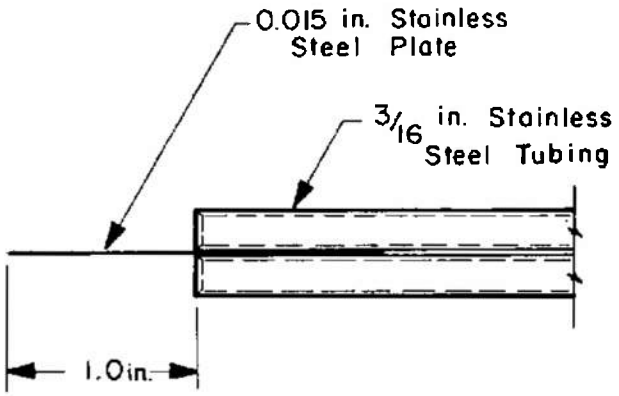

c. Flow Angularity Probe

Fig. 8 Concluded

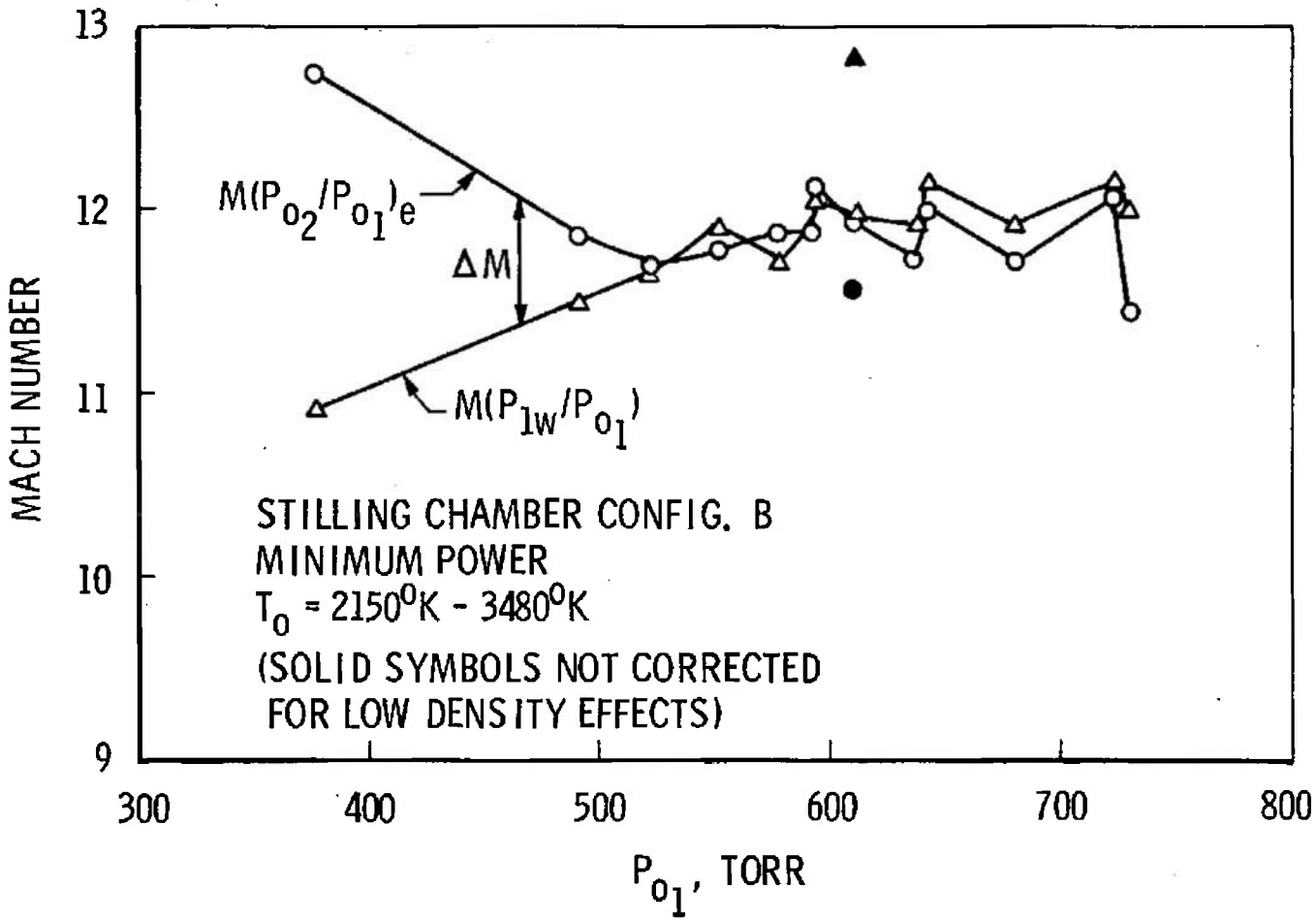

Fig. 9 Mach Number versus p_{o_1}, No Suction

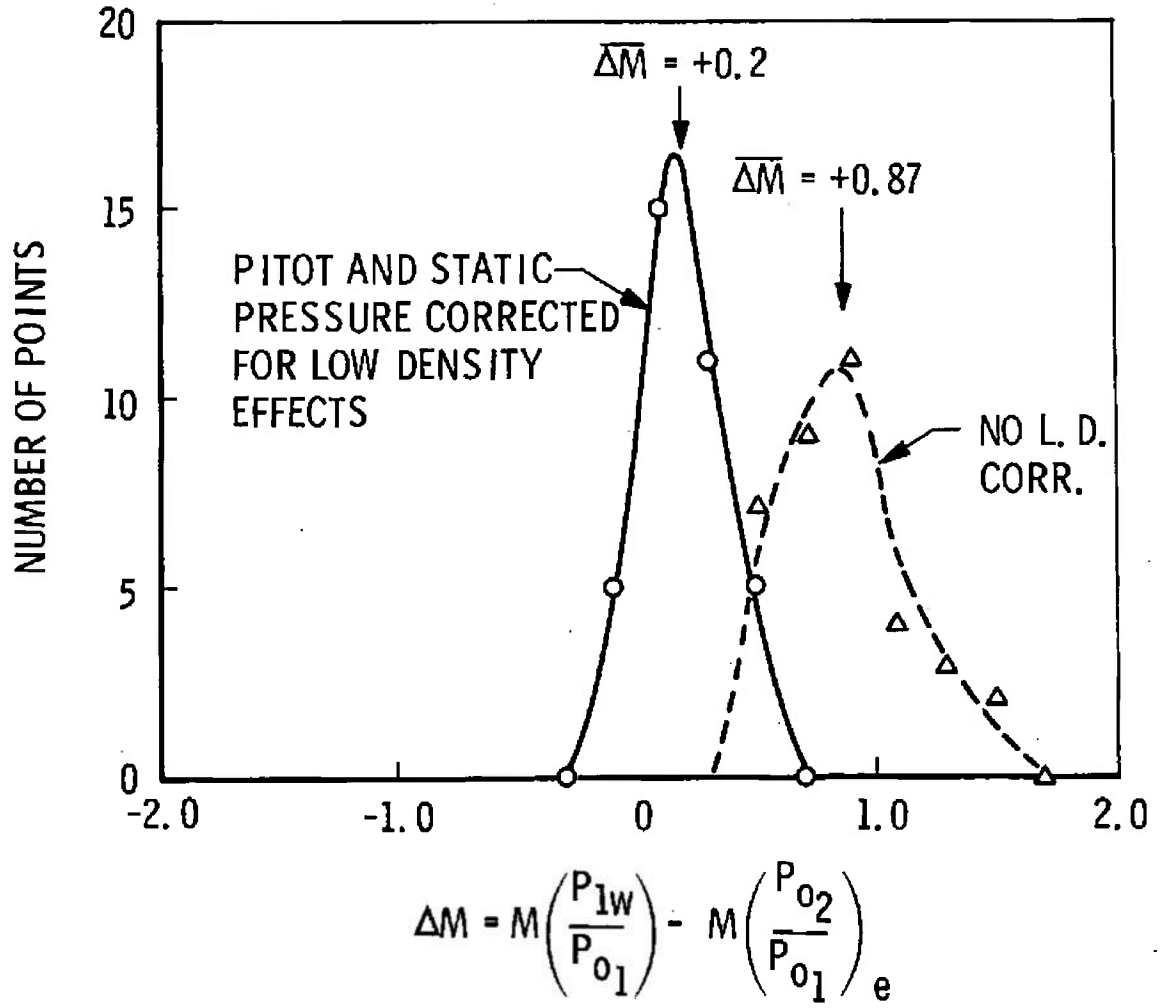

Fig. 10 Frequency Distribution of ΔM, No Suction

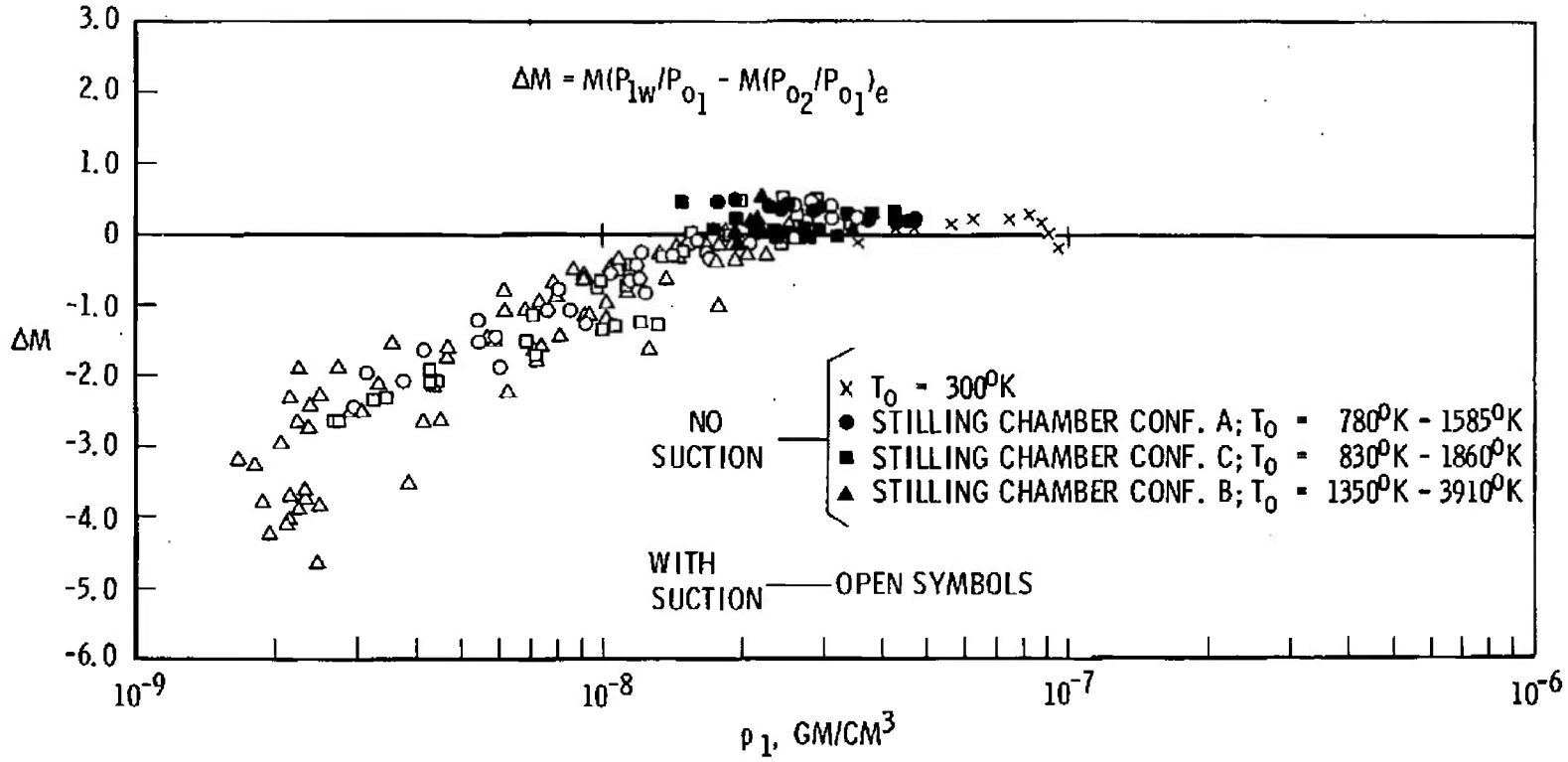

Fig. 11 Correlation of ΔM with Static Density

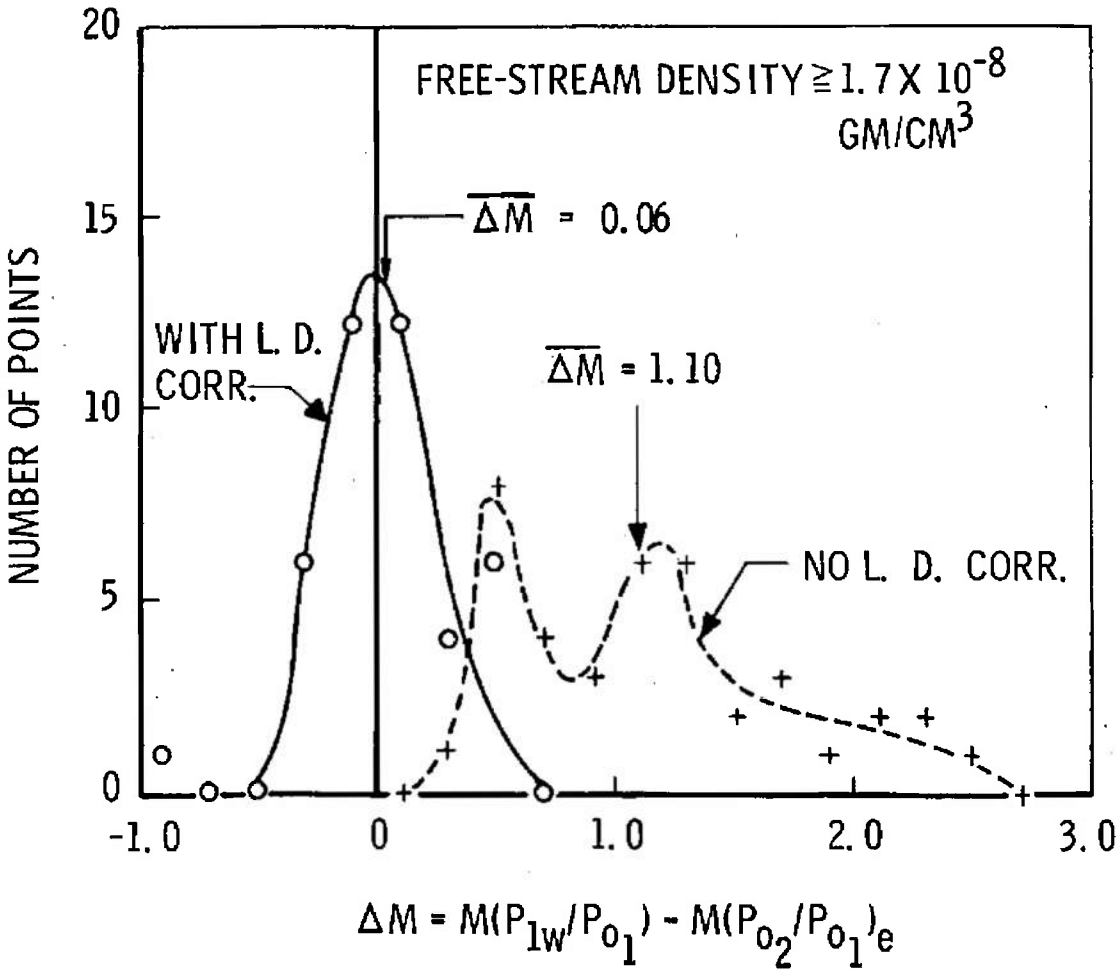

Fig. 12 Frequency Distribution of ΔM, with Suction

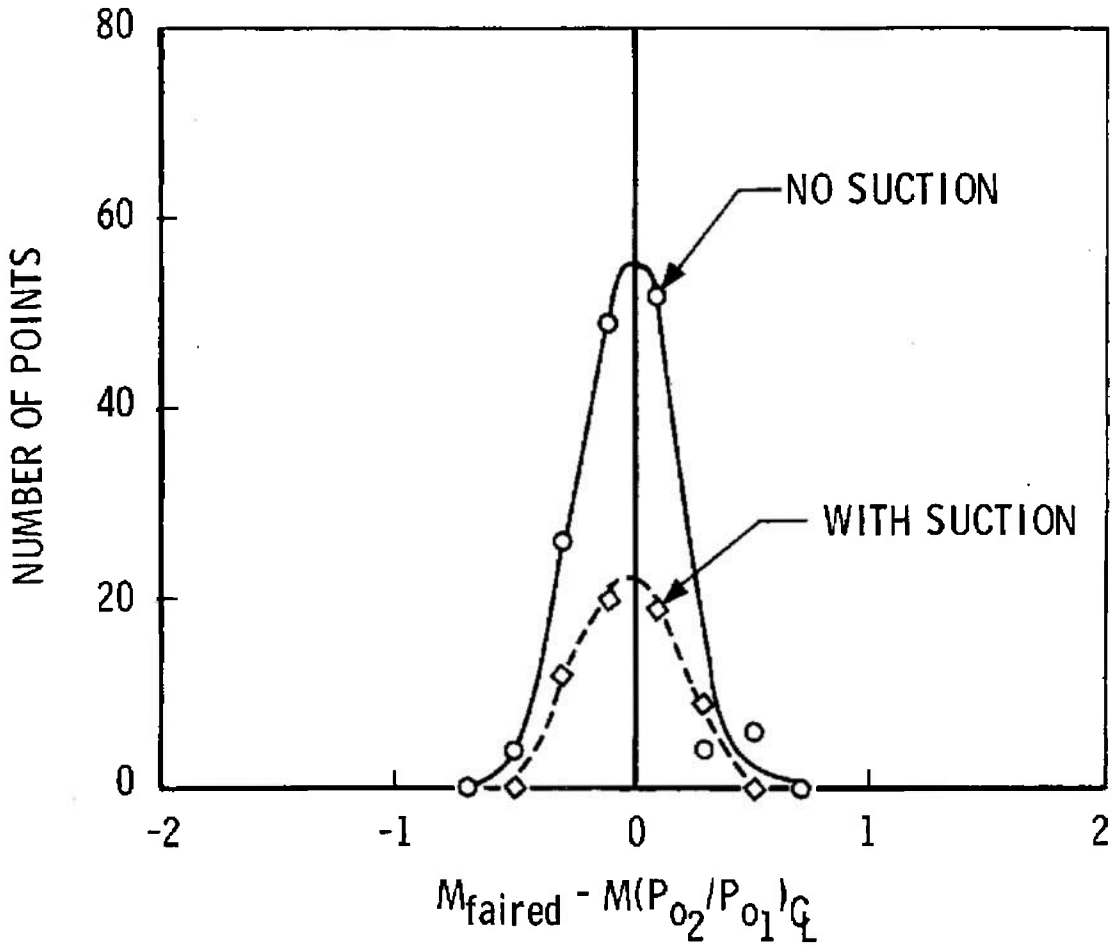

Fig. 13 Distribution of Differences between Individual Data Points and Faired Mach Number Curves

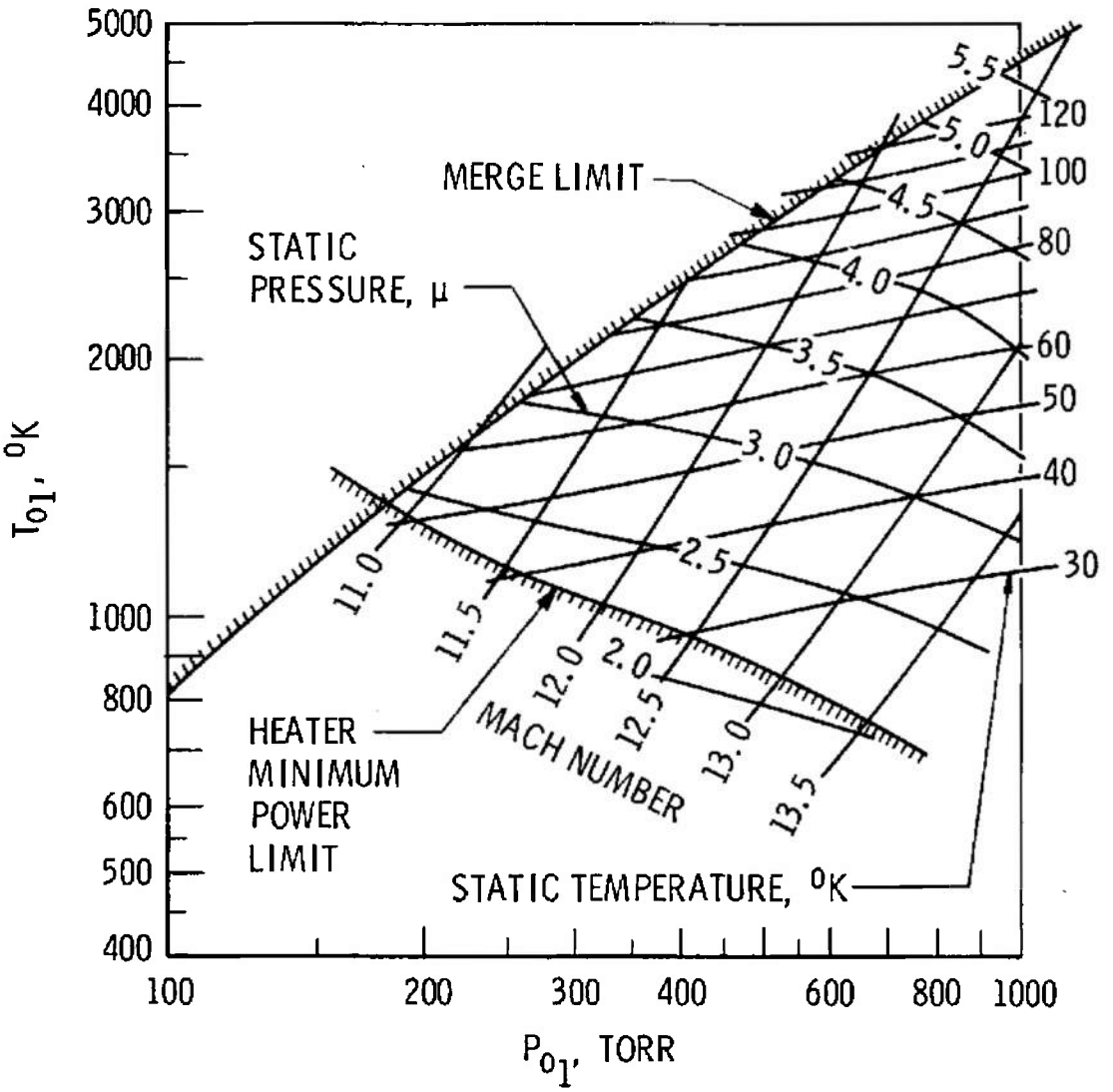

a. Mach Number, Static Pressure, Static Temperature

Fig. 14 Calibrated Flow Properties with No Suction versus p_{o_1} and T_{o_1}

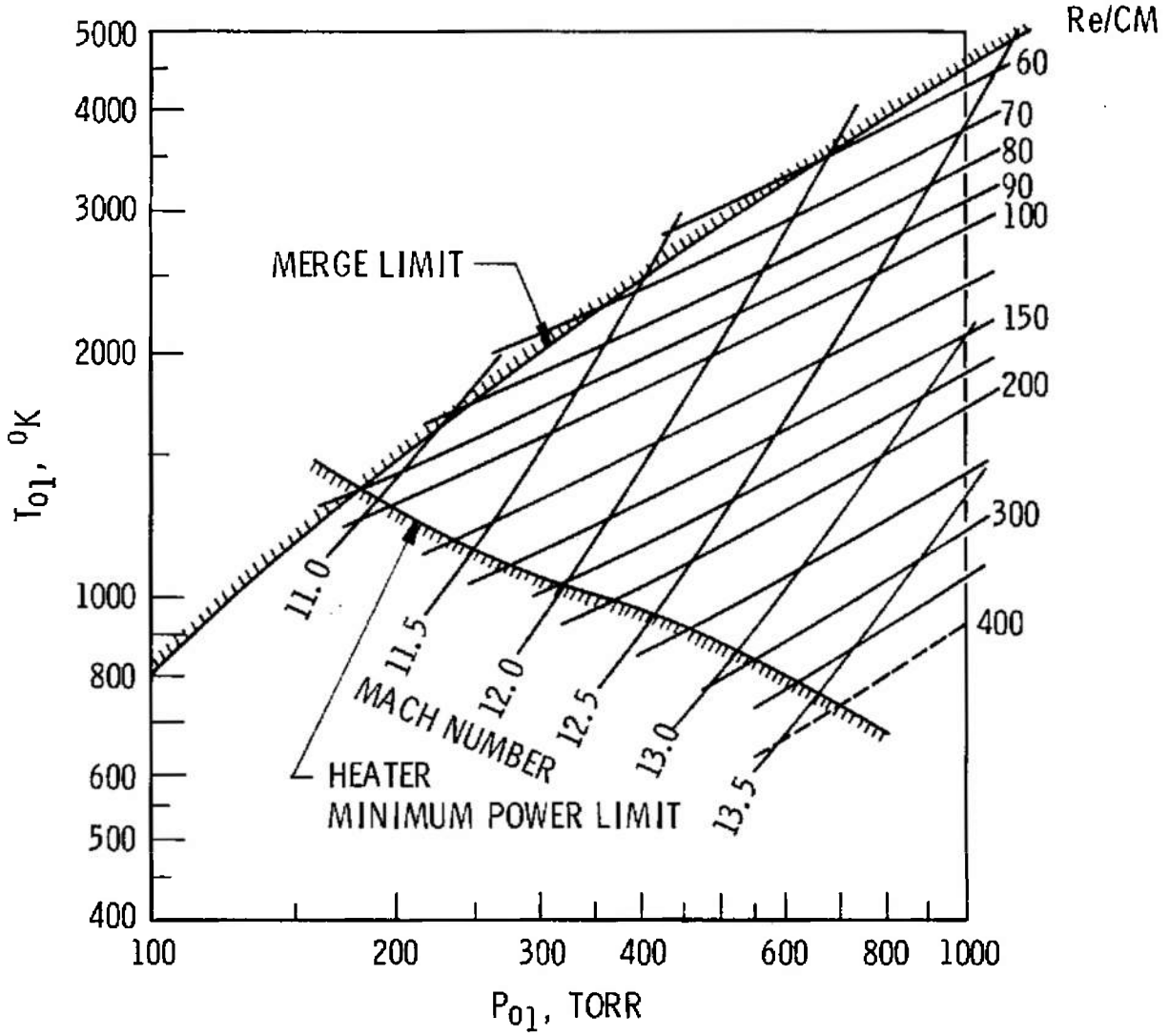

b. Mach Number and Unit Reynolds Number

Fig. 14 Continued

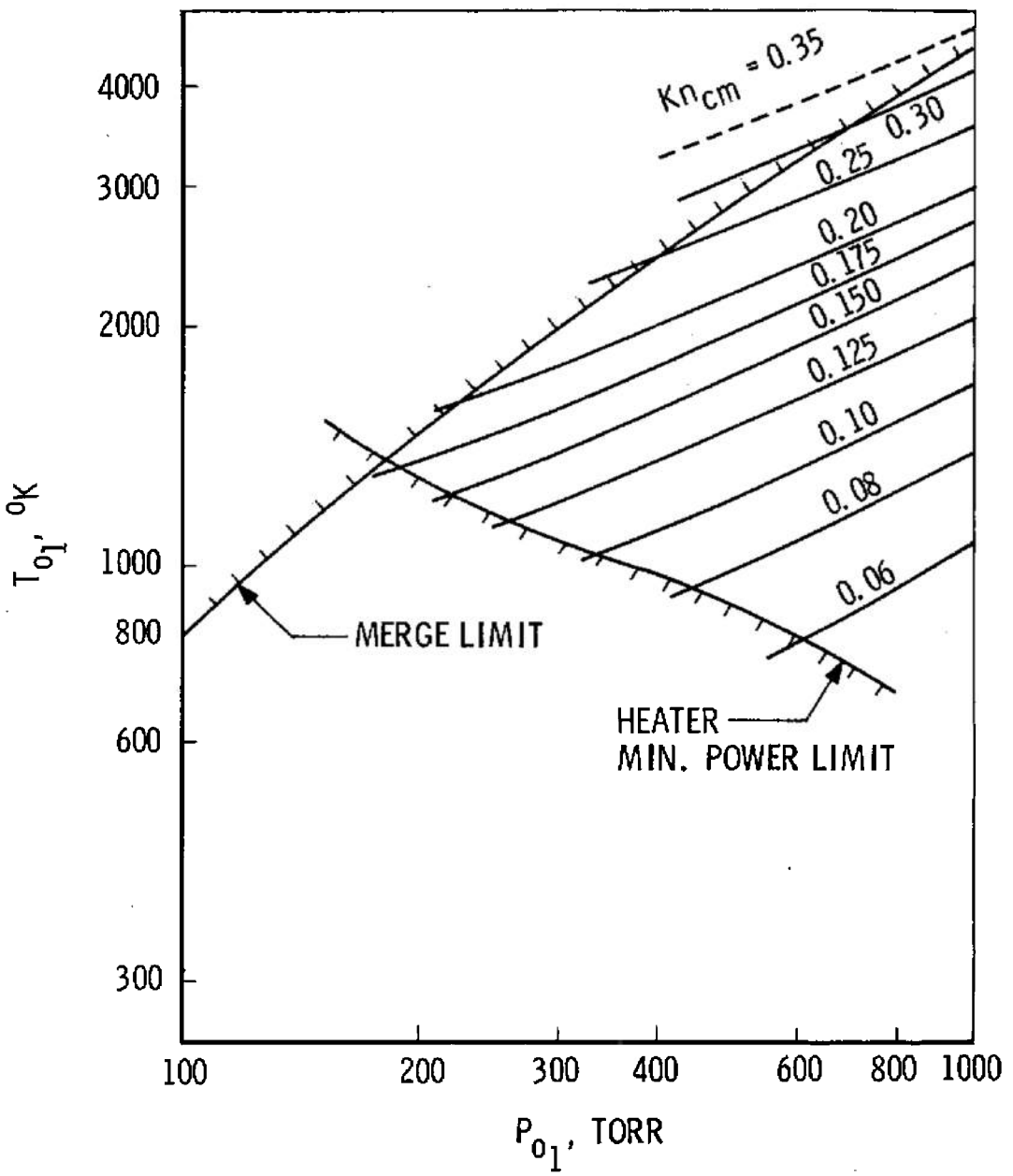

c. Knudsen Number for 1 cm at Nozzle Exit

Fig. 14 Concluded

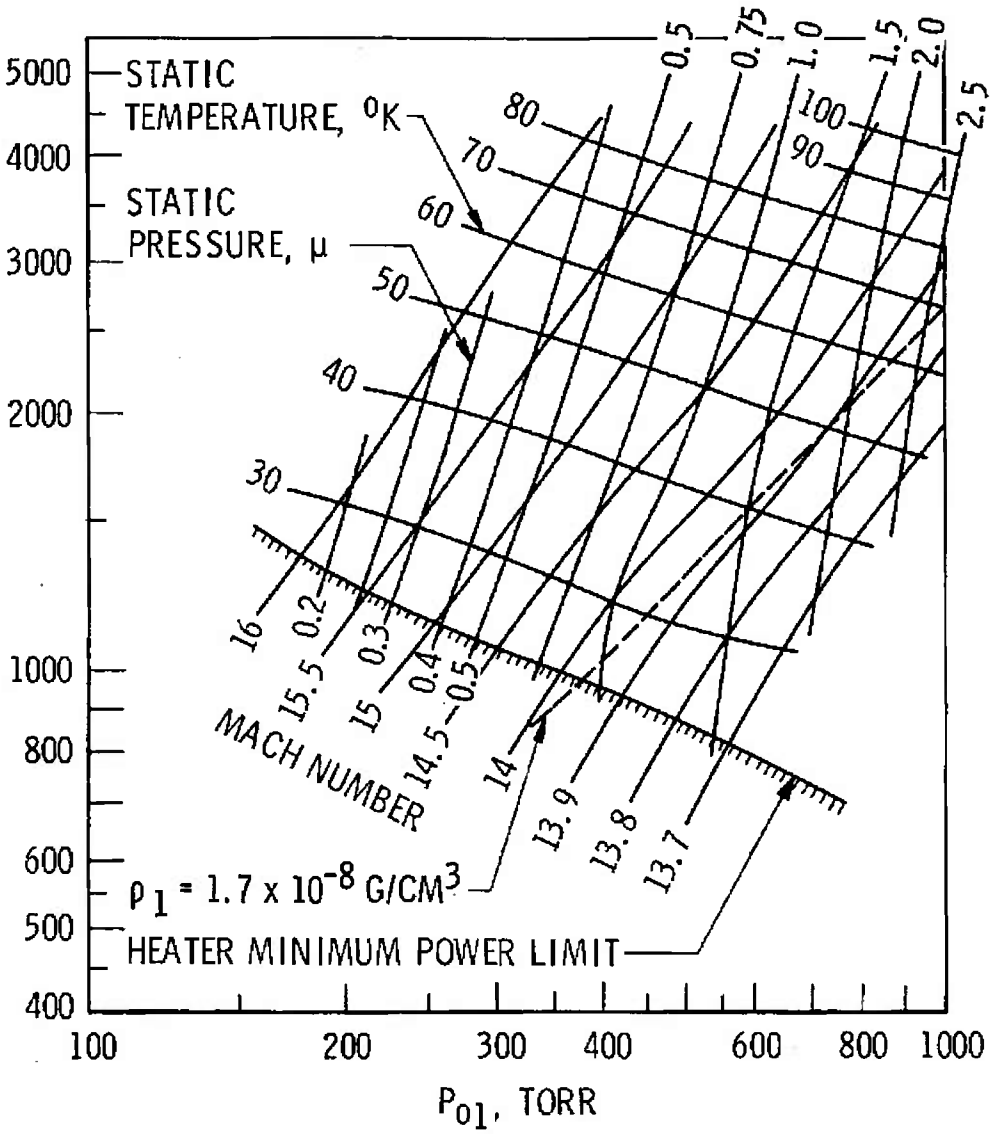

a. Mach Number, Static Pressure, Static Temperature

Fig. 15 Calibrated Flow Properties with Suction versus p_{o_1} and T_{o_1}

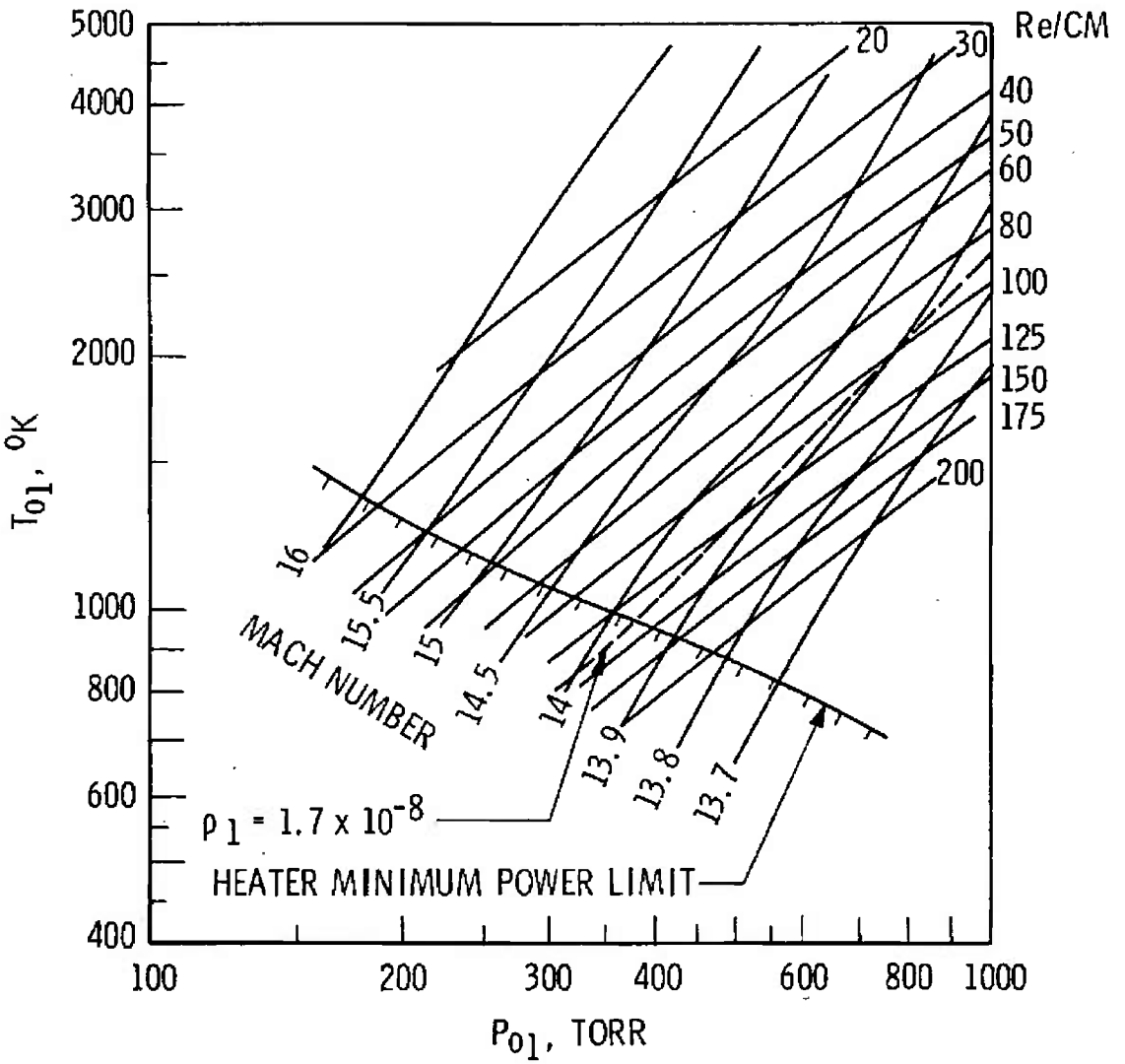

b. Mach Number and Unit Reynolds Number

Fig. 15 Continued

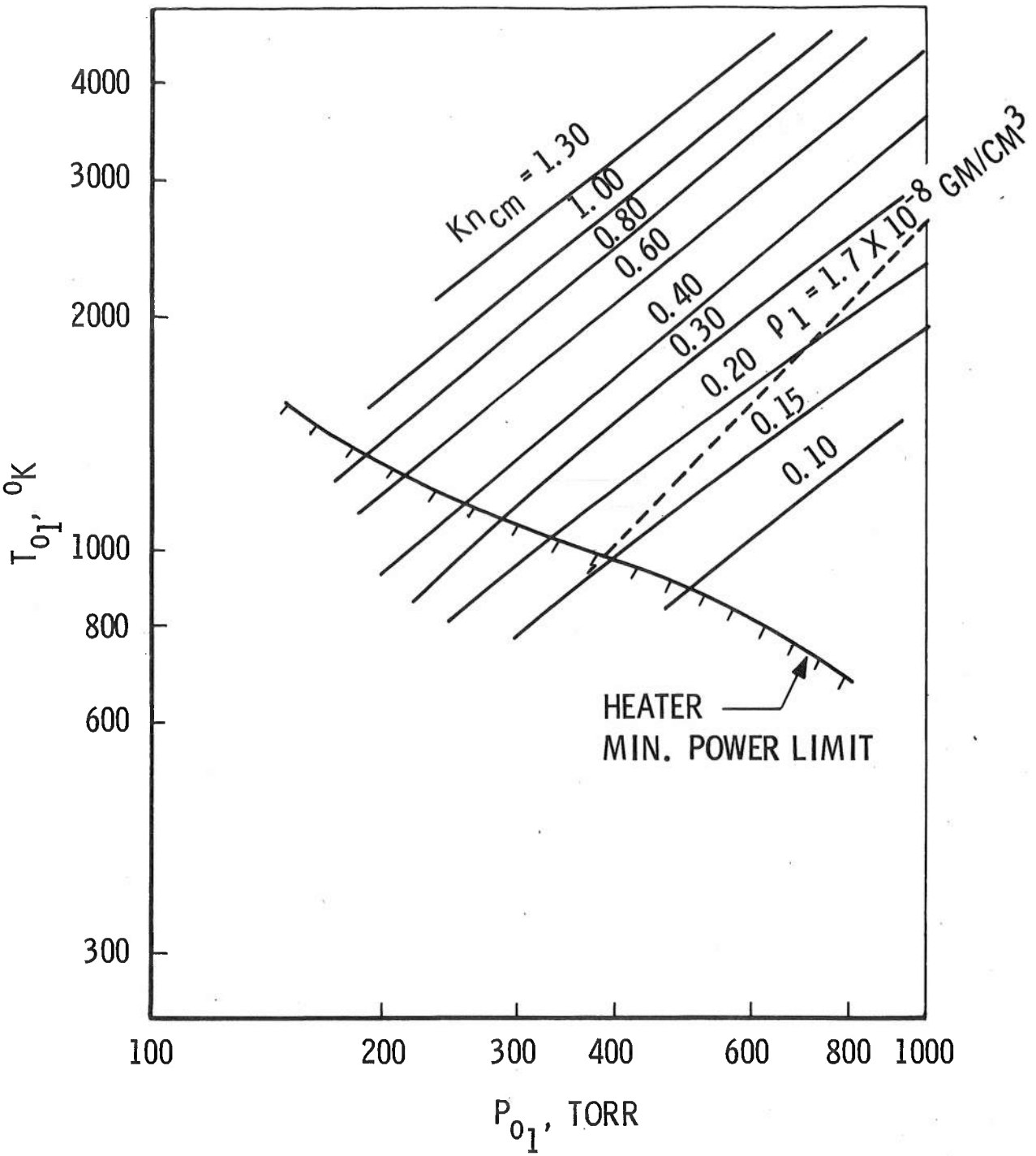

c. Knudsen Number for 1 cm at Nozzle Exit

Fig. 15 Concluded

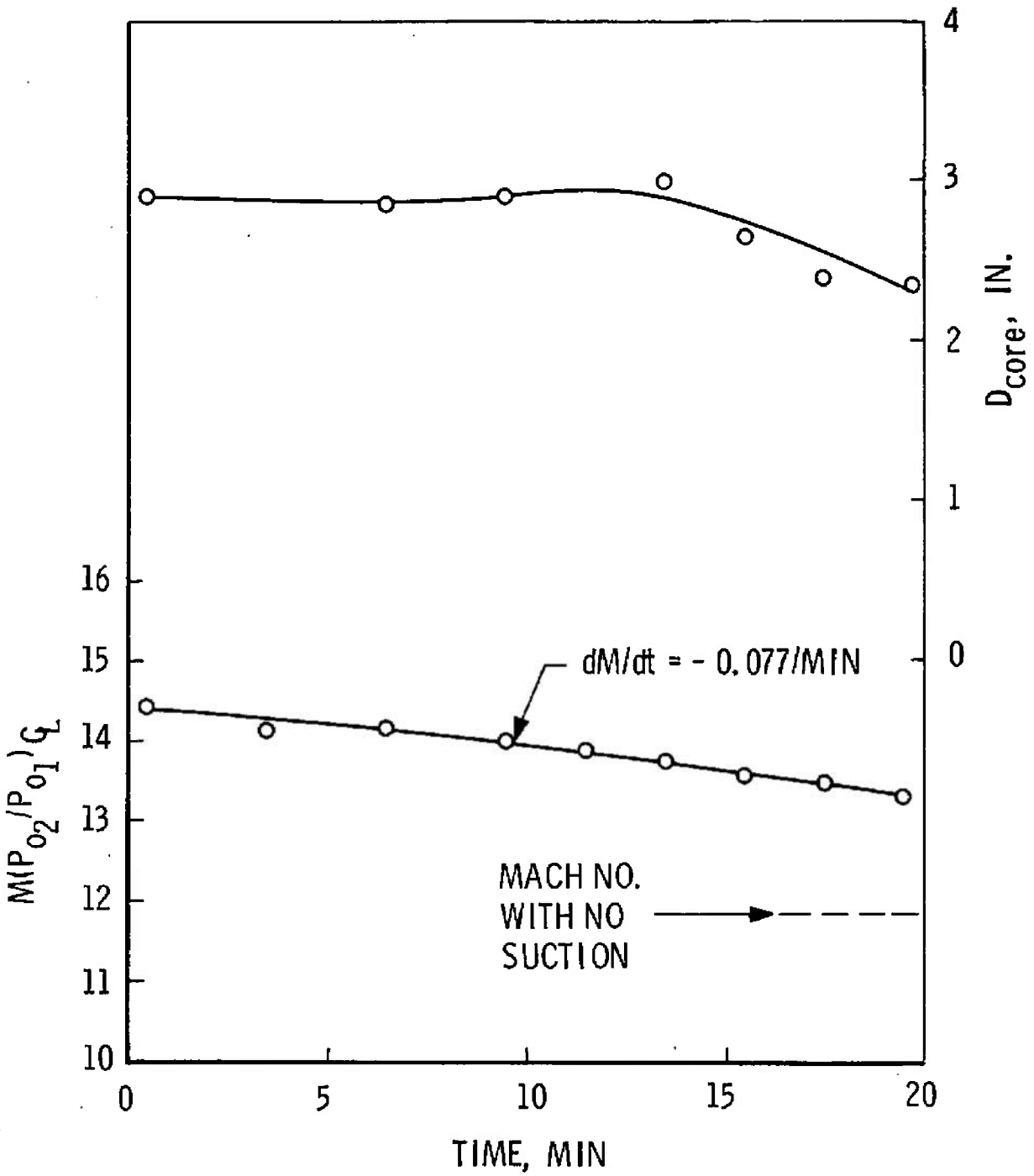

Fig. 16 Dependence of Mach Number and Core Size on Time, with Suction, p_{o_1} = 345 torr, T_{o_1} = 1080°K

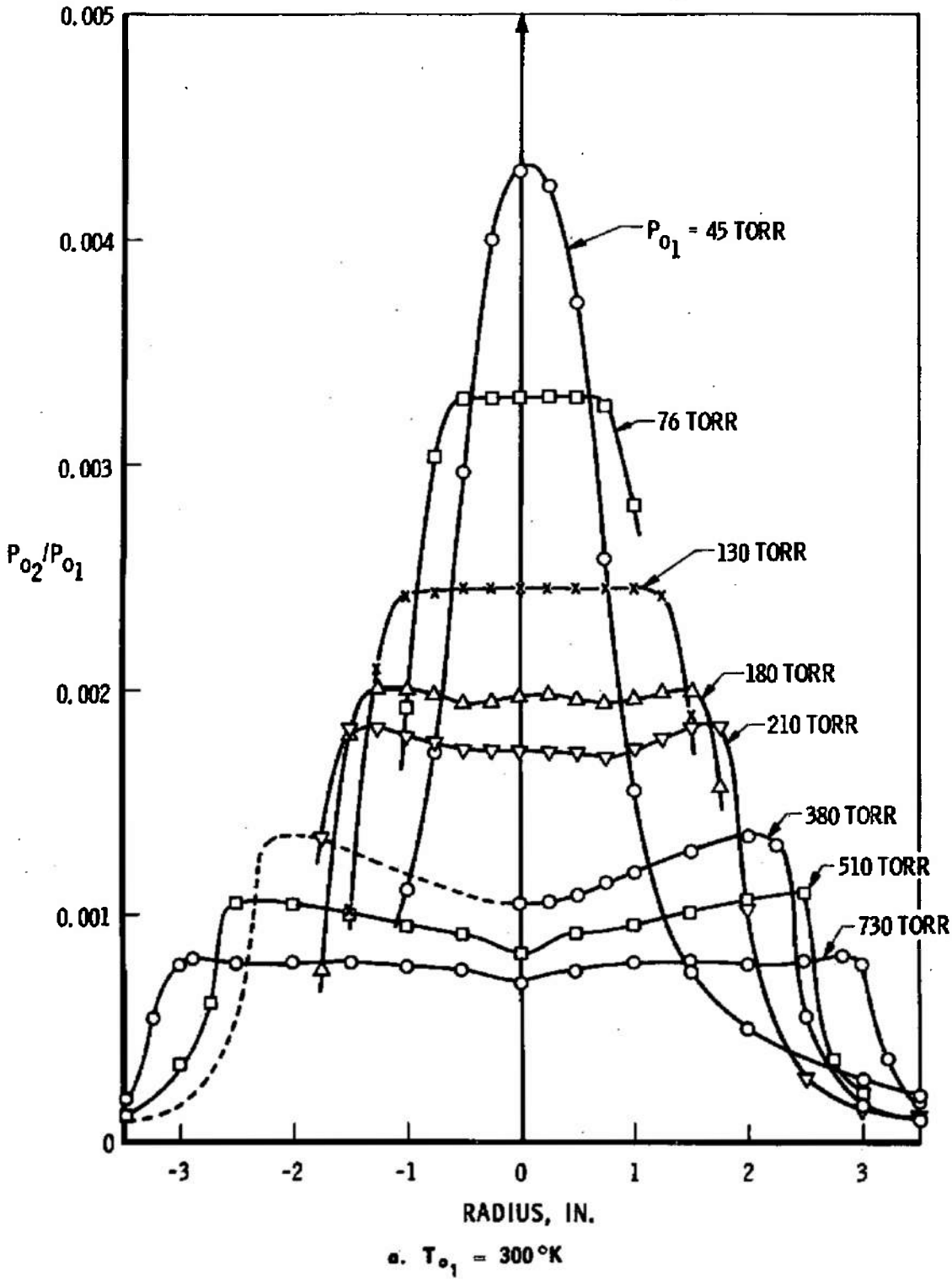

a. T_{o_1} = 300°K

Fig. 17 Pitot Pressure Profiles, No Suction

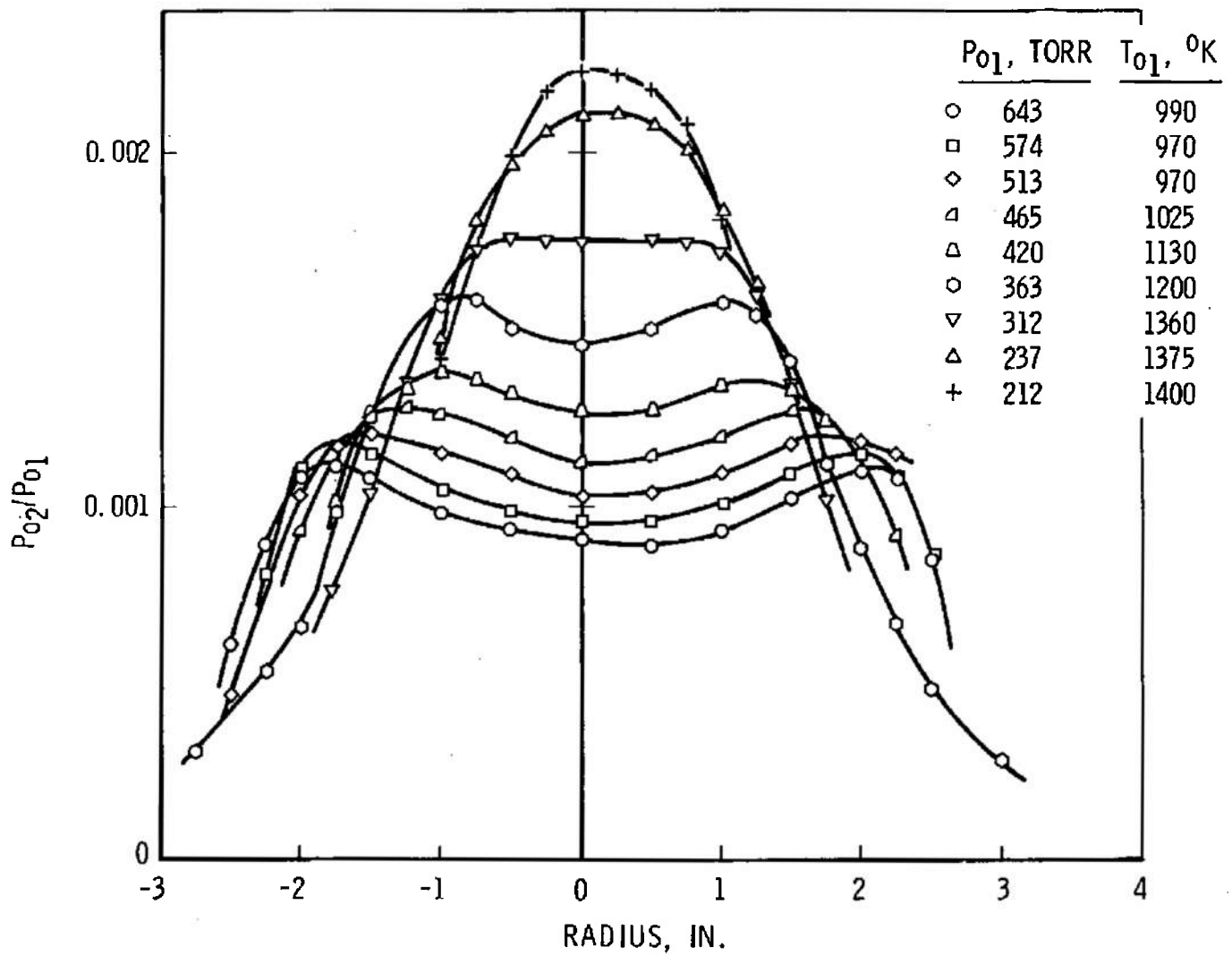

b. Stilling Chamber A, T_{o_1} = 970 to 1400 °K

Fig. 17 Continued

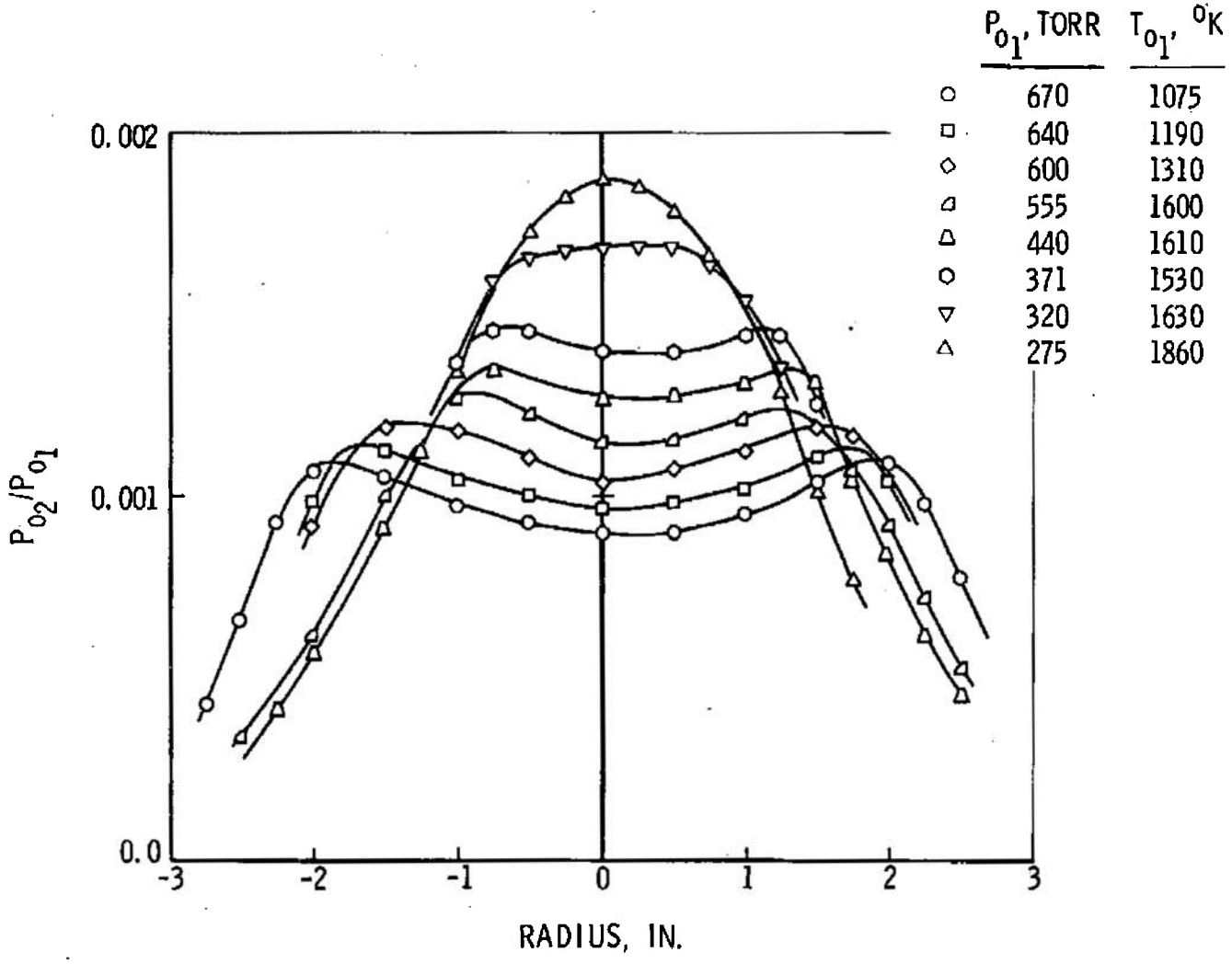

c. Stilling Chamber C, T_{o_1} = 1075 to 1860 °K

Fig. 17 Continued

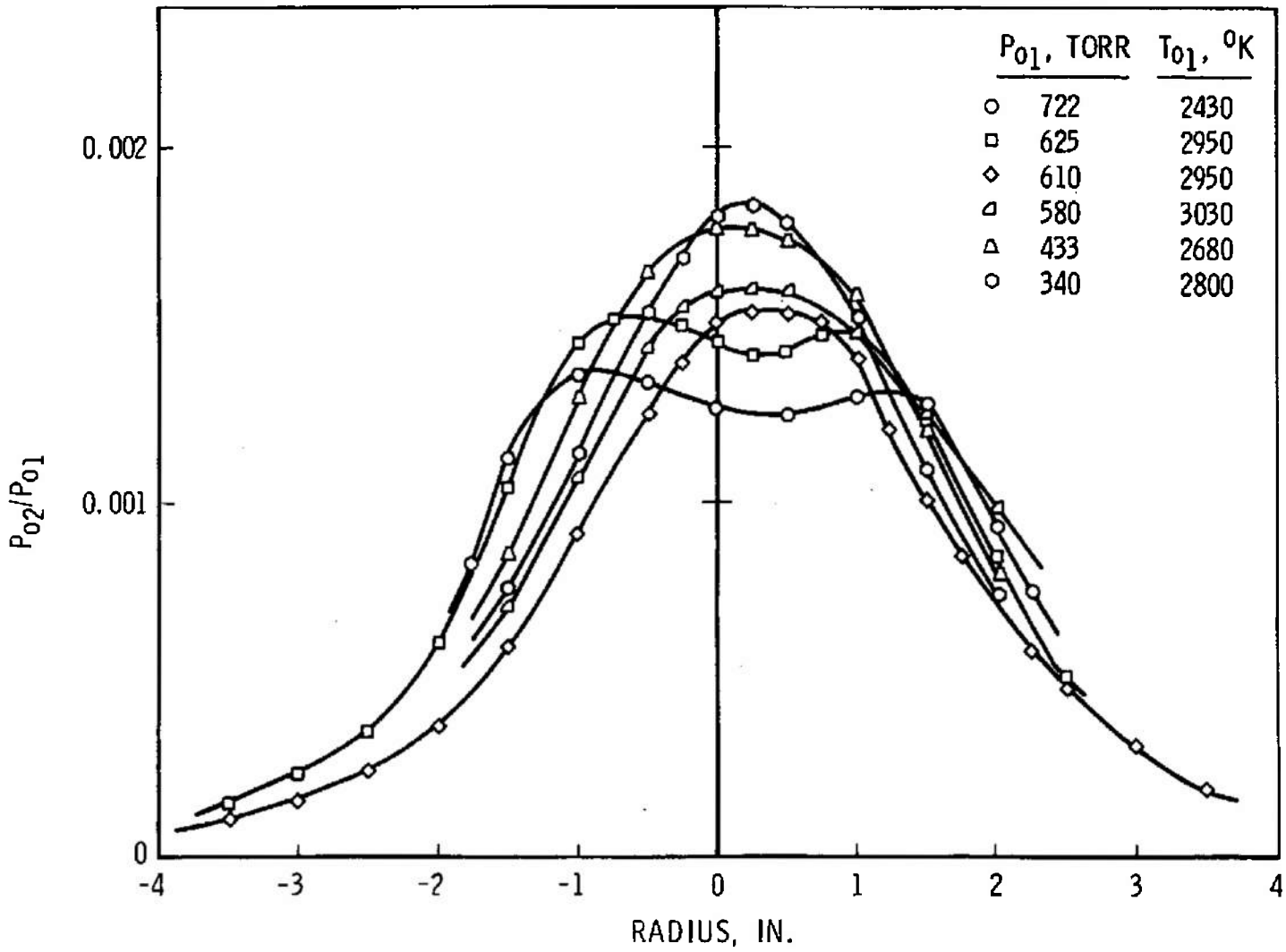

d. Stilling Chamber B, T_{o_1} = 2430 to 3030 °K

Fig. 17 Concluded

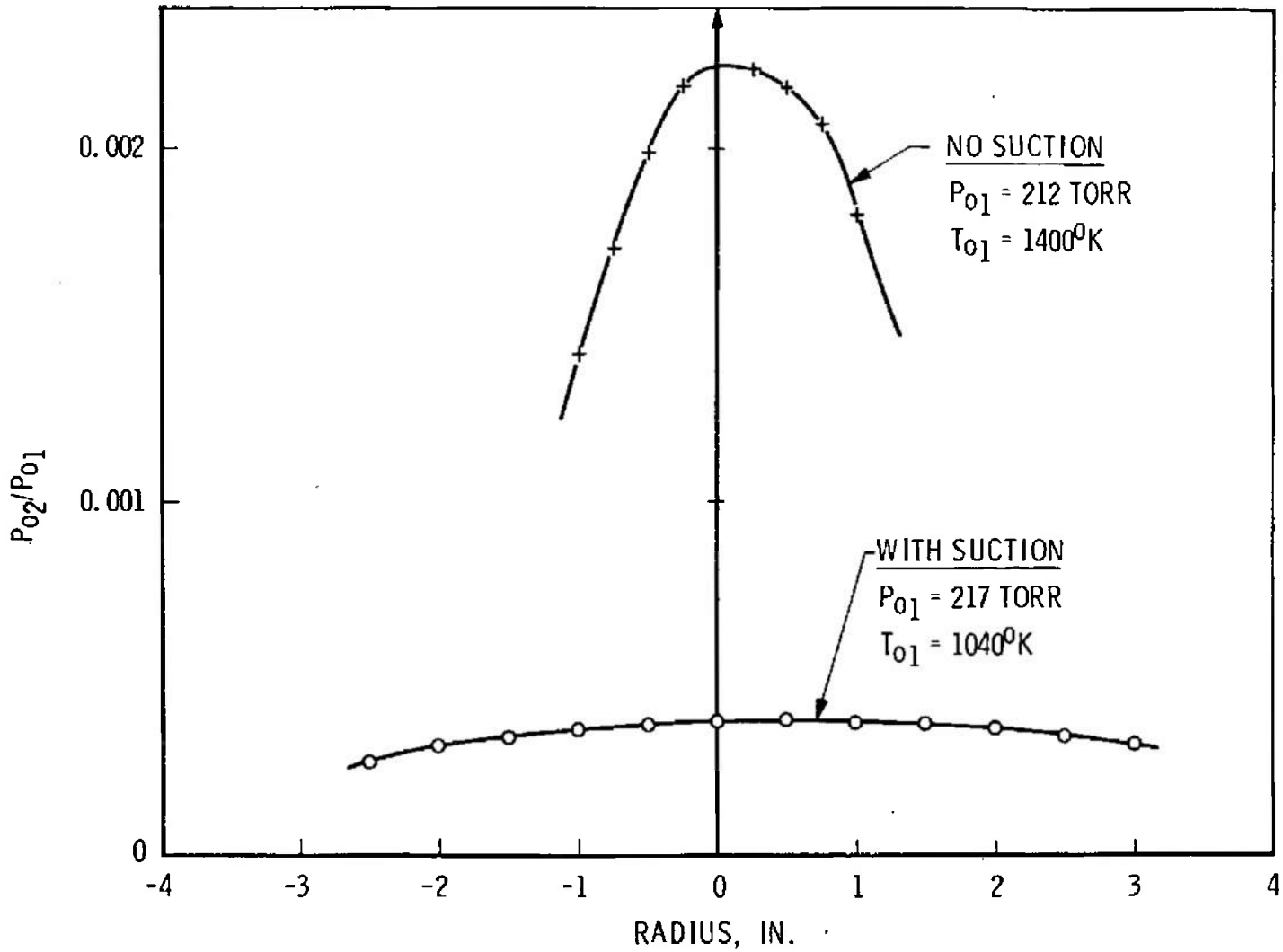

a. p_{o_1} = 215 torr, T_{o_1} = 1040 to 1400 °K

Fig. 18 Effect of Suction on Pitot Pressure Profiles

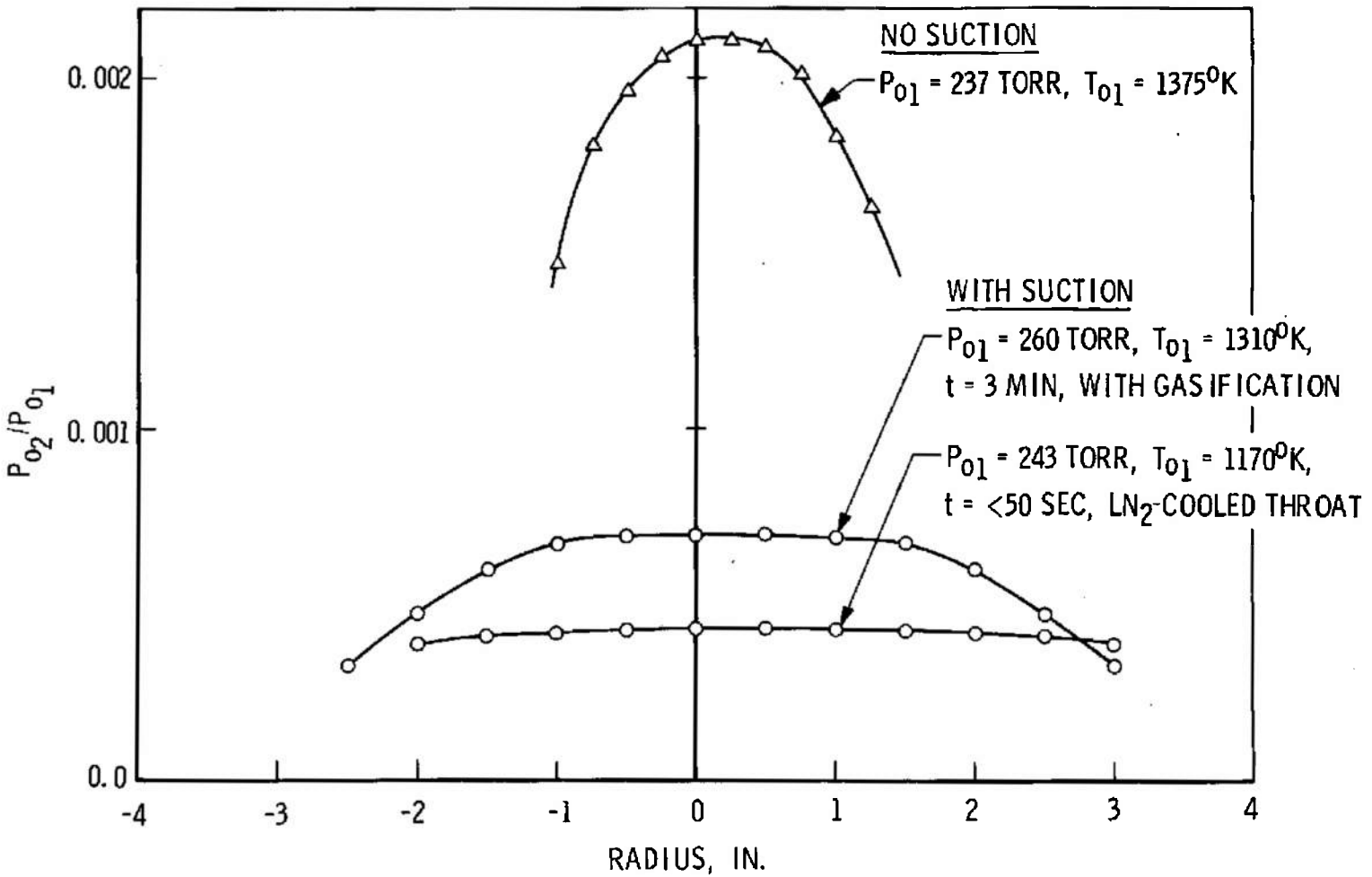

b. p_{o_1} = 237 to 260 torr, T_{o_1} = 1170 to 1375 °K

Fig. 18 Continued

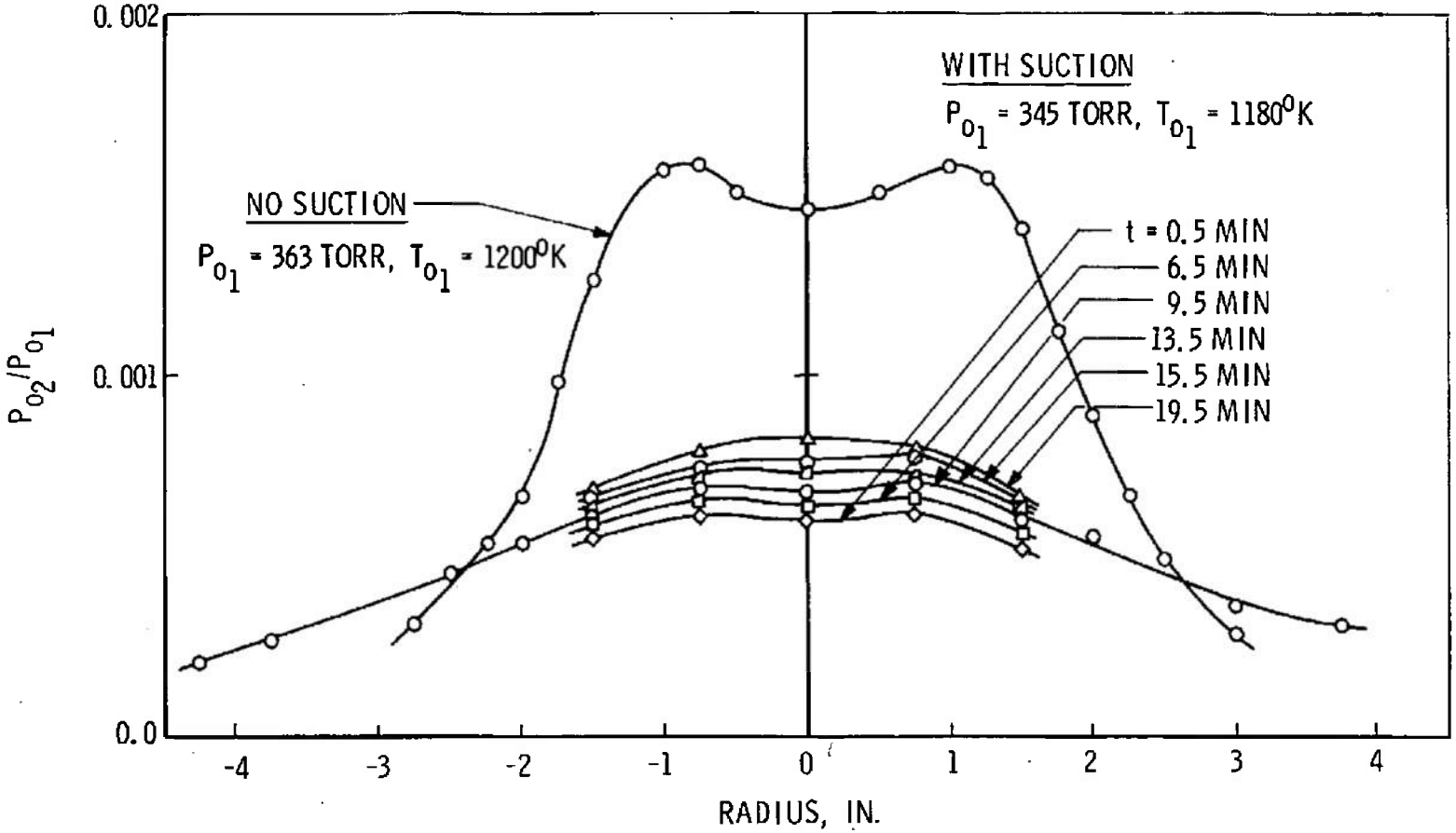

c. p_{o_1} = 345 to 363 torr, T_{o_1} = 1180 to 1200 °K

Fig. 18 Continued

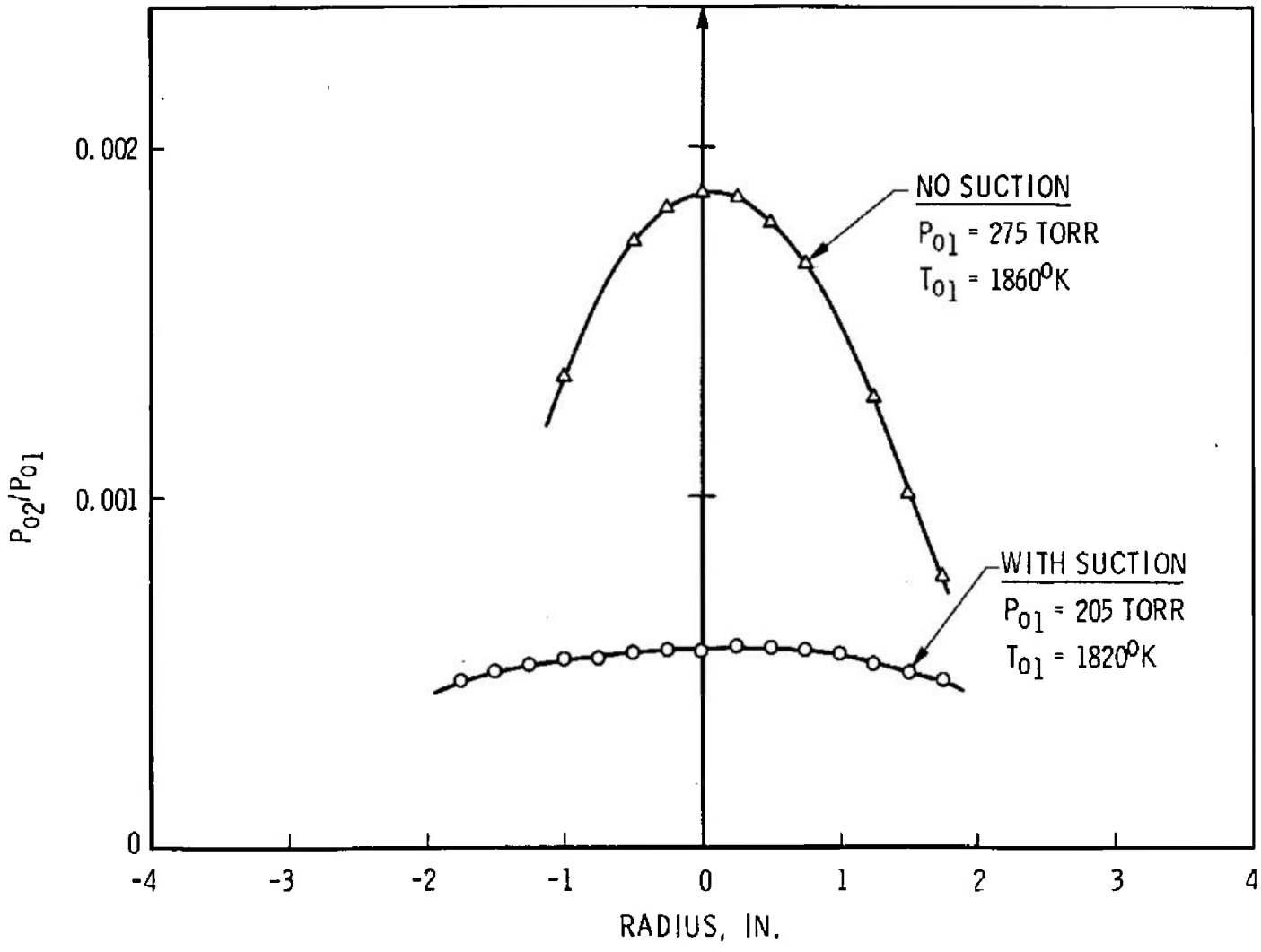

d. p_{o_1} = 205 to 275 torr, T_{o_1} = 1820 to 1860 °K

Fig. 18 Continued

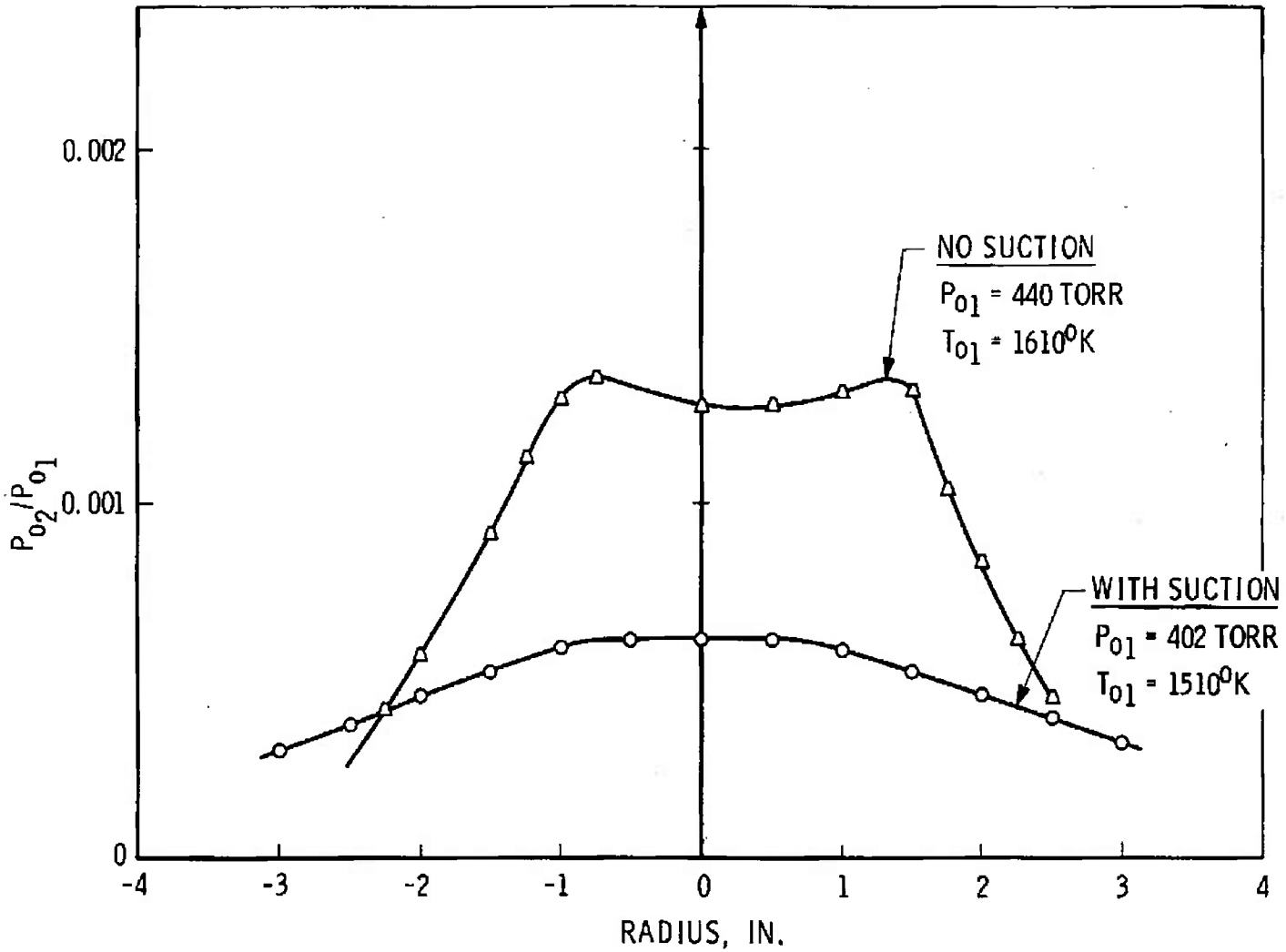

e. p_{o_1} = 402 to 440 torr, T_{o_1} = 1510 to 1610 °K

Fig. 18 Continued

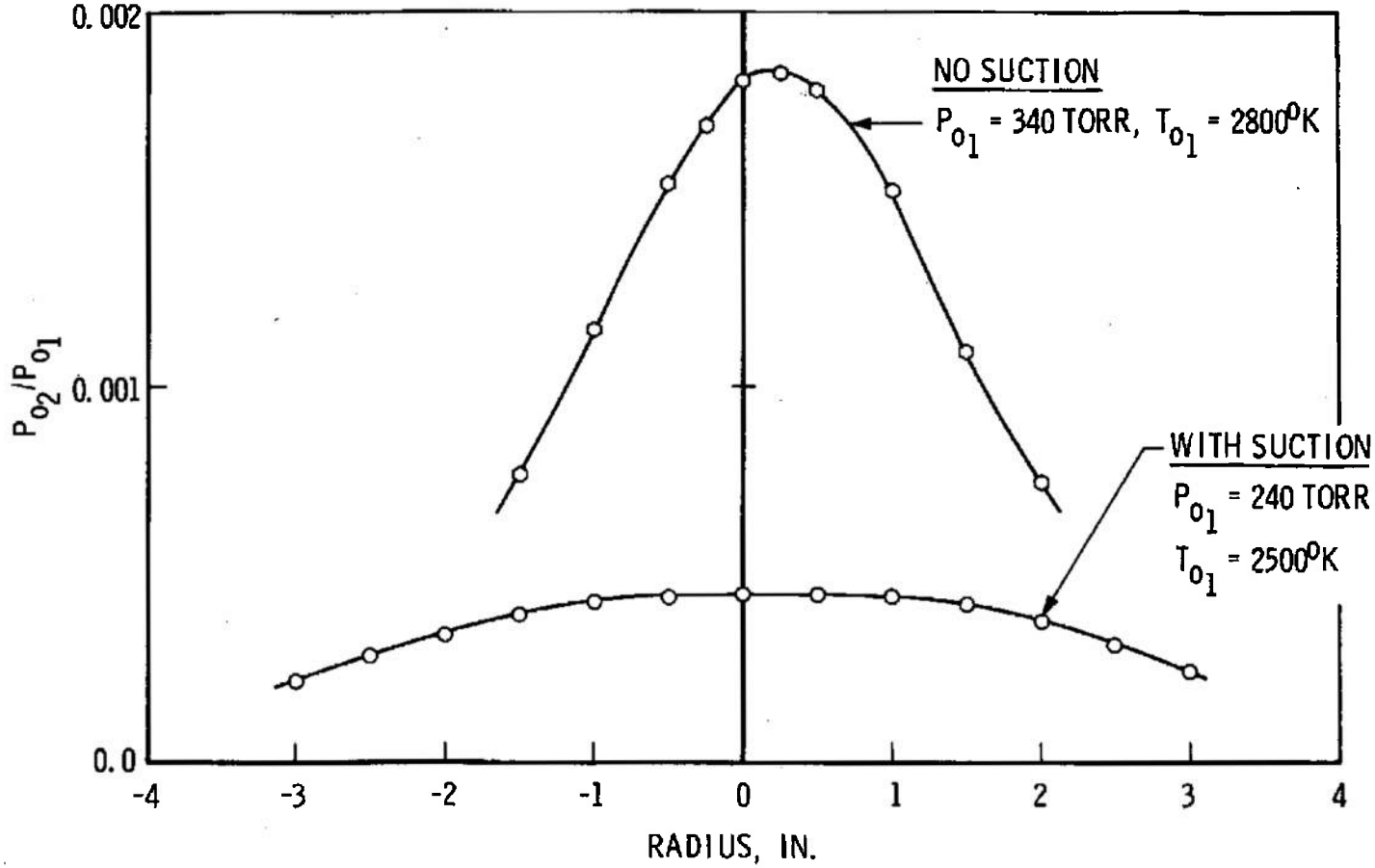

f. P_{o_1} = 240 to 340 torr, T_{o_1} = 2500 to 2800 °K

Fig. 18 Concluded

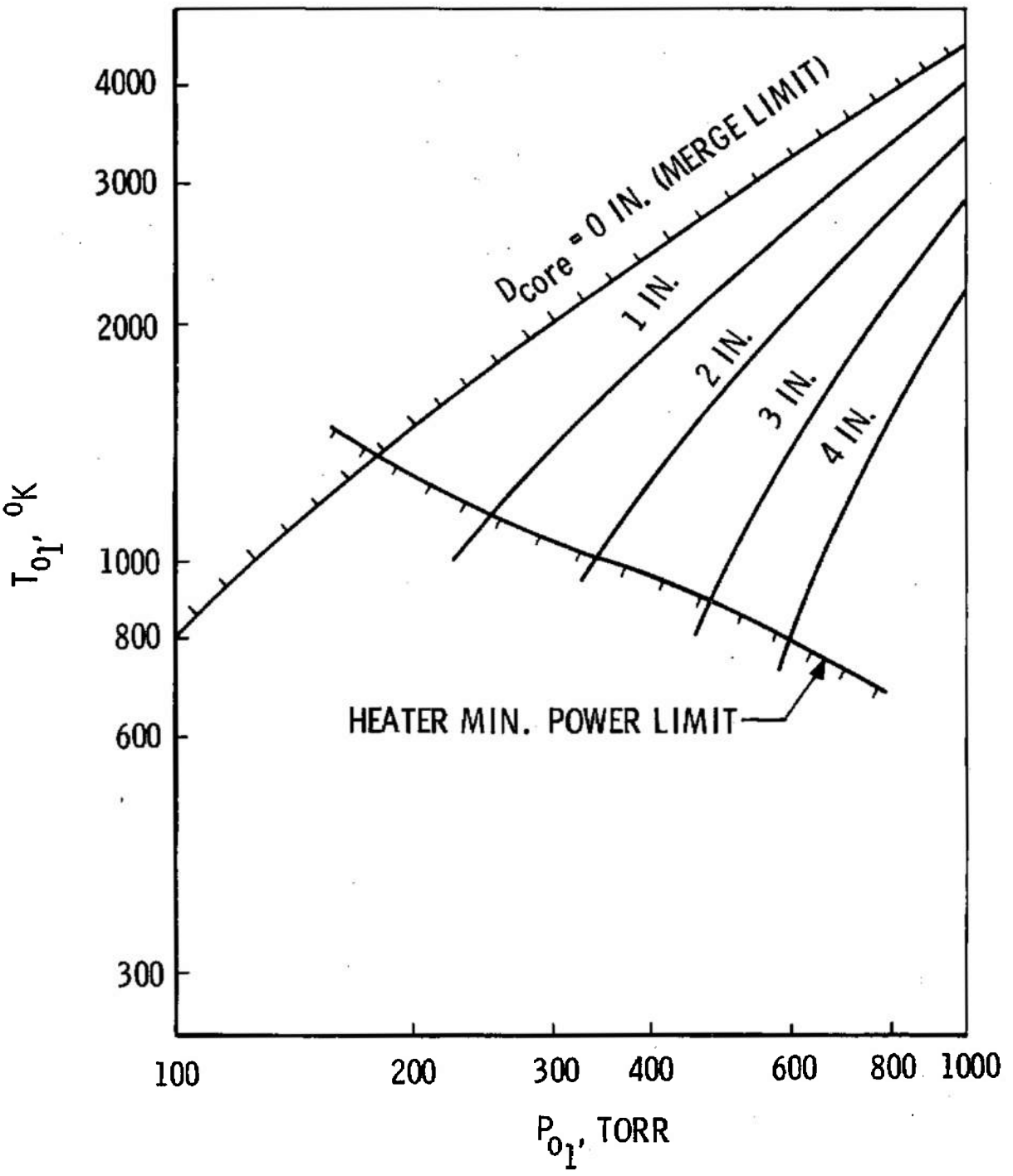

Fig. 19 Core Diameter versus Reservoir Conditions, No Suction

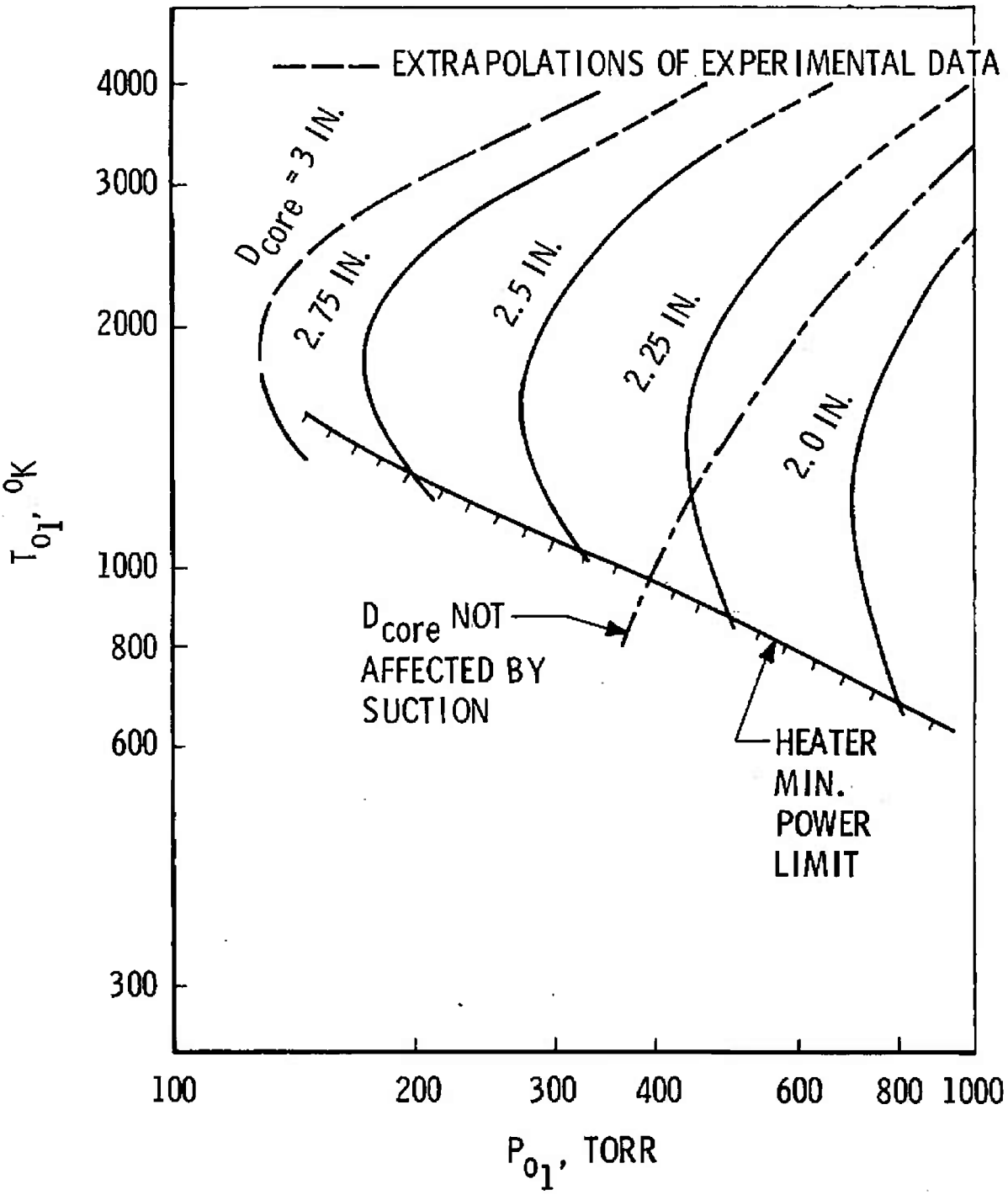

Fig. 20 Core Diameter versus Reservoir Conditions, with Suction

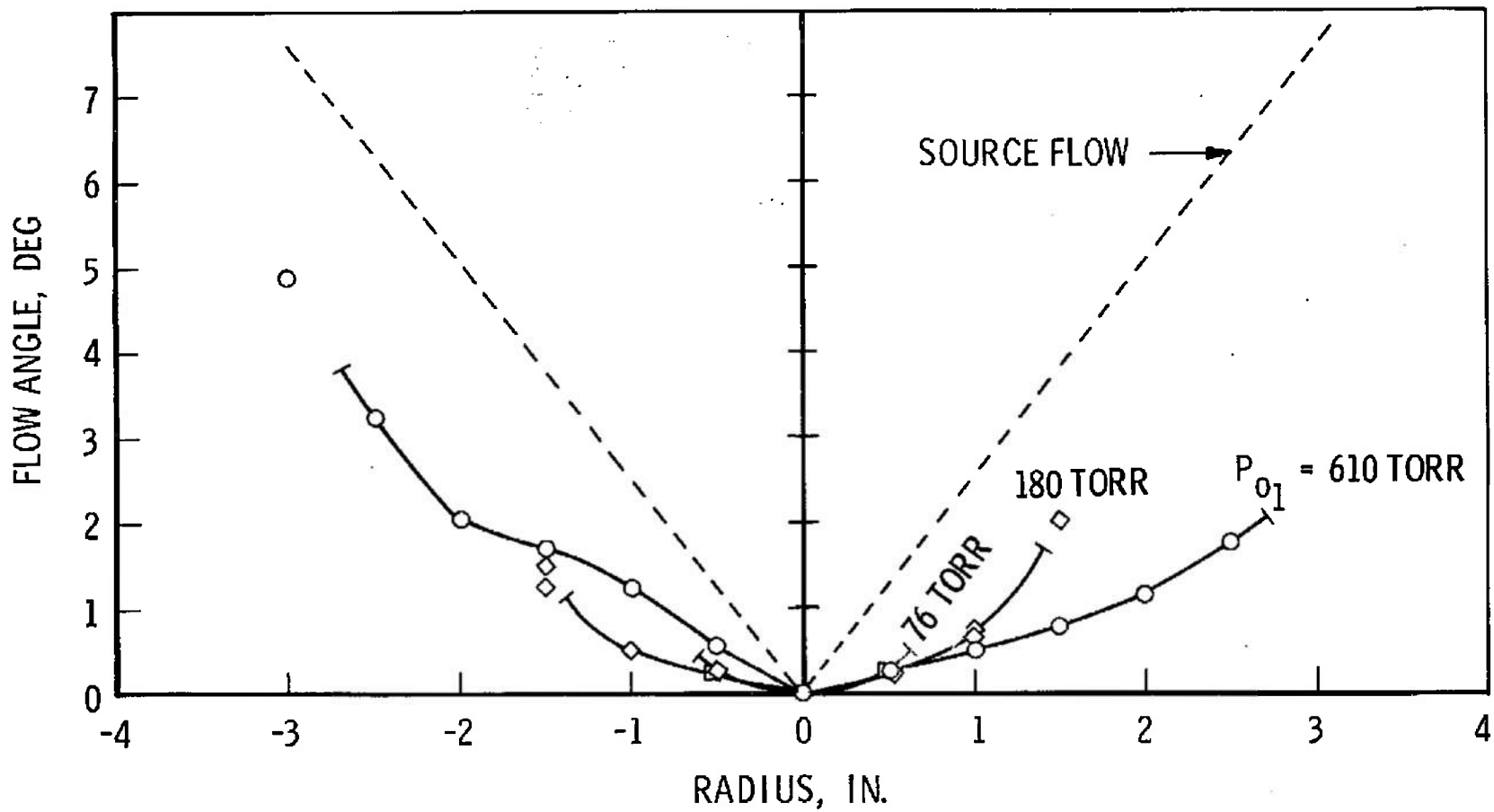

Fig. 21 Flow Angle in Core with No Suction, T_{o_1} = 300 °K

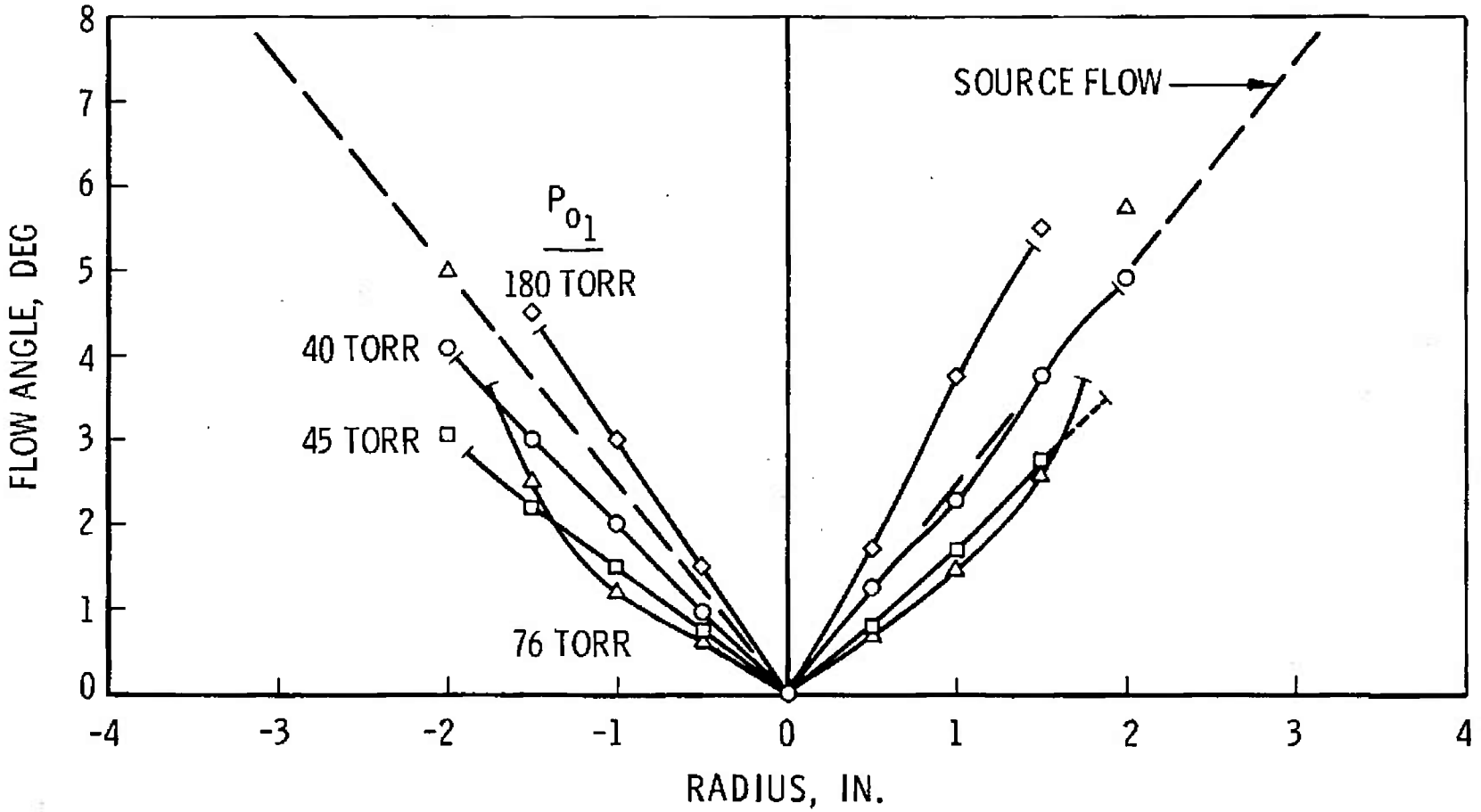

Fig. 22 Flow Angle in Core with Suction, T_{o_1} = 300°K

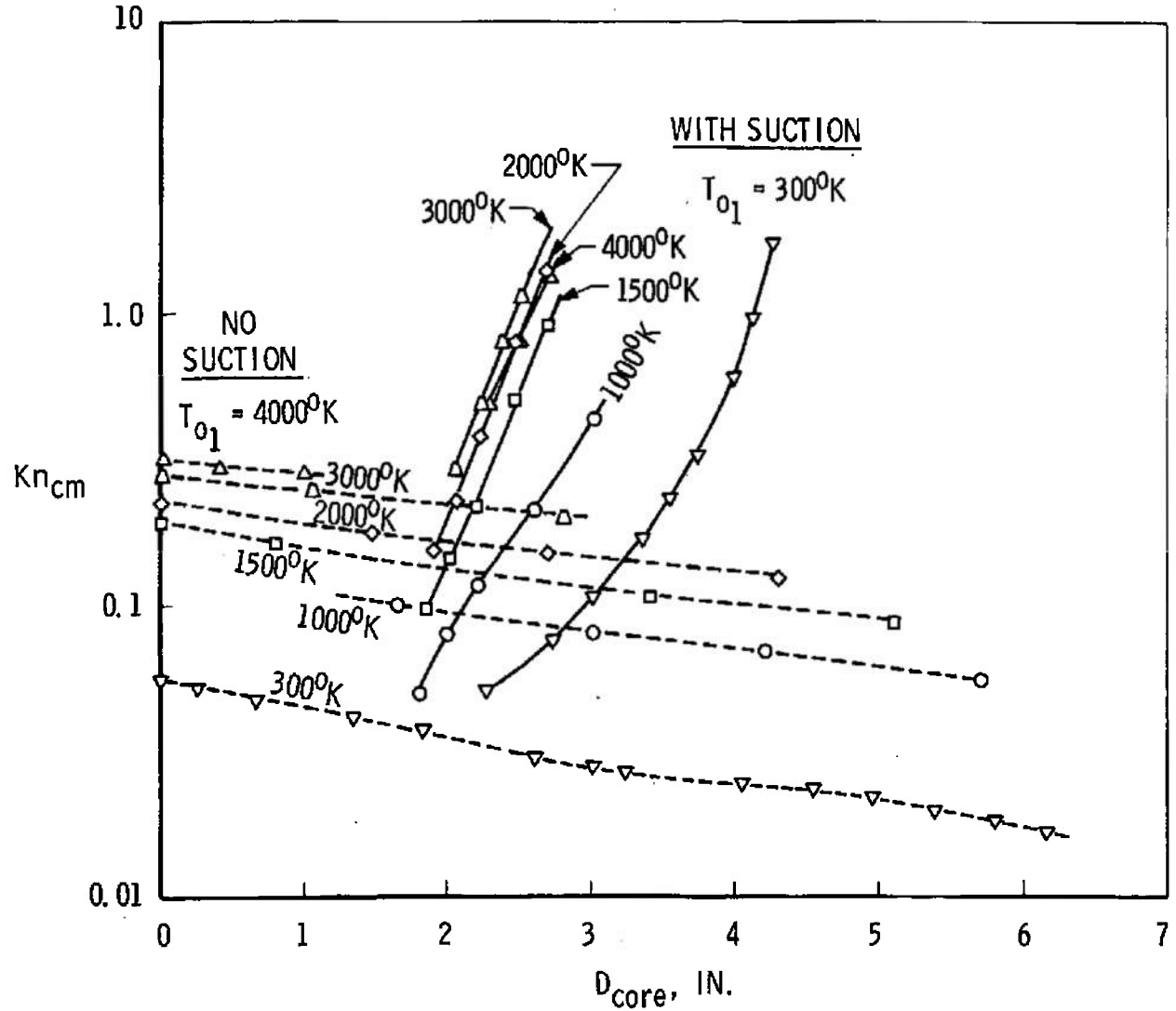

Fig. 23 Knudsen Number for 1-cm Characteristic Length versus Core Diameter

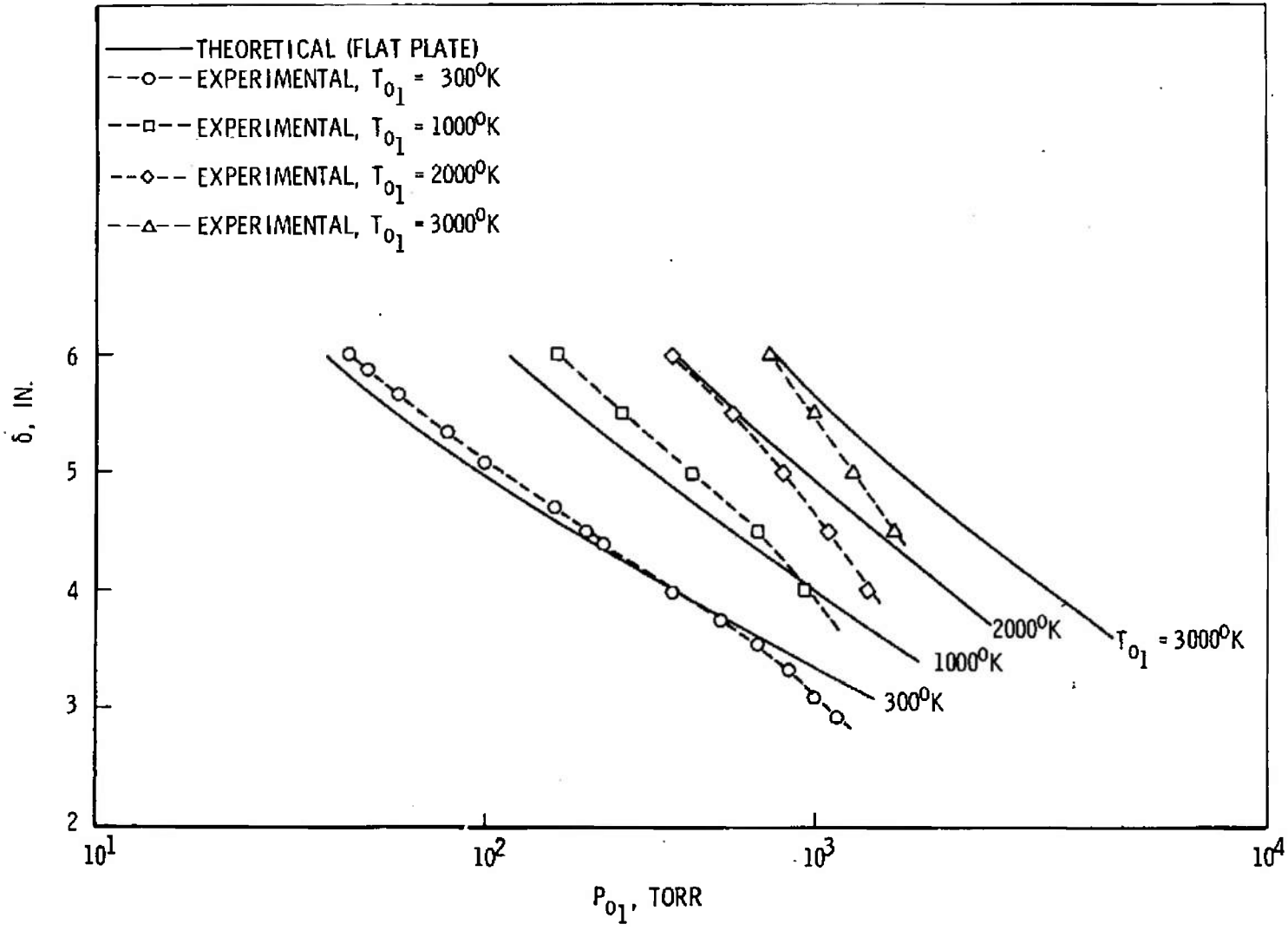

Fig. 24 Boundary-Layer Thickness at Nozzle Exit versus p_{o_1} at Constant T_{o_1}, No Suction

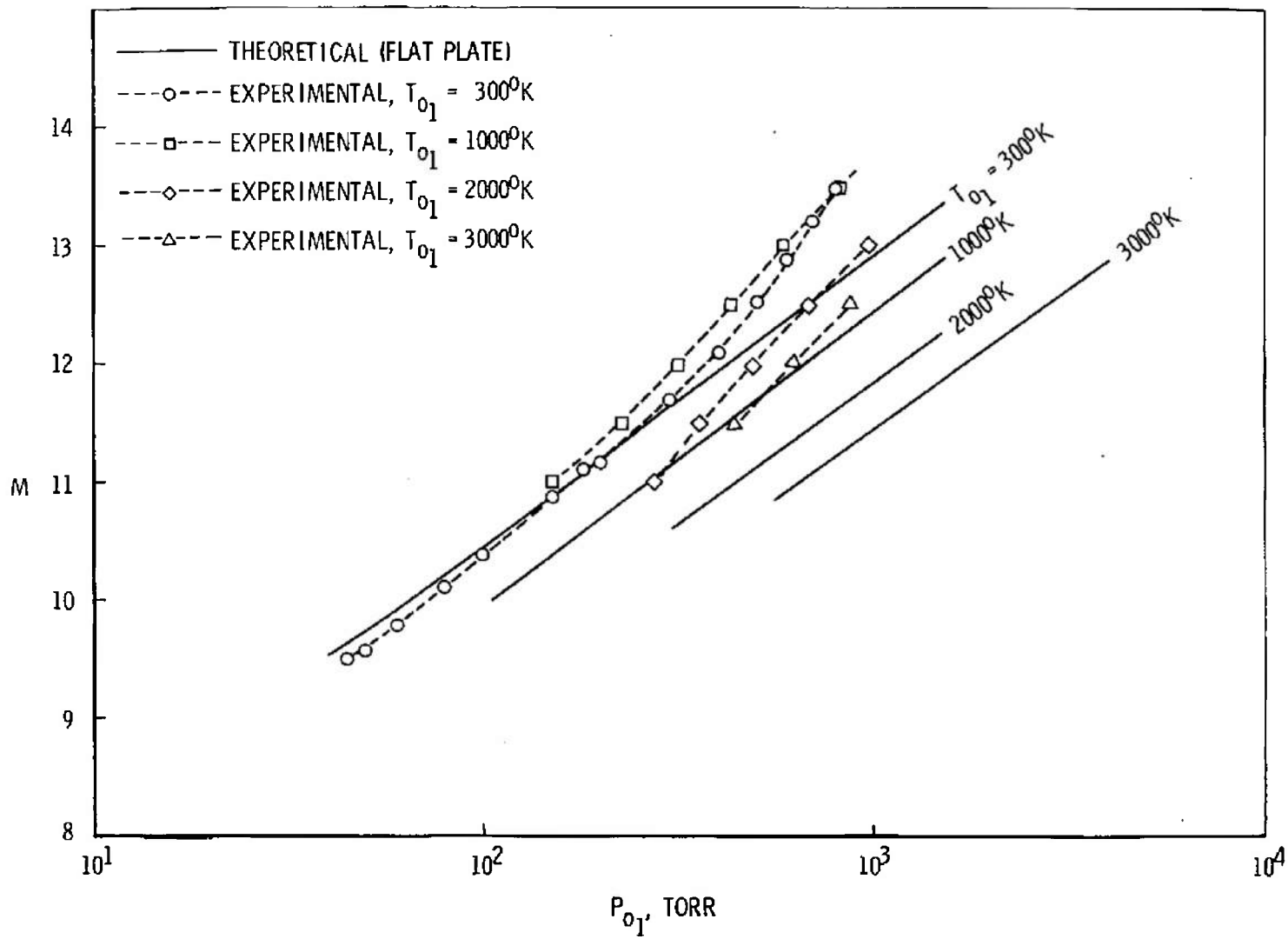

Fig. 25 Mach Number at Nozzle Exit versus p_{o_1} at Constant T_{o_1}, No Suction

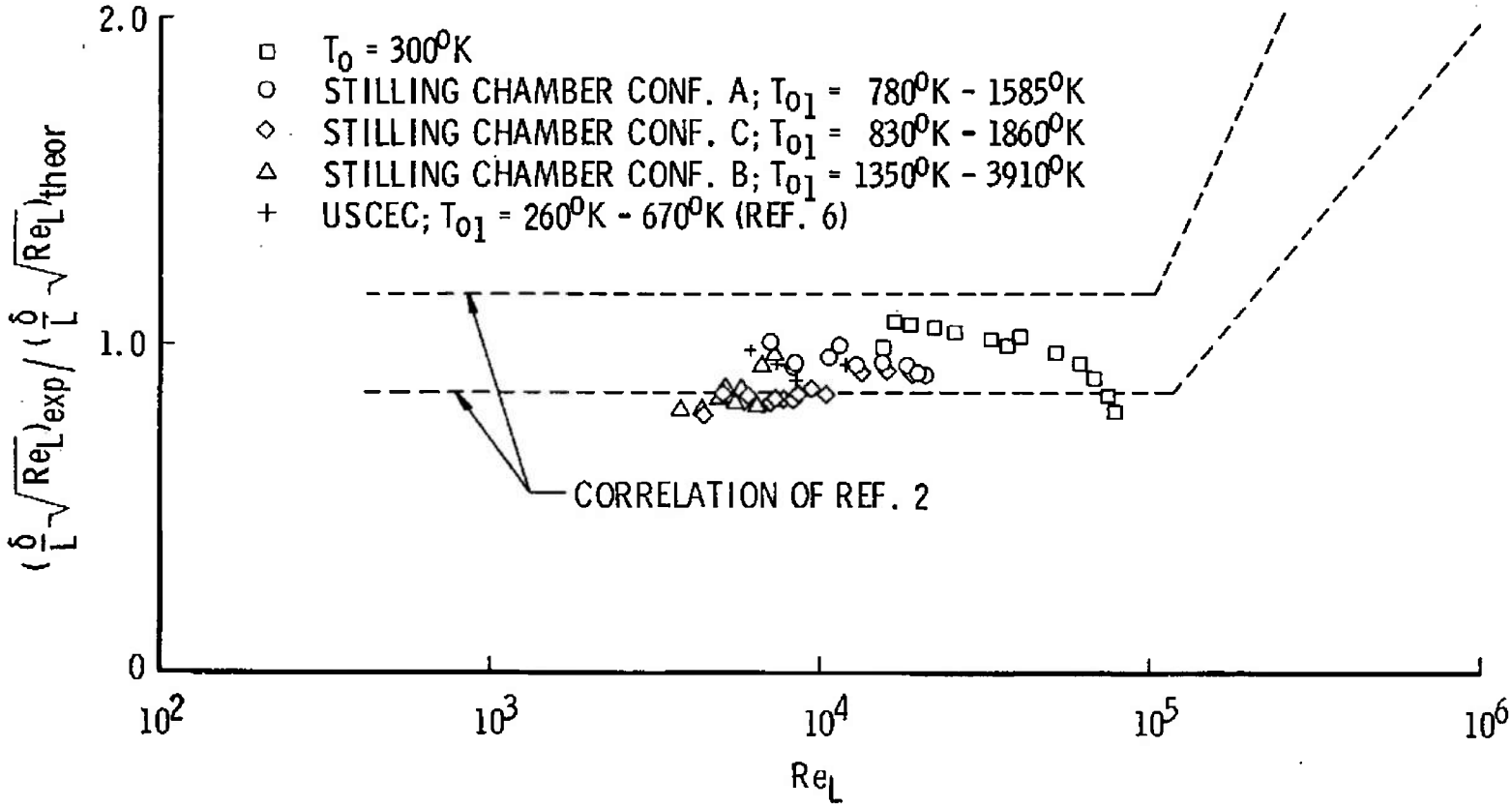

Fig. 26 Correlation of Experimental Boundary-Layer Thicknesses with Flat Plate Theory, No Suction

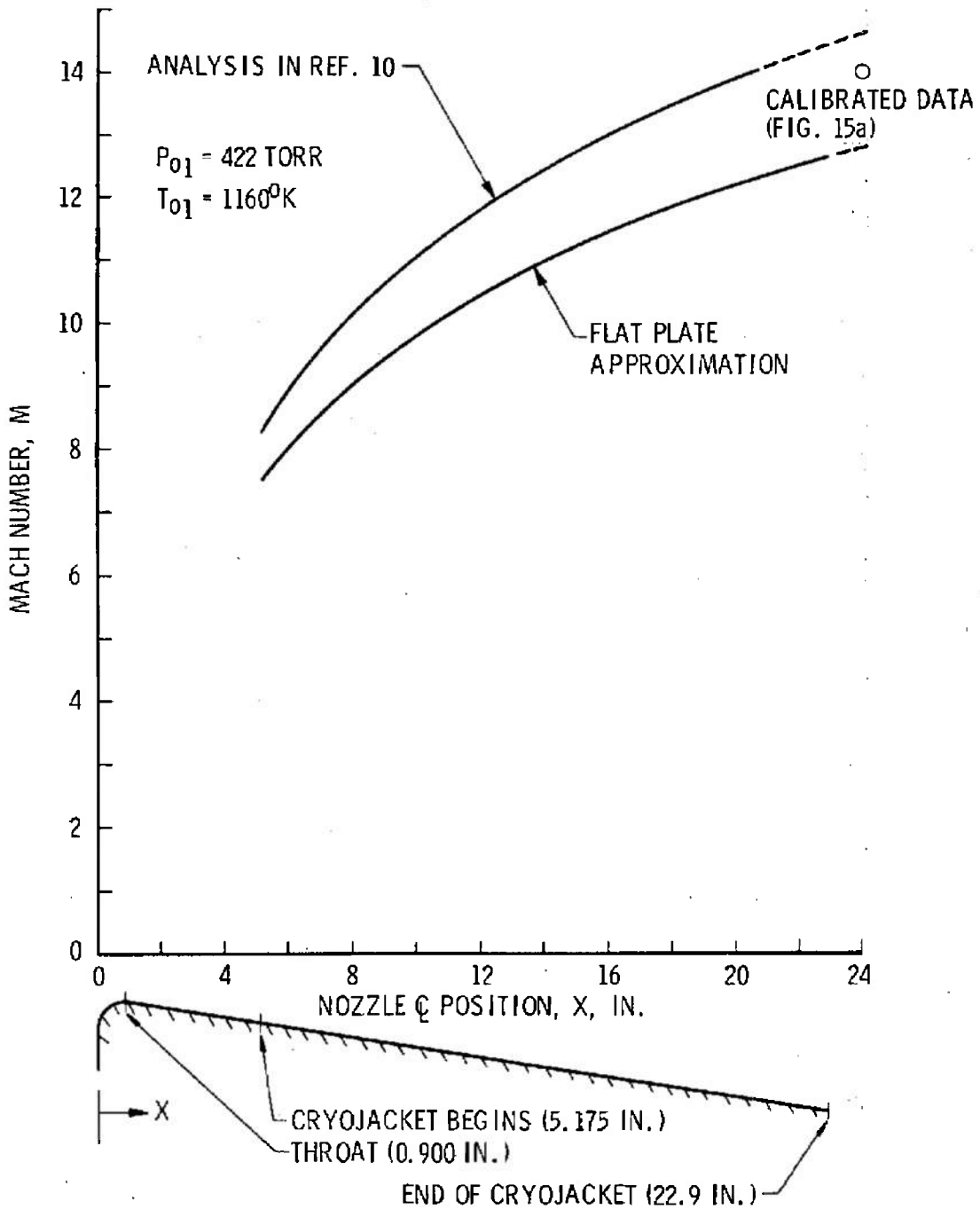

Fig. 27 Theoretical Mach Number Distribution in Nozzle with Suction

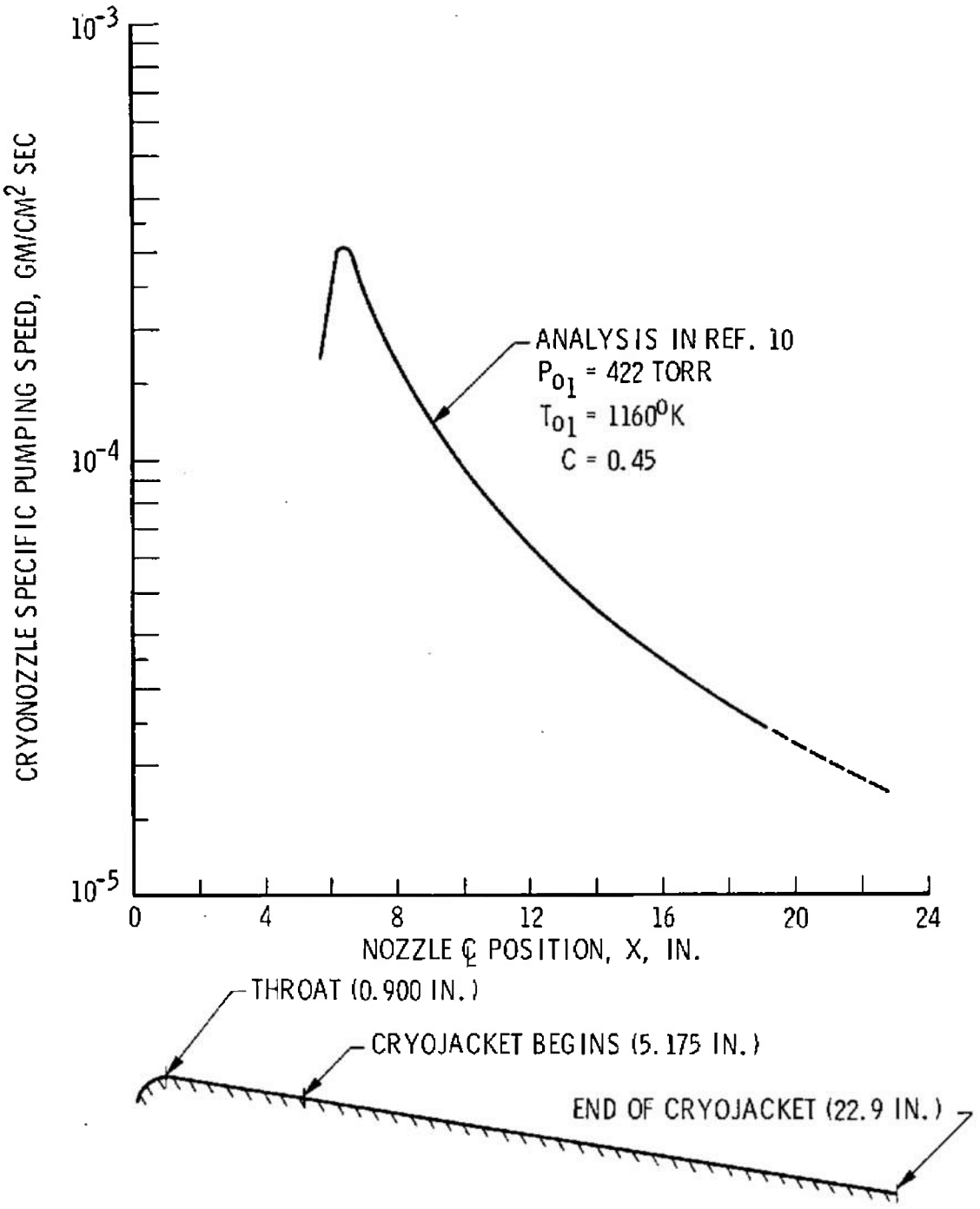

Fig. 28 Theoretical Distribution of Mass Flux to Wall

UNCLASSIFIED

Security Classification

DOCUMENT CONTROL DATA - R&D

(Security classification of title, body of abstract and indexing annotation must be entered when the overall report is classified)

1. ORIGINATING ACTIVITY (Corporate author)

Arnold Engineering Development Center
ARO, Inc., Operating Contractor, Arnold Air Force Station, Tennessee

2a. REPORT SECURITY CLASSIFICATION

UNCLASSIFIED

2b. GROUP

N/A

3. REPORT TITLE

High Temperature, Low Density Boundary-Layer Control by Cryogenic Pumping

4. DESCRIPTIVE NOTES (Type of report and inclusive dates)

N/A

5. AUTHOR(S) (Last name, first name, initial)

MacDermott, W. N., Dix, R.E. and Shepard, J.E., ARO, Inc.

6. REPORT DATE	7a. TOTAL NO. OF PAGES	7b. NO. OF REFS
December 1966	86	17

8a. CONTRACT OR GRANT NO.	9a. ORIGINATOR'S REPORT NUMBER(S)
AF 40(600)-1200	AEDC-TR-66-177
b. Program Element 62410034	
c.	9b. OTHER REPORT NO(S) (Any other numbers that may be assigned this report)
d.	N/A

10. AVAILABILITY/LIMITATION NOTICES

Qualified users may obtain copies of this report from DDC. Distribution of this report is unlimited.

11. SUPPLEMENTARY NOTES	12. SPONSORING MILITARY ACTIVITY
N/A	Arnold Engineering Development Center Arnold AFS, Tennessee

13. ABSTRACT

Results are presented of a study of the flow in a hypersonic nozzle operated at low densities and high stagnation enthalpy levels with both natural and controlled boundary layers. The boundary-layer control was established by cryogenic pumping on the nozzle walls, using liquid hydrogen as the cryogen. A flow calibration procedure was evolved for this nozzle which included a fully frozen nitrogen flow model, large low density corrections to pitot and static pressure measurements, and a non-Sutherland viscosity variation. The regimes of isentropic flow in the nozzle were identified by this calibration, and flow conditions within these regimes are given. The boundary-layer control technique permitted the attainment of indicated Knudsen numbers one order of magnitude greater than those produced with no boundary-layer control. At the lowest levels of static density produced in the nozzle with boundary-layer control, evidence of an entropy-increasing process was found which was tentatively identified as a departure from rotational equilibrium in the flow.

DD FORM 1 JAN 64 1473

UNCLASSIFIED

Security Classification

14 KEY WORDS	LINK A		LINK B		LINK C	
	ROLE	WT	ROLE	WT	ROLE	WT
cryogenics boundary-layer control hypersonic flow flow calibration high temperature low density pitot pressures static pressures						

INSTRUCTIONS

1. ORIGINATING ACTIVITY: Enter the name and address of the contractor, subcontractor, grantee, Department of Defense activity or other organization *(corporate author)* issuing the report.

2a. REPORT SECURITY CLASSIFICATION: Enter the overall security classification of the report. Indicate whether "Restricted Data" is included. Marking is to be in accordance with appropriate security regulations.

2b. GROUP: Automatic downgrading is specified in DoD Directive 5200.10 and Armed Forces Industrial Manual. Enter the group number. Also, when applicable, show that optional markings have been used for Group 3 and Group 4 as authorized.

3. REPORT TITLE: Enter the complete report title in all capital letters. Titles in all cases should be unclassified. If a meaningful title cannot be selected without classification, show title classification in all capitals in parenthesis immediately following the title.

4. DESCRIPTIVE NOTES: If appropriate, enter the type of report, e.g., interim, progress, summary, annual, or final. Give the inclusive dates when a specific reporting period is covered.

5. AUTHOR(S): Enter the name(s) of author(s) as shown on or in the report. Enter last name, first name, middle initial. If military, show rank and branch of service. The name of the principal author is an absolute minimum requirement.

6. REPORT DATE: Enter the date of the report as day, month, year; or month, year. If more than one date appears on the report, use date of publication.

7a. TOTAL NUMBER OF PAGES: The total page count should follow normal pagination procedures, i.e., enter the number of pages containing information.

7b. NUMBER OF REFERENCES: Enter the total number of references cited in the report.

8a. CONTRACT OR GRANT NUMBER: If appropriate, enter the applicable number of the contract or grant under which the report was written.

8b, 8c, & 8d. PROJECT NUMBER: Enter the appropriate military department identification, such as project number, subproject number, system numbers, task number, etc.

9a. ORIGINATOR'S REPORT NUMBER(S): Enter the official report number by which the document will be identified and controlled by the originating activity. This number must be unique to this report.

9b. OTHER REPORT NUMBER(S): If the report has been assigned any other report numbers *(either by the originator or by the sponsor)*, also enter this number(s).

10. AVAILABILITY/LIMITATION NOTICES: Enter any limitations on further dissemination of the report, other than those imposed by security classification, using standard statements such as:

(1) "Qualified requesters may obtain copies of this report from DDC."

(2) "Foreign announcement and dissemination of this report by DDC is not authorized."

(3) "U. S. Government agencies may obtain copies of this report directly from DDC. Other qualified DDC users shall request through _____."

(4) "U. S. military agencies may obtain copies of this report directly from DDC. Other qualified users shall request through _____."

(5) "All distribution of this report is controlled. Qualified DDC users shall request through _____."

If the report has been furnished to the Office of Technical Services, Department of Commerce, for sale to the public, indicate this fact and enter the price, if known.

11. SUPPLEMENTARY NOTES: Use for additional explanatory notes.

12. SPONSORING MILITARY ACTIVITY: Enter the name of the departmental project office or laboratory sponsoring *(paying for)* the research and development. Include address.

13. ABSTRACT: Enter an abstract giving a brief and factual summary of the document indicative of the report, even though it may also appear elsewhere in the body of the technical report. If additional space is required, a continuation sheet shall be attached.

It is highly desirable that the abstract of classified reports be unclassified. Each paragraph of the abstract shall end with an indication of the military security classification of the information in the paragraph, represented as *(TS)*, *(S)*, *(C)*, or *(U)*.

There is no limitation on the length of the abstract. However, the suggested length is from 150 to 225 words.

14. KEY WORDS: Key words are technically meaningful terms or short phrases that characterize a report and may be used as index entries for cataloging the report. Key words must be selected so that no security classification is required. Identifiers, such as equipment model designation, trade name, military project code name, geographic location, may be used as key words but will be followed by an indication of technical context. The assignment of links, rules, and weights is optional.